RELATIVISTIC DISTORTED WAVE APPROACH TO ELECTRON IMPACT EXCITATION OF HEAVY RARE GASES USING A COMPLEX POTENTIAL

ALEX MAGEMBE MARUCHA
(M.Sc.)

I84/32279/2015

A thesis is submitted in fulfillment of the requirements for the award of the degree of Doctor of Philosophy (Physics) in the school of Pure and Applied Sciences of Kenyatta University

MAY, 2022

DECLARATION

This thesis is my original work and has not been presented for degree or other awards in any other University.

Signature …….. Date ……

Alex Magembe Marucha (I84/32279/2015)
Department of Physics

We confirm that the candidate, under our supervision, carried out the work reported in this thesis.

Signature …….. Date ……

Prof. Chandra S. Singh
Department of Physics
Kenyatta University

Signature …….. Date ……

Dr. Peter K. Kariuki
Department of Physics
Kenyatta University

Signature …….. Date ……

Prof. John Okumu
Department of Physics
Kenyatta University

DEDICATION

This thesis is dedicated to my parents, siblings, friends, colleagues at work, my three supervisors, my wife Sekeyian and son Ivan. They have always encouraged me throughout my research.

ACKNOWLEDGEMENTS

I appreciate all the support, encouragement, knowledge and skills accorded to me by my supervisors, Prof. C.S. Singh, Dr. P. K. Kariuki and Prof. J. Okumu throughout my research. I also thank all the members of the Physics department for the criticism and advice aimed at improving the outcome of this study during the weekly departmental seminars. This research is supported in part by grants from the National Research Fund Kenya, NRF /1ST CALL 2016/ PHD and a scholarship from the African Development Bank through Kenyatta University; also of 2016. I sincerely thank these government bodies for enabling me complete this research without financial strain. Furthermore, I thank my parents, my fellow colleagues at work, my brothers and sisters for encouraging me to pursue this degree. Above all, I give thanks to the almighty God for my good health throughout my studies.

TABLE OF CONTENTS

LIST OF FIGURES

LIST OF TABLES

COMMON SYMBOLS USED

a_0 / sr	Bohr radius/steradian
$\boldsymbol{A}$	Anti-symmetrizing operator
'ch'	Scattering channel
$\Psi^{\pm}_{\boldsymbol{ch}}$	Total electron-atom wavefunctions of channel 'ch'
$\chi_{\boldsymbol{km}}(\hat{\boldsymbol{r}})$	Electron spin angular momentum wavefunctions
$\Phi_{\boldsymbol{ch}}$	Total target atom wavefunctions of channel 'ch'
$\mathrm{F}_{ch,\mu}$	Free electron wavefunctions in channel 'ch'
$\phi(\hat{\boldsymbol{r}})$	Electron orbital wavefunction / Dirac orbitals
$P_{n,k}(r)$	Large component radial wavefunctions for a bound electron
$Q_{n,k}(r)$	Small component radial wavefunctions for a bound electron
$f_{\in_{ch} k_{ch}}(r)$	Large component radial wavefunctions for a continuum electron
$g_{\in_{ch} k_{ch}}(r)$	Small component radial wavefunctions for a continuum electron
$\overline{f}_{\kappa}$	Large component radial wavefunctions for plane waves only

$\bar{g}_{\kappa}$	Small component radial wavefunctions for plane waves only
Δ	Mean excitation energy
$\rho(\boldsymbol{r})$	Electron charge density
P_1, P_2, P_3	Stokes parameters
η_{ch}	Phase shifts for scattering channel '*ch*'
$\boldsymbol{N}$	Total number of electrons for an atom
Z	Atomic charge number
μ_{ch}	Spin projection of scattering channel '*ch*'
H	Hamiltonian operator
κ	Relativistic quantum number
k_{ch}	Free electron linear momentum in channel '*ch*'

ABBREVIATIONS

Ar	Argon
CC	Close-coupling
DCS	Differential Cross Sections
DWA	Distorted wave Approximation
DWB (A)	Distorted wave Born (Approximation)
FBA	First Born Approximation
FOMBT	First-order Many Body Theory
FORTRAN	Formula Translation Programming Language
GRASP	General-purpose relativistic atomic structure program
ICS	Integral Cross Sections
Kr	Krypton
MCDF	Multi-Configuration Dirac Fock
RDWBA	Relativistic Distorted Wave Born Approximations
RM	R-matrix
SEPA	Static + Exchange + Polarization + Absorption
SEP	Static + Exchange + Polarization
SE	Static + Exchange
T-matrix	Transition Matrix
UDWA	Unitarized distorted wave approximation
UFOMBT	Unitarized first order many body theory
WKB	Wentzel-Kramers-Brillouin
Xe	Xenon atom

ABSTRACT

Data on excitation of rare gases is important in the study of plasma displays, lighting and lasers. From literature, both relativistic and non-relativistic computations performed on electron impact excitation of low-lying states of rare gases often fail to give satisfactory agreement with available experimental data mostly at low impact energies and at intermediate scattering angles. With this in view, in the present study, we have applied relativistic effects in a fully-relativistic distorted-wave approach to excitation of the lowest lying resonance states of argon, krypton and xenon gases, by modifying the electron-atom interaction distortion potential in such a way that the complex part, the absorption potential, and the real part, which includes an energy dependent polarization potential, exchange and electrostatic potentials, form the complex distortion potential used in calculating radial wavefunctions. The atomic wavefunctions are constructed in the multi-configuration Dirac-Fock approach by modifying the general-purpose relativistic atomic structure code GRASP for numerical procedures. In this study, the WKB approximation is used to compute the free continuum electron wavefunctions which are then used in computing scattering cross sections and angular parameters using our program RDWBA1. Present results from this study predict that use of a complex distortion potential in the relativistic approach to excitation of argon, krypton and xenon generally lowers integral cross sections as impact energies of the incident electron increases, compared to those obtained using real distortion potentials only. For argon, the effect of the absorption potential, which accounts for loss of flux into other open scattering channels is more visible at electron impact energies above 50 eV, while for krypton, absorption becomes more dominant above 100 eV. For xenon, which is the heaviest of the three, absorption in the distortion potential generally has minimal effect on cross sections at impact energies below 50 eV then significantly improves these results when compared with experiments as kinetic energy of the electron increases. Furthermore, for all the rare gases under investigation, it is the energy dependent polarization potential adopted, that plays a major role in improving shapes of cross-sections at low and near threshold impact energies, where available distorted-wave methods fail to give satisfactory results when compared to experiments. We have also obtained angular correlation parameters lambda to predict the magnetic sublevel responsible for most excitations, and Stokes parameters to predict the polarization of the emitted photon during atomic decay. Cross section results obtained from this study are in good agreement with experiments at all impact energies under investigation, therefore it will be interesting to see how these cross sections vary when this present approach is used to investigate excitation of the metastable states of rare gases with both electron and positron impact.

CHAPTER 1

INTRODUCTION

1.1 Background

Studying electron impact excitation is important for the understanding of atomic structures and dynamics of their excitation process. The study of electron ejected spectra after the collisional excitation and subsequent ionization of atoms is a powerful tool for the investigation of the atomic states (Kaur and Srivastava, 1999). Furthermore, data from angular correlation and Stokes parameters, which describes correlation between the scattered electrons and the emitted photon, is useful in the study of lighting, plasma display technologies and lasers. Since large amount of collision data is needed in modeling and diagnostic of high temperature plasmas, such as X-ray lasers, inertial fusion and astrophysics (Chen, 1996), this area of study should motivate researchers in coming up with more data on collision cross sections and angular parameters. A major goal of theoretical atomic physics therefore has been to develop reliable and efficient computational methods to calculate the outcome of the various collision processes of interest.

Computational methods, relativistic and non-relativistic, performed on electron impact excitation of atoms aim to improve on cross sections and angular parameter results when compared with experimental data. The distorted wave Born (DWB) method, which is a kind of first-order perturbation theory in terms of distorted waves is known to be a very successful and not computationally demanding method for electron impact excitation of atoms and ions, especially at intermediate and high energies (Itikawa, 1986). For relativistic calculations using the DWB method, as the number of electrons in a target atom increases, spin-orbit interaction of individual

particles dominates the LS coupling. Relativistic effects in excitation of atoms generally refer to the effect of spin-orbit coupling of free and bound electrons. That is, the spin of an unpaired electron pairs with its own orbital motion inside a potential, resulting in splitting of the target atom's energy levels. The relativistic effects and the mechanism of electron exchange also lead to electron spin-flip during excitation (Zuo *et al.*, 1991). In a fully-relativistic distorted wave (RDW) approach, Dirac equations usually describe the wavefunctions for both the free and bound atomic electrons, unlike in semi-RDW where the Schrodinger equation is used to only derive the target's electron wavefunctions. The excitation of the ground state np^6 to the first excited state $np^5(n+1)s$ results in the excitation of four fine structure levels with total angular momentum J = 0, 1, 1 and 2, that is, the metastable or long-lived states (J = 0 and 2) and the remaining two with J=1 representing the resonance states.

For DWB methods, although inclusion of relativistic effects in computations for heavy rare gases improves cross-sections results when compared to experiments, this is not always the case at low impact energies, even after inclusion of static and electron exchange to the projectile-target interaction potential. Previous studies for excitation of the lowest resonance states of heavy rare gases using RDW, semi-RDW and non-RDW methods as described in the literature review in chapter 2 have neither included the absorption potential (the imaginary part of the complex distortion potential), which accounts for the loss of flux into other possible open inelastic channels, nor an energy dependent polarization potential in the distortion potential for the projectile electron.

In this study, we apply the RDW method and incorporate the electrostatic, polarization, exchange and absorption potentials to form a complex potential, hence find out its effect on cross

section and angular correlation results. Cross sections results presented are calculated with four treatments of the RDWBA model namely; S-RDWBA (static potential), SE-RDWBA (static + exchange potentials), SEP-RDWBA (static + exchange + polarization potentials) and SEPA-RDWBA (static + exchange + polarization + absorption potentials).

1.2 Problem Statement

In this study we have applied the relativistic distorted-wave method to investigate electron impact excitation of the first excited resonance states of rare gases at low excitation energies where other distorted-wave methods in literature fail to give satisfactory results when compared with experiments. As a result, cross sections obtained from this present study are in good agreement with experiments both at low and high impact energies because of the dynamic complex distortion potential and relativistic effects adopted in our calculations.

1.3 Justification

This study is justified on the following grounds:

i. Relativistic effects generally include spin-orbit coupling of the target. These effects, which are usually incorporated in calculation of target state wavefunctions, become important in electron-atom scattering as the atomic charge of the target increases, that is, for heavier atoms. The primary advantages of the RDW method are that it automatically incorporates the fine structure levels of the target atom and includes the possibility of spin-flip of the incident electron during the interaction. Thus, all the relevant physical quantities can be calculated directly from the distorted-wave T -matrix elements (Kaur *et al.*, 1997).

ii. From literature (Zuo *et al*., 1991, 1992; Madison et al., 1998), it is evident that inclusion of relativistic effects greatly improves the agreement of results for both cross-sections and angular correlation parameters as compared to non-relativistic calculations. It is also well known that, in order to obtain reliable phase-shifts for low-energy scattering of electrons from neutral atoms, one must accurately take into account the long-range polarization of the atomic charge cloud by the incident particle and electron exchange effects (McEachran and Stauffer, 1986). Furthermore, a method which has been quite successful for calculating the scattering cross-sections is the model potential approach which seeks to use a complex local potential (Sharma, 2014). Therefore, there is need to combine all these effects in order to yield a good complex distortion potential.

iii. The choice of using the distorted wave series method lies in the fact that more of the important physical effects may be included in the leading terms of the perturbation series expansion making it converge faster than the Born Series (Bartschat, 1996) providing results which are in good agreement with experimental data for intermediate and high incident energies. Also, DWBA methods are less expensive computationally as compared to other reliable theories like R-matrix (RM) and close-coupling (CC) methods (Katiyar and Srivastava, 1988).

iv. The choice to modify the GRASP code over the MCDF code (Grant *et al.*, 1980) used by previous groups who have studied excitation of rare gases lies in the fact that the Oxford MCP/MCDF and MCBP/BENA packages have been rewritten in FORTRAN 77 and combined in the new code, GRASP. This is more versatile than its predecessors, contains more stable and accurate numerical procedures and a simplified but more flexible interface (Dyall *et al*., 1989).

1.4 Research Questions

The study seeks to answer the following research questions:

i. Is it possible to formulate the distorted-wave method in a relativistic approach using a complex potential?

ii. How does inclusion of absorption combined with electron exchange and polarization affect the DCS and ICS results obtained in relativistic excitation of rare gases?

iii. How do cross sections obtained by use of dynamic complex distorting potentials affect results for angular parameters?

iv. How do the RDW cross sections and angular parameters compare with experiments and other theoretical distorted-wave calculations when the distortion potential is complex?

1.5 Hypotheses

i. Applying relativistic effects to electron impact excitation of heavy rare gases will yield similar results for ICS, DCS and angular parameters only at high projectile energies when compared to non-relativistic calculations, but better results at intermediate to near excitation threshold energies

ii. Absorption effects yield a complex distortion potential which should improve results when compared with experimental results at energies near excitation threshold energies.

iii. The static potential alone is unlikely to produce good results for electron scattering from rare gases, therefore a dynamic distortion potential should instead give better results for ICS, DCS and angular parameters.

1.6 Objectives of the Research

1.6.1 General Objective

To study the relativistic distorted-wave approach to electron impact excitation of the first excited states of rare gases Ar, Kr, and Xe using a complex potential.

1.6.2 Specific Objectives

i. To formulate the problem for relativistic distorted-wave calculations for electron impact excitation of the first excited states of rare gases and modify GRASP computer code for our calculations.

ii. To determine collision strengths, differential and total cross-sections for the electron-impact excitation of the first excited states of rare gases.

iii. To determine angular correlation and Stokes' parameters

iv. To compare the results obtained with available theoretical and experimental data in literature.

1.7 Significance and Anticipated Output

It is anticipated that results for ICS, DCS and angular parameters obtained at intermediate energies and near excitation threshold will be in better agreement with experimental data compared to non-relativistic DWBA and RDW results without complex potentials

1.8 Conceptual Framework

This study will apply relativistic, absorption and polarization effects to electron impact excitation of heavy rare gases.

1.9 Limitations of the Study

In literature, there are relatively few theoretical and experimental data to compare with our calculated results and mainly lack of experimental data for angular parameters beyond 50º scattering angles.

2 CHAPTER 2

LITERATURE REVIEW

2.1 Electron Impact Excitation of Argon

Zatsarinny *et al.* (2014) made semi-relativistic calculations for electron impact excitation of the lowest excited states of argon using the RM method with close-coupling with target state wavefunctions ranging from 5 up to 500 from threshold up to 300 eV. Their results show that cross sections obtained with less target states wavefunctions are very large compared to experimental results although inclusion of many more target states in calculations improves ICS and DCS results. Major disparities in ICS results are seen at excitation energies less than 50 eV.

Khakoo *et al.* (2004) obtained electron-impact differential cross section (DCS) and DCS-ratio measurements for electron impact excitation of lowest excitation levels of argon using both relativistic and semi relativistic calculations which include; 41-state RM, Unitarized first order many body theory (UFOMBT), RDW and semi-relativistic DWBA methods for energies between 14 to 100 eV. They also made measurements of DCS and DCS-ratios for the same excitation to compare with their calculations. Although all their relativistic and semi-relativistic calculations agree very well with measurements as energies approach 100 eV, they fail to give good agreement with experimental measurements at energies less than 30 eV, where our study seeks to improve by adopting a dynamic complex potential. Madison *et al.* (1998) calculated ICS and DCS for electron-impact excitation of argon to 12 different target states using a semi-relativistic first-order distorted-wave Born theory from excitation threshold to 150 eV. Comparing their results with experimental data from Chutjian and Cartwright (1981) and Tsurubuchi *et al*. (1996) for the excitation of the lowest resonance states of argon, their cross

sections results are very large at energies below 30 eV, but yield reasonably good agreement at higher energies up to 150 eV.

Zuo *et al.* (1992) computed DCSs using a RDW method for electron impact excitation of Ar from ground state to the lowest lying excited states at incident electron energies of 20, 30 and 50 eV. The type of distortion potential they applied is not complex but rather composed of a non-local exchange potential of McEachran and Stauffer (1986) and an energy independent polarization potential. They compared DCS results with the experimental results of Filipovic (1984) and theoretical results of da Paixao *et al.* (1984) and Bartschat and Madison (1987) in which satisfactory agreement is seen for the optically allowed transitions at 50 eV, but the singlet transition results do not give satisfactory agreement below 30 eV. Bartschat and Madison (1987) carried out a non-relativistic DWBA study on electron impact excitation of rare gases with a real distortion potential comprising of the excited-state static potential plus the dynamic local electron-exchange potential. No polarization or absorption potential was applied in this study. Except for impact energies of 30 eV and below, DCS results yield an overall satisfactory agreement at all scattering angles for both singlet and triplet excited states with the available experimental data at incident electron energies above 50 eV.

2.2 Electron Impact Excitation of Krypton

Mityureva and Smirnov (2016) presented a collection of data made up of results of direct and effective cross sections available in literature for the process of electron impact excitation with the cascade population of the $4p^5 5s$ levels of the krypton atom. Significant disparities in cross sections results appear at low impact energies, more visibly below 50 eV.

Dasgupta *et al.* (2001) presented ICS calculations up to 50 eV using close-coupling and non-relativistic distorted-wave (NRDW) method with exchange and polarization potentials included in the distortion of the free electron. They also presented semi-RDW computations which did not include the polarization and absorption potentials. Their sets of results differ with experimental results significantly at impact energies below 25 eV but very good agreement is seen above this in all their calculations.

Zuo *et al.* (1992) presented results for electron impact excitation of heavy noble gases where calculations of DCS of krypton are given at 20, 30 and 50 eV. They used the RDW method with a non-local exchange potential and energy independent polarization potentials. Comparing their data with the experimental results of Filipovic (1988) and DWBA results of Bartschat and Madison (1987), good agreement in cross sections is seen with shape, but not magnitude for impact energies below 30 eV. The same is the case with the semi-relativistic distorted-wave Born approximation results of Bartschat and Madison (1987) on electron impact excitation of rare gases, where static and exchange potentials are used in calculation of the radial wavefunctions. Although the DCS for Kr have an overall satisfactory agreement at all scattering angles for both singlet and triplet excited states with the experimental data, their results are slightly larger than those of Filipovic (1988) and no results are presented for impact energies below 20 eV.

2.3 Electron Impact Excitation of Xenon

Khakoo *et al.* (1996) carried out an experiment to obtain differential cross sections (DCS) for electron impact excitation of xenon using conventional electrostatic electron energy-loss spectrometers and compared their data with earlier measurements of Nishimura *et al.* (1985) and

Filipovic *et al.* (1987). Despite DCS results having satisfactory agreement in shape at all scattering angles, cross sections measured by Filipovic *et al.* (1987) give results much higher in magnitude than theirs at intermediate angles, which were rather puzzling, though this may be attributed to the difference in their experimental set-ups. They also made calculations using the Unitarized first-order many-body theory and Unitarized distorted-wave approximation (UDWA) calculations. They compared their results with calculations of Bartschat and Madison (1987) and Zuo *et al.* (1992), in which they concluded that it is inclusion of the exchange potential in those calculations that improves DCS results.

Nakazaki *et al.* (1997) made ICS and DCS calculations for electron impact excitation of the lowest nine excited levels of Xe up to 35 eV using the RM method. At electron impact energies below 15 eV, all the integral cross sections show resonance structure. Although the overall agreement with experiments for DCS results is satisfactory, comparison of their ICS results with the experimental results of Filipovic *et al.* (1987) and RDW results of Zuo *et al.* (1991) suggests that the experimental measurements are still very large for the resonance states.

Zuo *et al.* (1992) applied a fully RDW calculation of electron impact excitation of the lowest excited states of xenon at an energy range of 20 eV to 100 eV using a non-local exchange potential and energy independent polarization potentials in the distortion potential. Comparing their results with measurements of Nishimura *et al.* (1985), Filipovic *et al.* (1987) and semi-RDW results of Bartschat and Madison (1987) results, satisfactory agreement is seen for the optically allowed transitions at 50 eV and above. At 30 eV, there is need for further improvement in DCS calculations. Furthermore, their RDW calculations don’t have results for excitation below at 20 eV or below.

Filipovic *et al.* (1987) obtained absolute DCS data using an electron spectrometer for electron-impact excitation of xenon at incident energies between 15 and 80 eV at a scattering range from 5^o to 150^o. In comparing their obtained DCS results at 20eV with experimental results of Nishimura *et al.* (1985), satisfactory agreement in shape but not absolute value.

2.4 Summary on Literature

Generally, for all the gases discussed in this chapter, though inclusion of relativistic, exchange and polarization effects in the distorted-wave methods greatly improves the agreement of results for both cross-sections and angular correlation parameters, they still fail to yield an overall satisfactory agreement at all scattering angles and at low impact energies, especially below 30 eV. In this study, we have applied an energy dependent polarization potential in addition to a local exchange potential of Furness and McCarthy (1973) and the absorption potential due to Staszewska et al. (1984), unlike the distortion potentials used in the distorted-wave methods described in this chapter, which are real potentials. For example, the RDW method by Zuo *et al.* (1992) used a dynamic non-local exchange potential derived by McEachran and Stauffer (1986) and an energy independent polarization potential.

Despite the numerous data available for scattering cross sections, from the experimental studies in the literature given in this chapter, it is evident that only a small amount of the data on angular parameters has been determined experimentally, and when available, it is mostly at scattering angles less than 50 degrees (Martus *et al.*, 1991). This probably is due to the difficulties and costs associated with setting up and performing such experiments. Despite this, it is still important to give theoretical data for angular parameters to act as reference for other researchers and hence the reason for this study.

CHAPTER 3

METHODOLOGY

3.1 The Relativistic Distorted-Wave Theory

3.1.1 Relativistic atomic structure description

In a relativistic approach, following the formulation by Zuo *et al.* (1991) and Grant (1970), the transition of the ground state electron for an argon (n=3), krypton (n=4) or xenon (n=5) gas atom from a singlet ground state will result in a singlet or triplet excited state which can be represented by transitions $n\bar{p}^2np^4\ {}^1S_0^e \rightarrow n\bar{p}np^4(n+1)s\ {}^1P_1^o$ or $n\bar{p}^2np^4\ {}^1S_0^e \rightarrow n\bar{p}^2np^3(n+1)s\ {}^3P_1^o$ respectively. The Dirac form of the Hamiltonian for an atom with N electrons is (in atomic units)

$$H = \sum_{i=1}^{N} H_i + \sum_{\substack{i,j \\ i<j}}^{N} \frac{1}{r_{ij}} \tag{1}$$

where $r_{ij} = \left| r_i - r_j \right|$ is the inter-particle distance and r_i is the position vector of the electron *i*, and;

$$H_i = c\alpha.p + \beta c^2 + V(r_i) \tag{2}$$

The central field $V(r_i) = -Z / r_i$ represents the potential energy of the electron due to nucleus, *Z* is the atomic number, c is the speed of light in free space, and $p = -i\nabla_i$ is the momentum operator, while the Dirac matrices α and β have their conventional representation;

$$\alpha = \begin{pmatrix} 0 & \sigma^P \\ \sigma^P & 0 \end{pmatrix} \quad \beta = \begin{pmatrix} I & 0 \\ 0 & -I \end{pmatrix} \tag{3}$$

where I is the 2×2 unit matrix and σ^{P} represent the Pauli matrices;

$$\sigma_x^{P} = \begin{pmatrix} 0 & 1 \\ 1 & 0 \end{pmatrix}, \ \sigma_y^{P} = \begin{pmatrix} 0 & i \\ -i & 0 \end{pmatrix}, \ \sigma_z^{P} = \begin{pmatrix} 1 & 0 \\ 0 & -1 \end{pmatrix} \tag{4}$$

The electron impact excitation of the atom is represented by a T-matrix given by;

$$T_{a\to b}^{RDW} = \left\langle \Psi_b^- \mid \mathrm{V} - U \mid A\Psi_a^+ \right\rangle \tag{5}$$

$U(r)$ is the distortion potential which is a function of the coordinates of the incident free electron only while A is the anti-symmetrizing operator which account for electron exchange and ensures conformity with the Pauli's exclusion principle. The total wavefunctions for the initial channel (a) and final channel (b) is a product of the free electron wavefunction and the target atom wavefunctions of the form;

$$\Psi_a^+ = \Phi_a^{rel}(1,2,...,N)\,\mathrm{F}_{\mathrm{a},\mu_a}^{DW+}(\mathrm{N}+1) \tag{6a}$$

$$\Psi_b^- = \Phi_b^{rel}(1,2,...,N)\,\mathrm{F}_{b,\mu_b}^{DW-}(\mathrm{N}+1) \tag{6b}$$

Generally, an N-electron-atom wavefunction, which is a solution to Dirac equation, is constructed from central field Dirac-Fock orbitals for an electron defined by quantum numbers n and κ, usually given by a four-component spinor as;

$$\phi(\mathbf{r},\sigma) = \frac{1}{r}\begin{pmatrix} P_{n\kappa}(r)\chi_{\kappa m}(\hat{\mathbf{r}},\sigma) \\ iQ_{n\kappa}(r)\chi_{-\kappa m}(\hat{\mathbf{r}},\sigma) \end{pmatrix} \tag{7}$$

$P(r)$ and $Q(r)$ represent the 'large' and 'small' components of the radial wavefunctions for the target atom, which are usually obtained by solving Dirac equations with the Hamiltonian given

in equation (1). The spin angular momentum functions are expressed in terms of a product of Clebsch-Gordan coefficients, spherical harmonics $\mathrm{Y}_{l\mu}$ and two component spinors $\psi_{\pm 1/2\upsilon}$ as;

$$\chi_{\kappa m}(\hat{\mathbf{r}},\sigma) = \sum_{\mu\upsilon} (l\mu\, 1/2\, \upsilon \mid jm)\, \mathrm{Y}_{l\mu}(\hat{\mathbf{r}})\psi_{1/2\upsilon}(\sigma) \tag{8a}$$

$$\chi_{-\kappa m}(\hat{\mathbf{r}},\sigma) = \sum_{\mu\upsilon} (\tilde{l}\mu\, 1/2\, \upsilon \mid jm)\, \mathrm{Y}_{\tilde{l}\mu}(\hat{\mathbf{r}})\psi_{1/2\upsilon}(\sigma) \tag{8b}$$

An angular state with relativistic orbitals is usually characterized by the relativistic quantum number κ or alternatively by quantum numbers (*l*, *j*). These quantum numbers are related by the expressions $l = j \pm 1/2$ and $j = |\kappa| - 1/2$. The orbital quantum numbers $\tilde{l}$ and *l* in equations (8) represent two possible states with same *l* but different total angular momentum *j*. The Dirac orbitals usually form an orthonormal set given by;

$$\int_0^\infty dr(P_{n'\kappa}(r)P_{n\kappa}(r) + Q_{n'\kappa}(r)Q_{n\kappa}(r)) = \delta_{nn'} \tag{9}$$

$$\langle \chi_{\kappa m} \mid \chi_{\kappa' m'} \rangle = \delta_{\kappa\kappa'}\delta_{mm'} \tag{10}$$

3.1.2 Ground state wavefunctions

Generally, the normalized total wavefunction of an *N*-electron atom with closed sub shells can be expressed as a single Slater determinant using the central field Dirac-Fock orbitals as (Grant, 1970);

$$\Phi_{ch}^{rel} = \frac{1}{\sqrt{N!}} A\{\phi_1, \phi_2, ..., \phi_N\} \tag{11}$$

The ground states of argon, krypton and xenon have the following configuration: $1s^2 2s^2 2\bar{p}^2 2p^4 3s^2 3\bar{p}^2 3p^4$ for argon, $1s^2 2s^2 2\bar{p}^2 2p^4 3s^2 3\bar{p}^2 3p^4 3\bar{d}^4 3d^6 4s^2 4\bar{p}^2 4p^4$ for krypton, and $1s^2 2s^2 2\bar{p}^2 2p^4 3s^2 3\bar{p}^2 3p^4 3\bar{d}^4 3d^6 4s^2 4\bar{p}^2 4p^4 4\bar{d}^4 4d^6 5s^2 5\bar{p}^2 5p^4$ for xenon. Since all the subshells are closed in the ground state (S state), their total angular momentum, $J_a = 0$ (see description in section 3.1.3). As a result, the wavefunctions for the ground states of the atoms can be expressed in the form (Zuo, 1991);

$$\Phi_a = \frac{1}{\sqrt{N!}} \frac{1}{\sqrt{2j_s + 1}} \sum_{mm'} (j_s m j m' \mid 00) \{..., j_s \bar{m} j_s \bar{m}'\} \tag{12}$$

where j_s and j are the angular momentum of the electron before and after the excitation, respectively, $j_s = ½$ for $\bar{p}$, $j_s = 3/2$ for p and $j = ½$ for the excited s orbital (see table 3.1). The curly brackets with $j_s m j m'$ and $j_s \bar{m} j_s \bar{m}'$ represent the corresponding orbitals in Slater determinants. The letters m, m', $\bar{m}$ and $\bar{m}'$ represent magnetic quantum numbers corresponding to the angular momentum numbers j_s, j, j_s and j_s respectively

3.1.3 Excited state wavefunctions

The wavefunctions for an excited state are generally expressed as (Zuo, 1991);

$$\Phi_b = \frac{1}{\sqrt{N!}} \sum_{mm'} (j_s m j m' \mid J_b M_b) \{..., j_s m j m'\} \tag{13}$$

The excited state of argon has the following configuration: $1s^2 2s^2 2\bar{p}^2 2p^4 3s^2 3\bar{p} 3p^4 4s$ (or in shorthand form $(3\bar{p}4s)$) or $1s^2 2s^2 2\bar{p}^2 2p^4 3s^2 3\bar{p}^2 3p^3 4s$ (or in shorthand form $(3p^3 4s)$).

Similarly, krypton has the excited state configuration $4\bar{p}5s$ or $4p^3 5s$, while xenon has the excited state configuration $5\bar{p}6s$ or $5p^3 6s$.

Taking for example, the krypton configuration $4\bar{p}5s$, and then using table 3.1 values for allowed j values for coupling of this state, the $4\bar{p}$ electron with occupation number $q = 1$ has $j_1 = ½$ and the $5s$ with same value of q has $j_2 = ½$. Therefore, the total angular momentum J_b = 0 and 1 of this state using the triangle inequality $|j_1 - j_2| \leq J_b \leq j_1 + j_2$. Similarly, the configuration $4p^3 5s$ will have the total angular momentum J_b =1 and 2. In this study, the focus is only on excitation of the two lowest resonance states (J_b =1) and not the two metastable states (J_b = 0 and 2). This procedure is also used to show that the angular momentum for a closed shell such as the ground state is always zero.

Table 3.1: Allowed j values for coupling of states j^q for occupation number q (Dyall *et al*., 1989).

l_j	$q \leq 2j+1$	seniority of coupling	j value
$s, \bar{p}$	0,2	0	0
	1	1	½
$p, \bar{d}$	0,4	0	0
	1,3	1	3/2
	2	0	0
		2	2
$d, \bar{f}$	0,6	0	0
	1,5	1	5/2
	2,4	0	0
		2	2,4
	3	1	5/2
		3	3/2 , 9/2
$f, \bar{g}$	0,8	0	0
	1,7	1	7/2
	2,6	0	0

		2	2,4,6
	3,5	1	$^7/_2$
		3	$^3/_2$, $^5/_2$, $^9/_2$, $^{11}/_2$, $^{15}/_2$
	4	0	0
		2	2, 4, 6
		4	2, 4, 5, 8

A calculation for the first two excited J = 1 states wavefunctions using the GRASP program (Dyall *et al*., 1989) generates particular configuration mixing coefficients; c_1 =0.8978 and c_2=0.4405 for Ar, c_1 =0.9917 and c_2 =0.1289 for Kr and, c_1 =0.998 and c_2 =0.059 for Xe, which are used in expressing the excited states as a linear combination, that is;

$$ns[1/2]_1^o = c_1\Phi(\alpha_{n\bar{p}(n+1)s}JM) - c_2\Phi(\alpha_{np^3(n+1)s}JM) \tag{14a}$$

$$ns[3/2]_1^o = c_2\Phi(\alpha_{n\bar{p}(n+1)s}JM) + c_1\Phi(\alpha_{np^3(n+1)s}JM) \tag{14b}$$

The wavefunctions in equations (14) are expressed in the common Racah notation $[l+s]_J^{parity}$. Parity of the orbital is given in terms of the orbital quantum number as $(-1)^l$, so that 'o' represents odd parity and 'e' represents even parity. For this study, the ground S-state $n\bar{p}^2np^4\ \ ^1S_0^e$ is of even parity, while the excited states represent odd parity.

The radial distorted waves $f_\kappa(r)$ and $g_\kappa(r)$ for the free electrons in channel '*ch*' are usually expanded in terms of relativistic partial waves that are expressed as (Zuo *et al.,* 1991);

$$\mathrm{F}_{\mu_{ch}}^{DW\pm} = \frac{1}{(2\pi)^{3/2}}\sum_{\kappa m} e^{\pm i\eta_{k_{ch}}} a_{\kappa m}^{\mu_{ch}}(\hat{\boldsymbol{k}}_{ch})\frac{1}{r}\begin{pmatrix} f_\kappa(r)\chi_{\kappa m} \\ ig_\kappa(r)\chi_{-\kappa m}\end{pmatrix} \tag{15a}$$

where;

$$a_{\kappa m}^{\mu_{ch}}(\hat{\boldsymbol{k}}_{ch}) = 4\pi i^{l}\left[\frac{E_{ch}+c^{2}}{2E_{ch}}\right]^{\frac{1}{2}}\sum_{m_l}(lm_l\,½\,\mu_{ch}\mid jm)\mathrm{Y}^{*}_{lm_l}(\hat{\boldsymbol{k}}_{ch}) \qquad (15b)$$

The minus and plus signs indicate the incoming and outgoing asymptotic boundary conditions. The *l* and *j* refer to the orbital and total angular momentum of the projectile electron while μ_{ch} denotes the spin orientation of the channel '*a'* or '*b'*. Furthermore, $\eta_{\kappa_{ch}}$ is the phase shift of the partial wave and $(lm_l\,½\,\mu_{ch}\mid jm)$ is a Clebsch-Gordan expansion coefficient. The radial distorted waves $f_{\kappa}(r)$ and $g_{\kappa}(r)$ are obtained by solving the following pair of coupled Dirac equations (Zeman *et. al.*, 1994; and Zuo *et. al*., (1991));

$$(\frac{d}{dr}+\frac{k}{r})f_{\kappa}(r)-\frac{1}{\hbar c}(2mc^{2}-U+E_{ch})g_{\kappa}(r)-\frac{1}{\hbar cr}\mathrm{W}_{Q}(\kappa;r)=0 \qquad (16a)$$

$$(\frac{d}{dr}-\frac{k}{r})g_{\kappa}(r)+\frac{1}{\hbar c}(-U+E_{ch})f_{\kappa}(r)+\frac{1}{\hbar cr}\mathrm{W}_{P}(\kappa;r)=0 \qquad (16b)$$

The radial distorted wavefunctions satisfy the asymptotic conditions;

$$f_{\kappa}(r)\ \square\ \frac{1}{k}\sin(k_{ch}r-\frac{l\pi}{2}+n_{\kappa_{ch}}) \qquad (17a)$$

$$g_{\kappa}(r)\ \square\ \frac{\hbar c}{E_{ch}+2c^{2}}\cos(k_{ch}r-\frac{l\pi}{2}+n_{\kappa_{ch}}) \qquad (17b)$$

In equations (16), $W_{Q}(\kappa,r)$ and $W_{P}(\kappa,r)$ are non-local exchange potentials, E_{ch} is the relativistic kinetic energy of the scattered electron and k_{ch} is the corresponding linear momentum. In this study, we have neglected the non-local exchange potentials, in a similar manner as pointed out

by Grant (1970) on page 752 and further utilized the local exchange potential V_{ex} in *U(r)* for the calculation of the distorted waves $f_\kappa(r)$ and $g_\kappa(r)$ as described in section 3.2.

3.2 Complex Distortion Potential

The distortion potential *U* used in calculating electron radial wavefunctions by solving the Dirac equations for the free electron in the RDW approach is usually chosen arbitrarily. The complex distortion potential adopted in this study consist of the electrostatic potential V_{st} that takes care of the electrostatic force of attraction between the projectile by the target positive nucleus, exchange potential V_{ex} that accounts for projectile exchange with the target electrons, polarization potential V_{pol} which accounts for long-range alignment of target electron cloud by the projectile and, the absorption potential V_{abs} which accounts for scattering of electrons to other available open channels rather than the one under investigation. That is;

$$U = (V_{st} + V_{ex} + V_{pol}) + iV_{abs}\,. \tag{18}$$

The electrostatic potential is given by;

$$V_{st}(r) = -\frac{Z}{r} + \int \frac{\rho(r')}{r_>} r'^2\, dr' \tag{19}$$

where $r_>$ is the greater of *r* (the free electron's position) and *r*' and $\rho(r')$ represents the atom's charge density;

$$\rho(r) = \frac{1}{4\pi r^2} \sum_{n'\kappa'} N_{n'\kappa'} [P^2_{n'\kappa'}(r) + Q^2_{n'\kappa'}(r)] \tag{20}$$

The occupation number of an orbital is represented by $N_{n'\kappa'}$, given in terms of quantum number *n* and κ.

In the initial scattering channel, the ground state static potential is used as the distortion potential while in the final channel the static potential of the excited state is used. This also applies to the exchange and absorption potentials. The ground state polarization potential is used for both scattering channels since no other version for the excited states of the rare gases is reported in literature. This choice is justified since the distortion potential is usually subject to individual discretion, as long as the asymptotic forms of the distorted waves fulfill the appropriate boundary conditions (Itikawa, 1986).

The absorption potential is adopted from the work of Sharma (2014) and Staszewska *et al.* (1984) which is given in terms of the local velocity of the scattering electron $[2(E-V^{SE})]^{1/2}$ and the mean binary collision cross section $\bar{\sigma}$ as;

$$V_{abs}(r,E) = -\frac{1}{2}[2(E-V^{SE})]^{1/2}\rho(r)\bar{\sigma}_{bx} \tag{21}$$

The polarization potential (Khare *et al*., 1985) adopted for this study is given in terms of dipole and quadrupole polarizabilities α_d and α_q , and an energy dependent parameter $d = 3k_{ch}/8\Delta$. That is;

$$V_{pol}(r,E) = -\frac{\alpha_d r^2}{2(r^2+d^2)^3} - \frac{\alpha_q r^4}{2(r^2+d^2)^5} \tag{22}$$

The symbol Δ represents the mean excitation energy, which is taken as an average of the excitation and ionization threshold energy. The value of dipole and quadrupole polarizabilities of

the rare gases are 11.07 and 52.25 for argon, 17.08 and 97.39 for krypton and 27.82 and 209.85 for xenon (Andreas *et al.*, 1995).

The local exchange potential adopted is (Furness and McCarthy, 1973);

$$V_{ex}(r,E) = -\frac{1}{2}\left\{\left[(E - V_{st}(r))^2 + \rho(r)\right]^{\frac{1}{2}} - [E - V_{st}(r)]\right\} \tag{23}$$

3.3 Transition Matrix Elements

The general procedure to obtain T -matrix elements of equation (5) is by algebraically combining equations (12), (13) and (15) and substituting into equation (6) and then substituting it in equation (5) in a lengthy but straightforward angular momentum algebra to achieve a simplified total T-matrix;

$$T_{a\to b}^{RDW} = \sum_{k_a k_b \mu_a \mu_b} e^{i(\eta_{k_a}+\eta_{k_b})} i^{l_a - l_b}\left[\frac{2l_a+1}{4\pi}\right]^{1/2}\left\{T_{a\to b}^{D} + (-1)^S T_{a\to b}^{E}\right\}\begin{pmatrix} j_a & J_b & j_b \\ -\mu_a & M_b & m_b \end{pmatrix}$$

$$\times\left(l_a 0 \tfrac{1}{2}\mu_a \mid j_a \mu_a\right)\left(l_b m_{l_b} \tfrac{1}{2}\mu_b \mid j_b m_b\right) Y^*_{l_b m_{l_b}}(\hat{k}_b) \tag{24}$$

This procedure involves deriving the direct ($T_{a\to b}^{D}$) T-matrix elements of the form (Zuo *et al.*, 1991);

$$T_{a\to b}^{D} = (2j_s+1)^{1/2} \sum_{mm'\bar{m}\bar{m}'} \left(j_s m j m' \mid J_b M_b\right)\left(j_s \bar{m} j_s \bar{m}' \mid 00\right)\delta_{m\bar{m}}$$

$$\times\left\langle jm'(N)\, \mathrm{F}_b^{DW-}(\mathrm{N}+1)\left|\frac{1}{|\boldsymbol{r}_{N+1} - \boldsymbol{r}_N|}\right|\mathrm{F}_a^{DW+}(\mathrm{N}+1)\, j_s \bar{m}'(N)\right\rangle \tag{25}$$

Since the target wavefunction is expressed as a linear combination of products of one-electron orbital as described in section 3.1.2, and the distorted wave is orthogonalized to the target atom orbitals, the exchange term ($T^{E}_{a\to b}$) takes the form (Itikawa, 1986);

$$T^{E}_{a\to b} = -(2j_s+1)^{1/2}\sum_{mm'\bar{m}\bar{m}'}\left(j_s m j m'\,|\,J_b M_b\right)\left(j_s \bar{m} j_s \bar{m}'\,|\,00\right)\delta_{m\bar{m}}$$

$$\times\left\langle jm'(N)\,\mathrm{F}_b^{DW-}(\mathrm{N}+1)\left|\frac{1}{|r_{N+1}-r_N|}\right|\mathrm{F}_a^{DW+}(\mathrm{N})\,j_s\bar{m}'(N+1)\right\rangle \qquad (26)$$

Then using the formula for Coulomb interaction (Grant, 1970);

$$\left\langle A(1)B(2)\left|\frac{1}{|\boldsymbol{r}_{N+1}-\boldsymbol{r}_N|}\right|C(1)D(2)\right\rangle = \sum_{\lambda\rho} d^{\lambda}_{\rho}(j_C m_C, j_A m_A)\,d^{\lambda}_{\rho}(j_B m_B, j_D m_D)$$

$$\times\int_0^\infty\int_0^\infty(\mathrm{P}_A(1)\,\mathrm{P}_C(1)+Q_A(1)\,\mathrm{Q}_C(1))\gamma_\lambda(1,2)(f_B(2)\,f_D(2)+g_B(2)g_{_D}(2))dr_1dr_2 \qquad (27)$$

where;

$$d^{\lambda}_{\rho}(j'm', jm) = (-1)^{\frac{1}{2}}(2j+1)^{\frac{1}{2}}(2j'+1)^{\frac{1}{2}}\begin{pmatrix} j & \lambda & j' \\ \frac{1}{2} & 0 & -\frac{1}{2}\end{pmatrix}\begin{pmatrix} j & \lambda & j' \\ -m & \rho & m'\end{pmatrix} \qquad (28)$$

As a result, the direct and exchange matrix elements of equation (24) are;

$$T^{D}_{a\to b} = \frac{2}{\pi}\sum_{k_a k_b}\left[\frac{E_a+c^2}{2E_a}\right]^{\frac{1}{2}}\left[\frac{E_b+c^2}{2E_b}\right]^{\frac{1}{2}}(2j+1)^{1/2}(2j_s+1)^{1/2}(2j_a+1)^{1/2}(2j_b+1)^{1/2}$$

$$\times\left(\sqrt{3}\right)^{-1}\begin{pmatrix} j & J_b & j_s \\ 1/2 & 0 & -1/2\end{pmatrix}\begin{pmatrix} j_a & J_b & j_b \\ 1/2 & 0 & -1/2\end{pmatrix}(-1)^{j_s+\mu_a}\Gamma_{J_b}(n_s\kappa_s, n\kappa;\in_a \kappa_a, \in_b \kappa_b) \qquad (29)$$

and;

$$T^{E}_{a\to b}=\frac{2}{\pi}\sum_{\lambda k_a k_b}\left[\frac{E_a+c^2}{2E_a}\right]^{\frac{1}{2}}\left[\frac{E_b+c^2}{2E_b}\right]^{\frac{1}{2}}(2j+1)^{½}(2j_s+1)^{½}(2j_a+1)^{½}(2j_b+1)^{½}$$

$$\times\left(\sqrt{3}\right)\begin{pmatrix} j & \lambda & j_a \\ ½ & 0 & -½\end{pmatrix}\begin{pmatrix} j_s & \lambda & j_b \\ ½ & 0 & -½\end{pmatrix}\begin{Bmatrix} j_a & j_b & J_b \\ j_s & j & \lambda\end{Bmatrix}(-1)^{j_s-\mu_a+\lambda}\Gamma_{\lambda}(n\kappa,\in_a\kappa_a;n_s\kappa_s,\in_b\kappa_b) \quad (30)$$

The radial slater integrals $\Gamma_{J_b}(n_s\kappa_s,n\kappa;\in_a\kappa_a,\in_b\kappa_b)$ and $\Gamma_{\lambda}(n\kappa,\in_a\kappa_a;n_s\kappa_s,\in_b\kappa_b)$ for the T-matrix elements $T^{D}_{a\to b}$ and $T^{E}_{a\to b}$ respectively are;

$$\Gamma_{J_b}(n_s\kappa_s,n\kappa;\in_a\kappa_a,\in_b\kappa_b)=\int_0^{\infty}\int_0^{\infty}(\mathrm{P}_{n_s\kappa_s}(r)\mathrm{P}_{n\kappa}(r)+Q_{n_s\kappa_s}(r)\mathrm{Q}_{n\kappa}(r))\gamma_{J_b}(r,s)$$

$$\times(f_{\in_a\kappa_a}(s)f_{\in_b\kappa_b}(s)+f_{\in_a\kappa_a}(s)f_{\in_b\kappa_b}(s))drds \quad (31)$$

which can be written as;

$$\Gamma_{J_b}(n_s\kappa_s,n\kappa;\in_a\kappa_a,\in_b\kappa_b)=\int_0^{\infty}ds(f_{\in_a\kappa_a}(s)f_{\in_b\kappa_b}(s)+g_{\in_a\kappa_a}(s)g_{\in_b\kappa_b}(s))\frac{r_<^2}{r_>^2}$$

$$\times\int_0^{\infty}dr(\mathrm{P}_{n_s\kappa_s}(r)\mathrm{P}_{n\kappa}(r)+Q_{n_s\kappa_s}(r)\mathrm{Q}_{n\kappa}(r)) \quad (32)$$

where;

$$\int_0^{\infty}dr(\mathrm{P}_{n_s\kappa_s}(r)\mathrm{P}_{n\kappa}(r)+Q_{n_s\kappa_s}(r)\mathrm{Q}_{n\kappa}(r))=\frac{1}{s^2}\int_0^{s}dr\,r(\mathrm{P}_{n_s\kappa_s}(r)\mathrm{P}_{n\kappa}(r)+Q_{n_s\kappa_s}(r)\mathrm{Q}_{n\kappa}(r))$$

$$+s\int_{s}^{\infty} dr\,\frac{1}{r^2}(\mathrm{P}_{n_s\kappa_s}(r)\,\mathrm{P}_{n\kappa}(r)+Q_{n_s\kappa_s}(r)\,\mathrm{Q}_{n\kappa}(r)) \tag{33}$$

At large s, $P(s)$ and $\mathrm{Q}(s)$ exponentially decay, therefore simplifying equation (33) since the last term eventually vanishes. Similarly;

$$\Gamma_\lambda(n\kappa,\in_a\ \kappa_a;n_s\kappa_s,\in_b\ \kappa_b)=\int_0^\infty\int_0^\infty(\mathrm{P}_{n\kappa}(r)\,f_{\in_a\kappa_a}(s)+\mathrm{Q}_{n\kappa}(r)g_{\in_a\kappa_a}(s))\gamma_\lambda(r,s)$$

$$\times(\mathrm{P}_{n_s\kappa_s}(s)\,f_{\in_b\kappa_b}(s)+Q_{n_s\kappa_s}(s)\,\mathrm{g}_{\in_b\kappa_b}(s))drds \tag{34}$$

The integrals can be separated as;

$$\Gamma_\lambda(n\kappa,\in_a\ \kappa_a;n_s\kappa_s,\in_b\ \kappa_b)=\int_0^\infty dr(\mathrm{P}_{n_s\kappa_s}(s)\,f_{\in_b\kappa_b}(s)+Q_{n_s\kappa_s}(s)\,\mathrm{g}_{\in_b\kappa_b}(s))$$

$$\times\int_0^\infty ds(\mathrm{P}_{n\kappa}(r)\,f_{\in_a\kappa_a}(s)+\mathrm{Q}_{n\kappa}(r)g_{\in_a\kappa_a}(s))\gamma_\lambda(r,s) \tag{35}$$

where;

$$\int_0^\infty ds\,(P_{n\kappa}(r)\,f_{\in_a\kappa_a}(s)+Q_{n\kappa}(r)g_{\in_a\kappa_a}(s))\gamma_\lambda(r,s)=\frac{1}{r}Y_\lambda(n\kappa;\in_a\ \kappa_a;r) \tag{36}$$

represents the Hartree Y-function given by (Dyall *et al*., 1989);

$$Y_\lambda(n\kappa,\in_a\ \kappa_a;r)=\int_0^r ds\,\frac{s^\lambda}{r^\lambda}(\mathrm{P}_{n\kappa}(r)\,\mathrm{f}_{\in_a\kappa_a}(r)+\mathrm{Q}_{n\kappa}(r)g_{\in_a\kappa_a}(r))$$

$$+\int_{r}^{\infty} ds \frac{r^{\lambda+1}}{s^{\lambda+1}} (\mathrm{P}_{n\kappa}(r) f_{\in_a \kappa_a}(s) + \mathrm{Q}_{n\kappa}(r) g_{\in_a \kappa_a}(s)) \qquad (37)$$

The integral from 0 to r is approximated using Simpson's rule with a recursive relationship obtained for the integral at each r, followed by an outward integration (starting from the origin). Similarly, a recursive relationship for the integral from r to ∞ is obtained followed by an inward integration (starting from values at infinity towards the origin)

The quantum numbers l_a and j_a represent the incoming electron partial wave while l_b and j_b represent the partial wave for the scattered electron. Furthermore, n_s, l_s and j_s are quantum numbers for the active $\overline{p}$ or p electron, while n, l and j represent the excited s electron. Parity conditions for the T-matrix elements require that the sum $l_a + l_b + J_B$ and $l + l_s + J_B$ is an even integer. Furthermore, the values of λ are determined by the triangle inequality $|j - j_a| \leq \lambda \leq j + j_a$. In this study, convergence is achieved with $\lambda \leq 65$.

The resulting $ns[1/2]_1^o$ or $ns[3/2]_1^o$ state T- matrix for both direct and exchange processes is a linear combination of their expressions with their corresponding j_s values in a similar manner as the excited state wavefunctions are expressed with the different configuration mixing.

3.4 Cross Sections

Using the calculated T -matrix elements, for the total scattering system total angular momentum J_a and J_b, and their projections M_a and M_b respectively, before and after excitation resulting from initial *unpolarized* electrons, the relativistic scattering amplitude arising from the T-matrix equations described in the previous section is defined as (Zuo *et. al.*, 1991; Kaur *et al.*, 1998);

$$f(J_b M_b, \mu_b; J_a M_a, \mu_a) = (2\pi)^2 \left(\frac{k_b}{k_a}\right)^{\frac{1}{2}} T(J_b M_b, \mu_b; J_a M_a, \mu_a) \tag{38}$$

Furthermore, the differential cross sections are given as;

$$\frac{d\sigma}{d\Omega} = \frac{1}{2(2J_a+1)} \sum_{M_b \mu_b M_a \mu_a} |\, f(J_b M_b, \mu_b; J_a M_a, \mu_a)|^2 \tag{39}$$

The angular integration of the DCS of equation (39) over the scattering solid angles and summed over the magnetic quantum states $M_b = 0, \pm 1$ gives the integral cross sections (ICS);

$$\sigma_{tot} = \int \frac{d\sigma}{d\Omega} d\Omega \tag{40}$$

3.5 Angular correlation parameters in the collision frame

Once a target is excited, this state undergoes relaxation or decay by photon emission. Usually, angular parameters are measured with respect to the emitted photon and the scattered electron. These parameters give finer details regarding population of magnetic sub-states for the collision process. For this study we considered the collision frame, where the z-axis is parallel to the linear momentum of the incoming electrons. If it was in the natural frame, the x-axis would have to be chosen parallel to the linear momentum of the incoming electrons. da Paixao *et al.* (1980) and Bartschat and Madison, (1987) presented the set of parameters;

$$\sigma(M_b) = \left\langle f(M_b)\, f^*(M_b) \right\rangle \tag{41}$$

$$\sigma = 2\left\langle f(1)\, f^*(1) \right\rangle + \left\langle f(0)\, f^*(0) \right\rangle \tag{42}$$

$$\lambda = \frac{\sigma(M_b = 0)}{\sigma} \tag{43}$$

$$\overline{\chi} = \arg\left\langle f(1) f^*(0) \right\rangle \tag{44}$$

$$\cos\varepsilon = -\frac{\left\langle f(1) f^*(-1) \right\rangle}{\sigma(1)} \tag{45}$$

$$\cos\Delta = \frac{\left|\left\langle f(1) f^*(0) \right\rangle\right|}{\sqrt{\sigma(1)\sigma(0)}} \tag{46}$$

$$\rho_{00} = \frac{1}{2}(1-\lambda)(1-\cos\varepsilon) \tag{47}$$

Due to limited data available for angular correlation parameters in literature, in this study much emphasis is given to the lambda parameter λ which is usually important in determining the magnetic sublevel of more scattering electron population. In the case where an electron transits from a p to s orbital, this parameter will then give information of which magnetic sublevel M_b more or less excitation takes place from. It can be seen that as λ approaches 1, which is its maximum value, then the most populated sublevel from which excitation takes place is $M_b = 0$. Furthermore, $\cos\varepsilon$ and $\cos\Delta$ are useful in checking for electron exchange and spin flip effects during collision. If there is no spin flip during collision $\cos\varepsilon = \cos\Delta = 1$. This also refers to a case where there are no relativistic effects during collision. Otherwise, if the contrary happens, the parameters are less than 1. The height of the charge cloud along the z-axis is ρ_{00}=0 for a pure

singlet excitation (no exchange). The parameters $\overline{\chi}$, $\cos\varepsilon$, $\cos\Delta$ and ρ_{00} are not discussed further but only used in calculating Stokes parameters.

3.6 Stokes parameters

The Stokes (coherence) parameters are used in the analysis of degree of polarization of the photon emitted from the target atom after excitation (during decay of the target atom). Following the definition by Bartschat (1996), then, for an incident electron moving along the z-axis (in the collision frame), three unit vectors $\boldsymbol{e}_1$, $\boldsymbol{e}_2$ and n defining the helicity (degree of rotation) of the photon can be defined such that; the scattered photon moves in the direction of n so that $\boldsymbol{e}_1$ is perpendicular to n but lie in the plane spanned by the z axis and n. Also, vector $\boldsymbol{e}_2$ is perpendicular to both $\boldsymbol{e}_1$ and n (see Kessler, 1985).

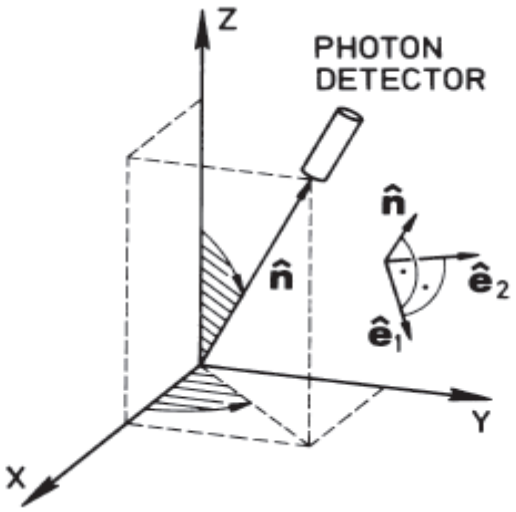

Figure 3.1: Geometry for observation of the Stokes parameters.

Furthermore, Stokes parameters P_1 and P_2 are defined with respect to axes in the plane spanned by $\boldsymbol{e}_1$ and $\boldsymbol{e}_2$ vectors. That is, P_1 is the degree of linear polarization with respect to $\boldsymbol{e}_1$ with axes at (0^o, 90^o) while P_2 is the degree of linear polarization with respect to an axis oriented at 45^o to $\boldsymbol{e}_1$

at (45^o, 135^o). P_3 is the degree of circular polarization in the direction of the photon n. In this study, we have obtained Stokes parameters using the collision frame parameters as (Andersen *et al*., 1988; Andersen and Bartschat 2017);

$$P_1 = \frac{\lambda(3+\cos\varepsilon)-(1+\cos\varepsilon)}{2(1-\rho_{00})} \tag{48}$$

$$P_2 = \frac{2[\lambda(1-\lambda)]^{1/2}\cos\Delta\cos\overline{\chi}}{1-\rho_{00}} \tag{49}$$

$$P_3 = \frac{2[\lambda(1-\lambda)]^{1/2}\cos\Delta\sin\overline{\chi}}{1-\rho_{00}} \tag{50}$$

3.7 Top-up partial waves

It is important to include high *l* partial wave contributions in the RDW calculations to obtain accurate cross sections. However, the lack of convergence of the partial wave expansion as *l* tends towards infinity makes it difficult to achieve this. The *analytic Born Subtraction Technique* detailed by Fontes and Zhang (2007) and Bostock *et al.* (2013) has been used therefore to give more accurate calculations of the excitation cross sections in a fully relativistic treatment and ensure convergence for high partial waves. That is;

$$T_{a\to b}^{RDW} = T_{a\to b}^{born} + \sum_{l=0}^{l\max}(T_{a\to b}^{D} - T_{a\to b}^{D,\mathrm{born}}) \tag{51}$$

For this procedure, first, exchange is neglected beyond a set limit for *l*, say *lmax*, and then it is assumed that beyond this point, it is only plane waves that exist. The plane wave expansion of the relativistic plane wave is similar to that of the distorted waves described with equation (15),

but with the distorted wavefunctions $f_\kappa(r)$ and $g_\kappa(r)$ replaced with radial wavefunctions corresponding to plane waves $\bar{f}_\kappa$ and $\bar{g}_\kappa$ which take the form of Ricatti-Bessel functions. That is;

$$\bar{f}_\kappa = \frac{1}{\kappa} j_l(k_{ch} r) \tag{52}$$

and;

$$\bar{g}_\kappa = \frac{q_\kappa}{E_{ch} + c^2} j_l(k_{ch} r) \tag{53}$$

where $q_k = \kappa / |\kappa|$ and κ represents the relativistic quantum number related to the total quantum number of the orbital by $j = |\kappa| - 1/2$. Therefore, the relativistic plane wave expansion in scattering channel '*ch*' takes the form;

$$\mathrm{F}^{PW\pm}_{\mu_{ch}} = \frac{1}{(2\pi)^{3/2}} \sum_{km} a^{\mu_{ch}}_{km}(\hat{k}_{ch}) \frac{1}{r} \begin{pmatrix} \bar{f}_\kappa(r)\chi_{km} \\ i\bar{g}_\kappa(r)\chi_{-km} \end{pmatrix} \tag{54}$$

As a result, the relativistic Born approximation T-matrix formula is;

$$T^{born}_{b\leftarrow a} = \left\langle \Phi^{rel}_b(N)\, \mathrm{F}^{PW}_{\mathrm{b},\mu_b}(\mathrm{N}+1) \,|\, \mathrm{V} - U \,|\, \Phi^{rel}_a(N)\, \mathrm{F}^{PW}_{\mathrm{a},\mu_a}(\mathrm{N}+1) \right\rangle \tag{55}$$

Therefore, in an exact procedure that was used to obtain the direct ($T^D_{a\to b}$) T-matrix $T^{D,\mathrm{born}}_{a\to b}$ is also obtained but by replacing the relativistic version of the partial wave expansion with a partial wave expansion of the relativistic plane wave (equation (54)). The phase shifts $\eta_{\kappa_{ch}}$ must also be set to zero, since this is the case for plane waves.

3.8 Data analysis

We modified the General Relativistic Atomic Structure Program, GRASP program (Dyall *et al,* 1989) in order to calculate the atomic radial wave-functions *P* and *Q* (see Appendix for details). Furthermore, we have developed a new program RDWBA1 and used it in computing continuum radial wave-functions, transition matrix elements, scattering amplitudes, differential cross-sections and integral cross sections. Atomic radial wavefunctions from the GRASP program (Dyall *et al,* 1989) together with their grid are used as input for the RDWBA1 program. Once the atomic radial wavefunctions are read in, the program RDWBA1 applies the Wentzel-Kramers-Brillouin (WKB) approximation in solving the Dirac equations (16a) and (16b) to obtain continuum wavefunctions. The continuum wavefunctions are then used in calculating the T-matrix elements and cross sections as described by equations (24-40). Further description of the program is given in the Appendix.

CHAPTER 4

RESULTS AND DISCUSSION

4.1 Introduction

Cross section results given using symbols represent experimental data while lines of any format represent theoretical results (calculations). It is also important to state that where experimental data lack error bars, then the uncertainty is smaller than the symbol used for plotting that result. Considering a calculation result (line) and an experiment (symbol): the term ‘very good agreement’ is used to compare two results that have matched both in shape and magnitude with the line passing through the all symbols; ‘good agreement’ for the line within the error bars of the majority symbols and ‘satisfactory’ for matching shapes of the line and symbols though ‘some’ part of the line may fail to fall within the error bars.

4.2 Electron-Argon Inelastic Scattering

4.2.1 Differential cross sections for argon

Present DCS results for electron impact excitation of the lowest J=1 states ($[1/2]_1^o$ for singlet state and $[3/2]_1^o$ for triplet state) of argon are compared with experimental results of Filipovic *et al.* (2000a and 2000b), Chutjian and Cartwright (1981) and Khakoo *et al.* (2004) and DWBA calculations of Bartschat and Madison (1987) and the RM , the UFOMBT, the semi-RDW, and the fully relativistic distorted-wave (RDW) results of Khakoo *et al.* (2004) for impact energies 17.5, 20, 30, 50 and 100 eV.

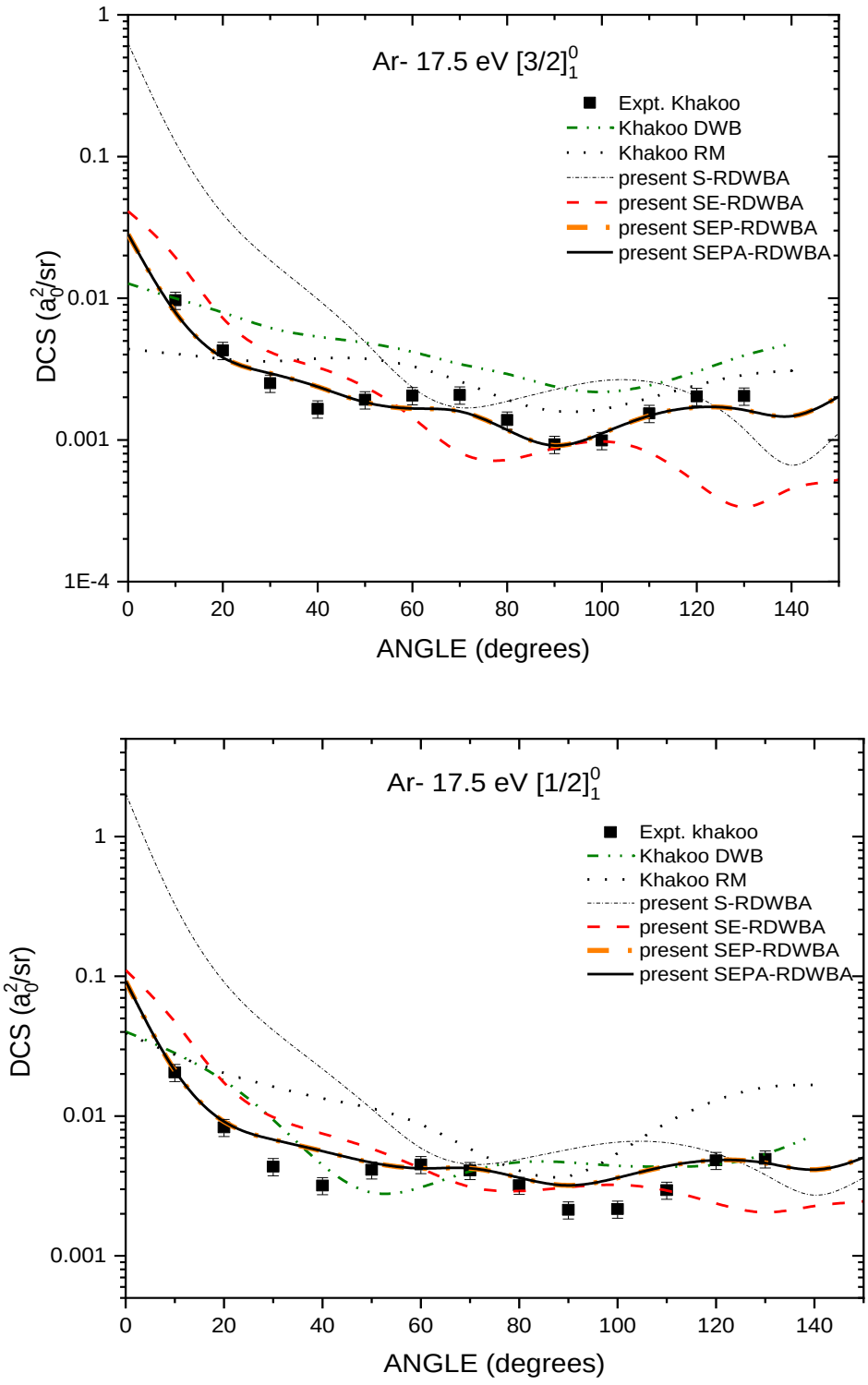

Figure 4.1: DCS results for electron impact excitation of the lowest resonance states $4s[3/2]^o_1$ and $4s[1/2]^o_1$ of argon at 17.5 eV. Experimental results: Expt. Khakoo, Khakoo *et al.* (2004). Calculations by Khakoo *et al.* (2004): Khakoo RM and Khakoo DWB. Present calculations: S-RDWBA, SE-RDWBA, SEP-RDWBA and SEPA-RDWBA.

At 17.5 eV (figure 4.1) electron impact energy, present SEPA (static + exchange + polarization + absorption potentials) -RDWBA and SEP (static + exchange + polarization potentials) -RDWBA results appear overlapped at all scattering angles and both have good agreement in shape and magnitude with the measurements of Khakoo *et al.* (2004) for both singlet and triplet states, although this is more pronounced for the excitation of $4s[3/2]_1^o$ (triplet) state which is the more dominant state of excitation as it takes care of more effects such as electron spin-flip.

On the contrary, present SE (static + exchange potentials) -RDWBA and S (static potential) -RDWBA results don't give satisfactory results when compared with the experimental measurements at all scattering angles. The semi relativistic DWB and RM results of Khakoo *et al.* (2004) differ in shape for the singlet excited state, and in magnitude for the triplet state with their experimental results at this low energy. This may be due to the different type of distortion potential they adopted (static + exchange only) in their distorted-wave, RM and UFOMBT calculations, and relativistic effects not being fully applied with their semi-RDW calculations.

At 20 eV (figure 4.2), experimental results of Chutjian and Cartwright (1981) are generally lower for both excitations compared with the more recent results of Filipovic *et al.* (2000a and 2000b) and Khakoo *et al.* (2004) who used more recent high resolution electron beam spectrometers, though the shapes are similar. Both present SEPA-RDWBA and SEP-RDWBA results again predict good agreement in DCS results as these experimental results. The overlap in present SEP-RDWBA and SEPA-RDWBA results suggests that the effect of the absorption potential is not yet very critical at this low electron impact energy. Absorption dominates due to the large number of other open scattering channels at high energy. Present SE-RDWBA and S-RDWBA results fail to predict satisfactory cross sections at this impact energy.

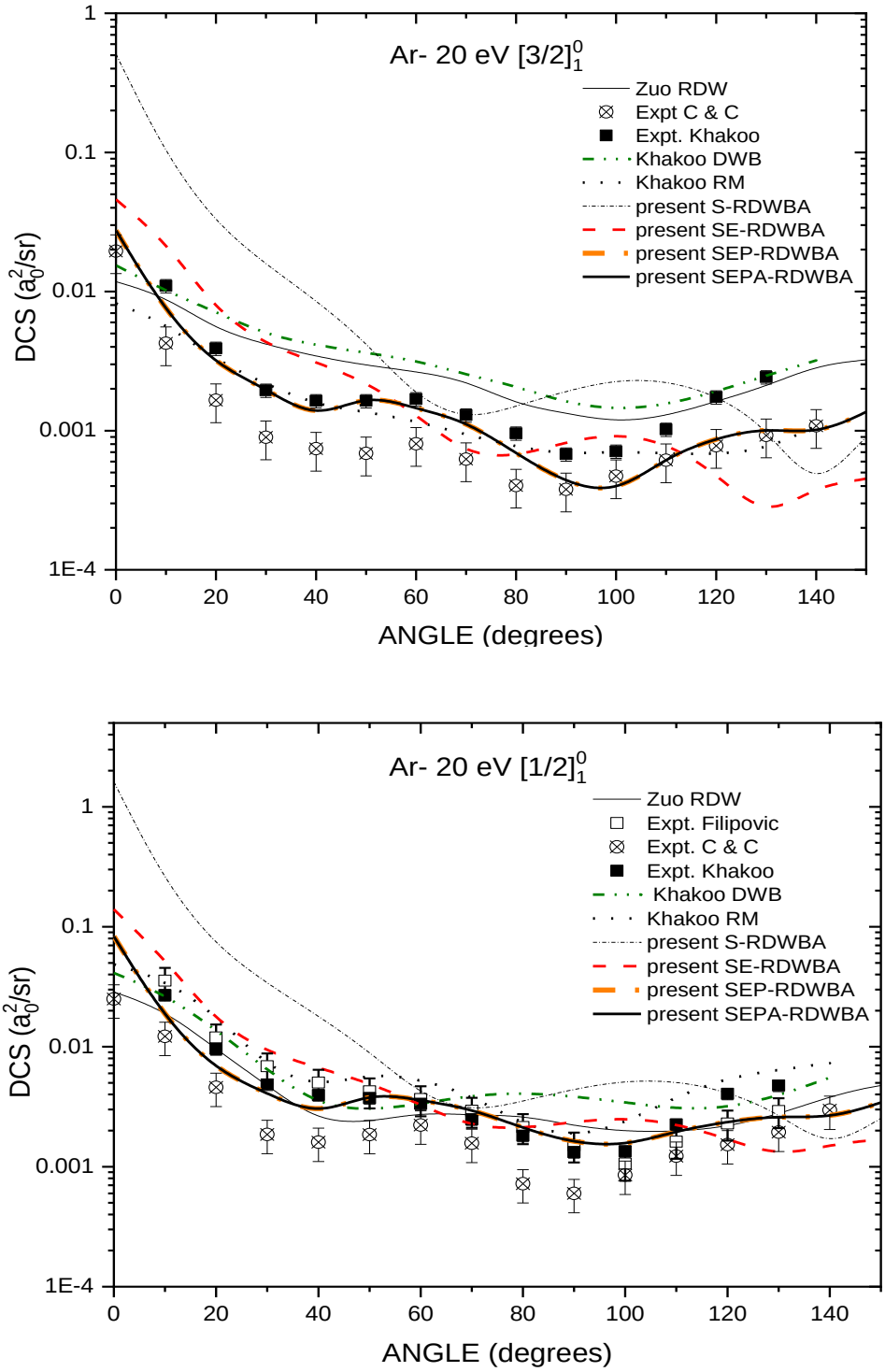

Figure 4.2: DCS results for electron impact excitation of the lowest resonance states $4s[3/2]^o_1$ and $4s[1/2]^o_1$ of argon at 20 eV. Experimental results: Expt. Khakoo, Khakoo *et al.* (2004); Expt. C & C, Chutjian and Cartwright (1981); Expt. Filipovic, Filipovic *et al.* (2000a and 2000b). Calculations: Khakoo RM, Khakoo *et al.* (2004); Khakoo DWB, Khakoo *et al.* (2004); Zuo RDW, Zuo *et al*,. (1992). Present calculations: S-RDWBA, SE-RDWBA, SEP-RDWBA and SEPA-RDWBA.

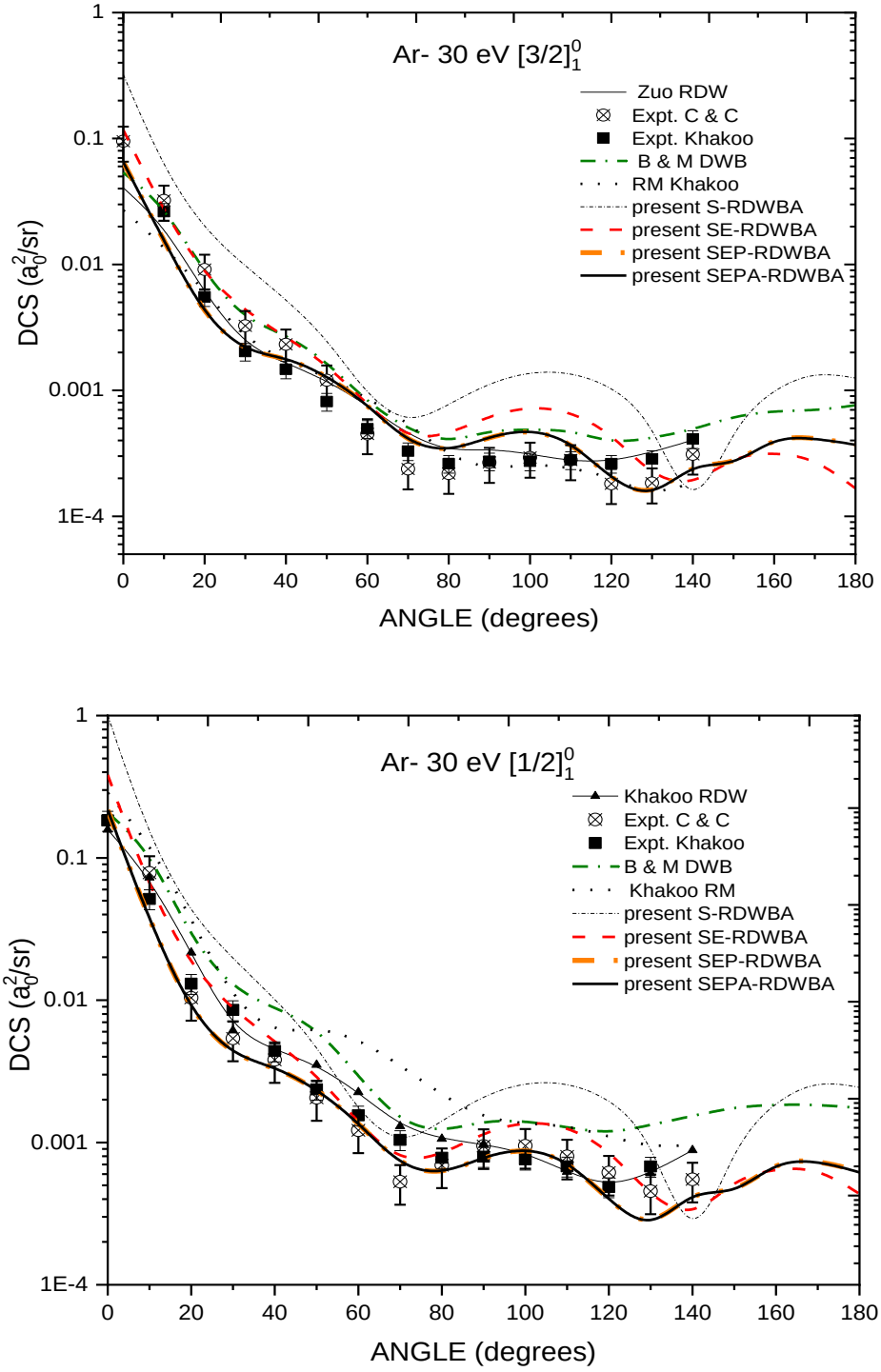

Figure 4.3: DCS results for electron impact excitation of the lowest resonance states $4s[3/2]^o_1$ and $4s[1/2]^o_1$ of argon at 30 eV. Experimental results: Expt. Khakoo, Khakoo *et al.* (2004); Expt. C & C, Chutjian and Cartwright (1981). Calculations: Khakoo RM, Khakoo RDW and Khakoo DWB by Khakoo *et al.* (2004); Zuo RDW, Zuo *et al.* (1992); B & M DWB, Bartschat and Madison (1987). Present calculations: S-RDWBA, SE-RDWBA, SEP-RDWBA and SEPA-RDWBA.

At 30 eV (figure 4.3), all present results start taking a similar shape of cross sections. The present SEP-RDWBA and SEPA-RDWBA results predict good DCSs results when compared both the experimental results of Chutjian and Cartwright (1981) and those of Khakoo *et al.* (2004). The R-matrix method of Khakoo *et al.* (2004) and the DWBA method of Bartschat and Madison (1987) present larger cross sections than the experimental values for the $4s[1/2]_1^o$ excited state. Present SE-RDWBA and S-RDWBA results predict larger cross sections for both $4s[1/2]_1^o$ and $4s[3/2]_1^o$ excitations probably because polarization of the target-atom electrons and absorption of the incident electrons to other open channels is not accounted for by the static and exchange potentials. For $4s[3/2]_1^o$ excitations, while the RDW method of Zuo *et al.* (1992) has better agreement with the experimental results of Khakoo *et al.* (2004), our SEP-RDWBA and SEPA-RDWBA results tend to match in shape with the experimental results of Chutjian and Cartwright (1981) and of Khakoo *et al.* (2004) at larger scattering angles and lower scattering angles respectively. Present SE-RDWBA and S-RDWBA results which predict cross sections that lack agreement in both shape and magnitude also verify the importance of including the polarization potential at low impact energies in order to achieve improved results.

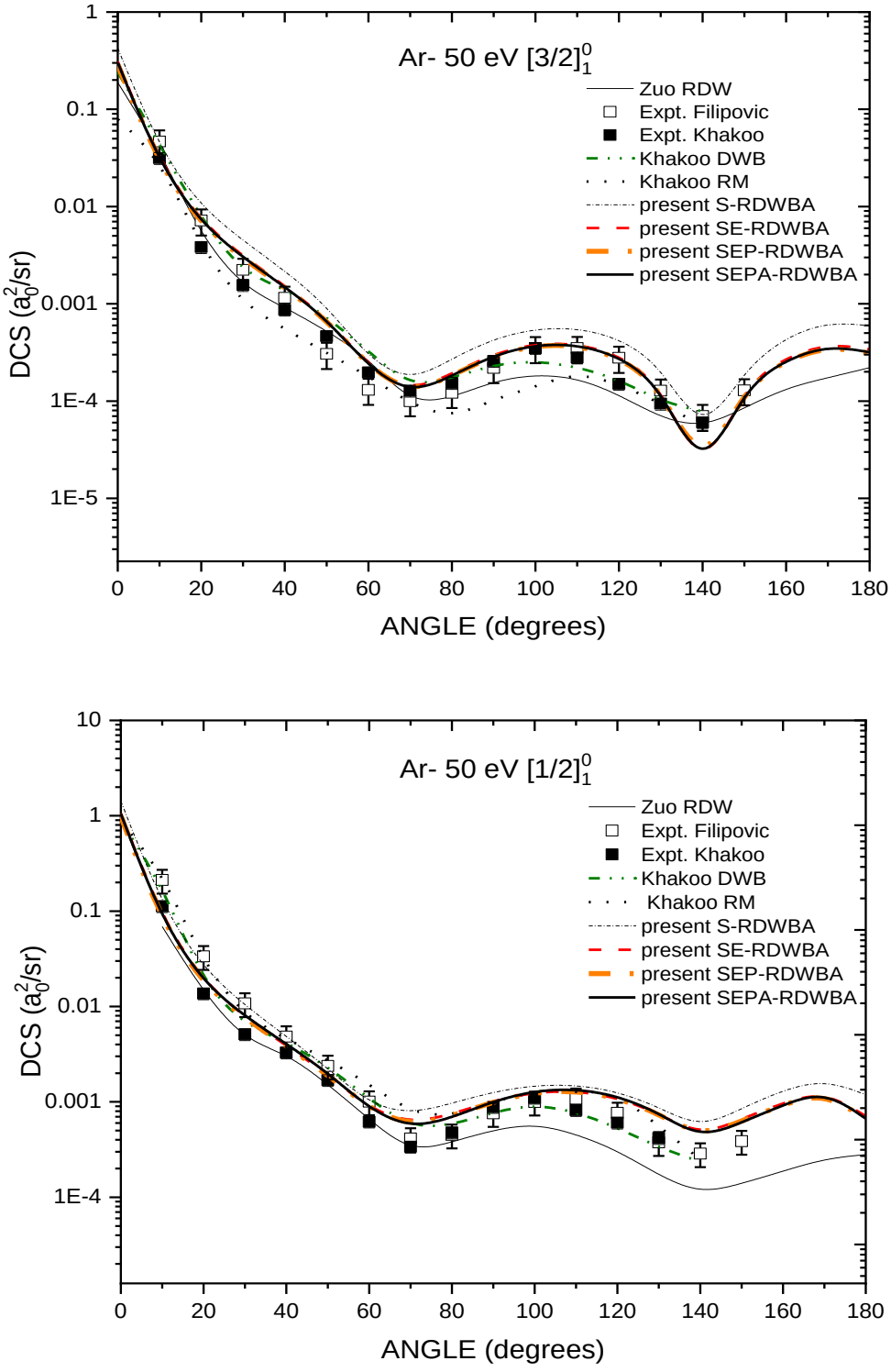

Figure 4.4: DCS results for electron impact excitation of the lowest resonance states $4s[3/2]_1^o$ and $4s[1/2]_1^o$ of argon at 50 eV. Experimental results: Expt. Khakoo, Khakoo *et al.* (2004); Expt. Filipovic, Filipovic *et al.* (2000a and 2000b). Calculations: Khakoo RM, Khakoo *et al.* (2004); Khakoo DWB, Khakoo *et al.* (2004); Zuo RDW, Zuo *et al*. (1992). Present calculations: S-RDWBA, SE-RDWBA, SEP-RDWBA and SEPA-RDWBA.

For impact energies of 50 eV and above (figures 4.4-4.5), all present results have similar shape and magnitude, an indication that the polarization potential takes less effect as impact energy increases. The trend of DCSs across the calculations and experimental measurements remains similar in shape, both for excitation of $4s[3/2]_1^o$ and $4s[1/2]_1^o$ levels, although the present SEPA and SEP results (figure 4.4) are still in good agreement with the experimental results compared to SE-RDWBA and S-RDWBA. At 50 eV, the RDW result of Zuo *et al*, (1992) (which adopted static, exchange and polarization potentials) differ with present SEP-RDWBA result mainly due to the difference in the type of exchange and polarization potentials used and lack of absorption potential in their calculations. Present SEPA-RDWBA calculations are done using an energy dependent polarization and a local exchange potential compared to the energy independent polarization and non-local exchange potential adopted by Zuo *et al.* (1992).

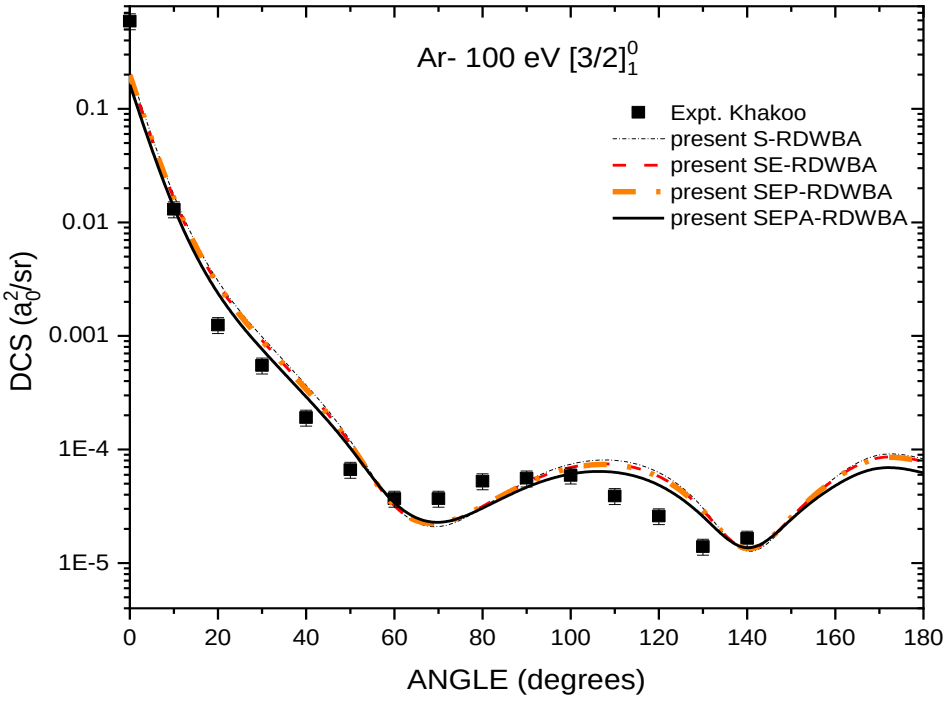

Figure 4.5: DCS results for electron impact excitation of the lowest resonance state $4s[3/2]_1^o$ of argon at 100 eV. Experimental results: Expt. Khakoo, Khakoo *et al.* (2004). Present calculations: S-RDWBA, SE-RDWBA, SEP-RDWBA and SEPA-RDWBA.

Generally, at low impact energies, there is more interaction between the projectile electron and the target electrons as the projectile tend to stay longer in the vicinity of the target-atom than for to larger impact energies where it exits faster. This means that the effect of the distortion potential is usually very high at low energies near excitation threshold. As a result, the electrons are scattered evenly in different directions. At high impact energies, the projectile electron tends to move in a near straight line inside the target atom electron cloud, and encounters less interaction with the target atom electrons, hence it is scattered at small angles as the effect of distortion potential fades.

4.2.2 Integral cross sections for argon

Integral cross sections (ICSs) for electron impact excitation of the lowest resonance states of Ar have been obtained by integrating the DCSs over all scattering angles. Present ICSs are compared with the experimental results of Filipovic *et al.* (2000b), Chutjian and Cartwright (1981), Khakoo *et al.* (2004) and Hoshino *et al.* (2013) and calculations of Bartschat and Madison (1987) done using DWBA, semi-RDW result of Madison *et al.* (1998), RM result of Zatsarinny *et al.* (2014), and UFOMBT and DWBA results of Khakoo *et al.* (2004) for impact energies from threshold up to 100 eV.

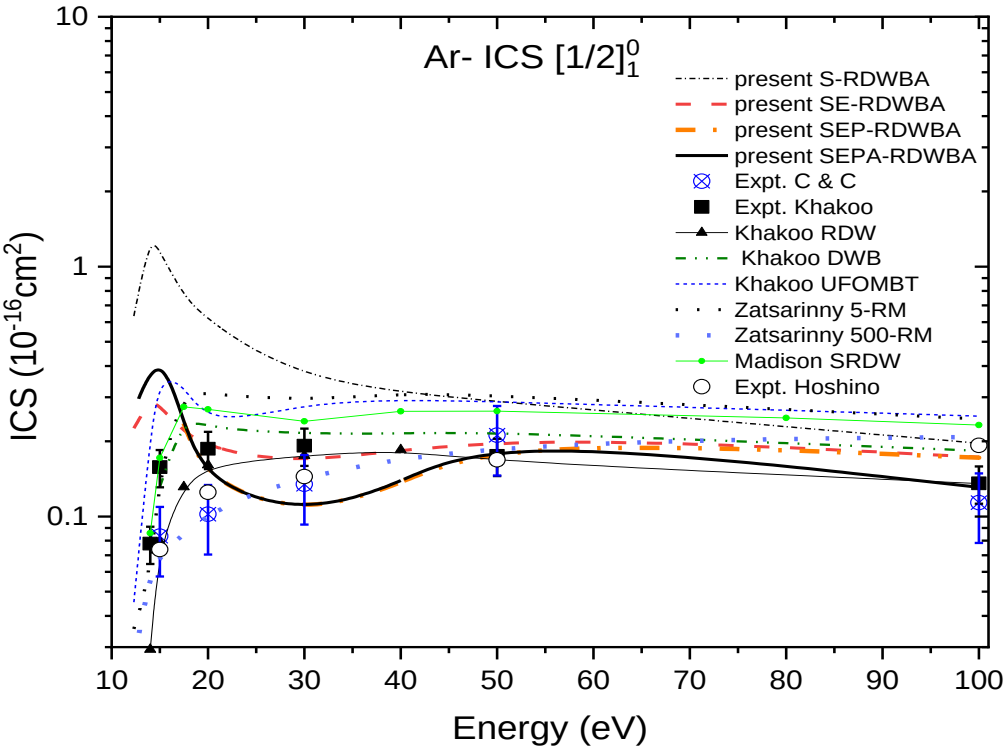

Figure 4.6: ICS results for electron impact excitation of the $4s[1/2]_1^o$ state of argon. Experimental results: Expt. Hoshino, Hoshino *et al.* (2013); Expt. Khakoo, Khakoo *et al.* (2004); Expt. C & C, Chutjian and Cartwright (1981). Calculations: Khakoo RDW, Khakoo *et al.* (2004); Khakoo DWB, Khakoo *et al.* (2004); Khakoo UFOMBT, Khakoo *et al.* (2004); Zatsarinny 5-RM, Zatsarinny *et al.* (2014): Zatsarinny 500-RM, Zatsarinny *et al.* (2014): Madison SRDW, Madison *et al.* (1998). Present calculations: S-RDWBA, SE-RDWBA, SEP-RDWBA and SEPA-RDWBA.

In figure 4.7, the present SEPA-RDWBA results predict ICS that are in a satisfactory agreement with the measurements for excitation of the $4s[3/2]_1^o$ level, while for $4s[1/2]_1^o$ level (figure 4.6), measurements of Khakoo *et al.* (2004) are in close agreement with our present SEPA-RDWBA results at impact energies of 50 and 100 eV, and those of Chutjian and Cartwright (1981) at lower energies up to 20 eV. For both excitations (figures 4.6-4.7), present results are close to the experimental results of Hoshino *et al.* (2013) in the range from 20 to 50 eV electron impact energy but they disagree at lower and higher energies. The sharp rise in cross sections near the threshold excitation energy is due to the large interaction between target electrons and projectile electrons which leads to an increase in the number of particles scattered.

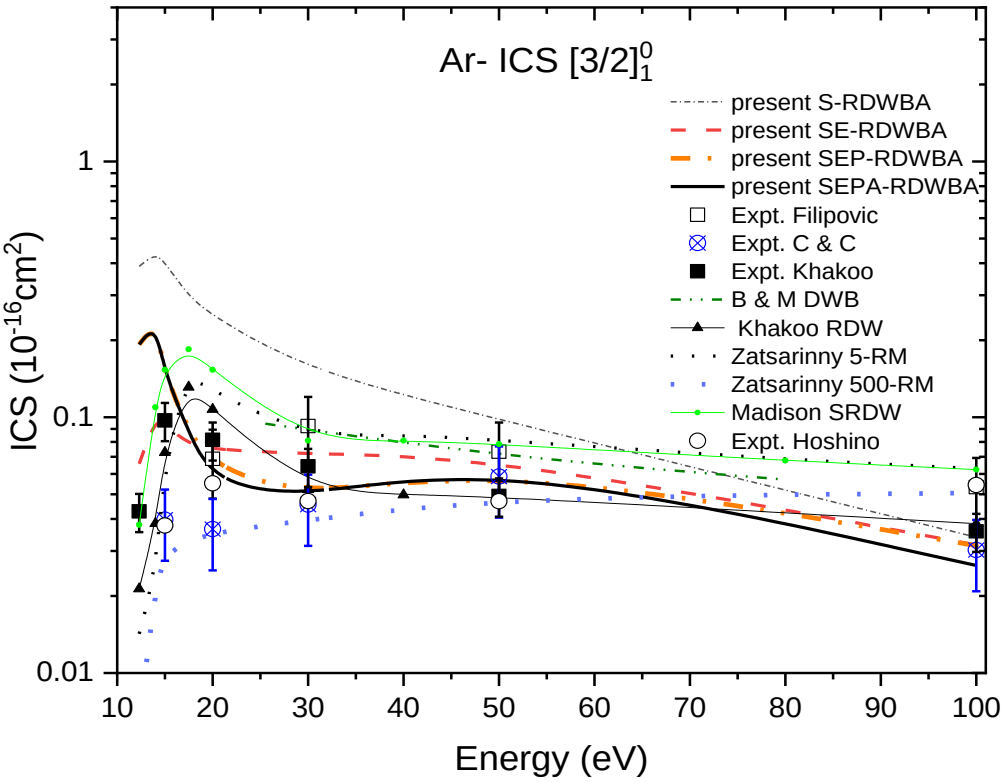

Figure 4.7: ICS results for electron impact excitation of the $4s[3/2]^o_1$ state of argon. Experimental results: Expt. Hoshino, Hoshino *et al.* (2013); Expt. Khakoo, Khakoo *et al.* (2004); Expt. Filipovic, Filipovic *et al.* (2000a and 2000b); Expt. C & C, Chutjian and Cartwright (1981). Calculations: Khakoo RDW, Khakoo *et al.* (2004); B & M DWB, Bartschat and Madison (1987)); Zatsarinny 5-RM, Zatsarinny *et al.* (2014): Zatsarinny 500-RM, Zatsarinny *et al.* (2014): Madison SRDW, Madison *et al.* (1998). Present calculations: S-RDWBA, SE-RDWBA, SEP-RDWBA and SEPA-RDWBA.

It can also be attributed to large interaction of the free and bound electrons due to a combination of exchange effects between electrons colliding at low energy, attraction of the incident electron by the positive nucleus as it enters the electron cloud and the polarization effect of the incident electron on the target atom electrons. The polarization potential is most dominant at low energy and hence plays a major role in improvement of cross sections near excitation threshold.

Table 4.1: Present integral cross section results for relativistic electron impact excitation of $4s[1/2]_1^o$ state of argon.

ENERGY (eV)	S-RDWBA ($10^{-16}cm^2$)	SE-RDWBA ($10^{-16}cm^2$)	SEP-RDWBA ($10^{-16}cm^2$)	SEPA-RDWBA ($10^{-16}cm^2$)
12.3	0.63398	0.22541	0.26538	0.26538
14	1.33600	0.29260	0.45174	0.45174
15	1.14950	0.27600	0.47979	0.47979
17.5	0.75978	0.21876	0.23602	0.23408
20	0.60514	0.18857	0.13504	0.13504
30	0.34083	0.15784	0.10152	0.10166
50	0.28763	0.21670	0.20519	0.21439
100	0.19649	0.17262	0.17184	0.13083

Table 4.2: Present integral cross section results for relativistic electron impact excitation of $4s[3/2]_1^o$ state of argon.

ENERGY (eV)	S-RDWBA ($10^{-16}cm^2$)	SE-RDWBA ($10^{-16}cm^2$)	SEP-RDWBA ($10^{-16}cm^2$)	SEPA-RDWBA ($10^{-16}cm^2$)
11.7	0.38900	0.06578	0.19220	0.19220
14	0.43790	0.09906	0.23259	0.23259
15	0.40310	0.09320	0.14715	0.14715
17.5	0.29659	0.07841	0.08781	0.08781
20	0.24865	0.07488	0.06415	0.05523
30	0.15105	0.07172	0.04774	0.04780
50	0.09796	0.06991	0.06576	0.06811
100	0.03396	0.03165	0.03147	0.02632

As impact energy increases, say beyond 50 eV, the effect of absorption becomes important in obtaining cross sections. This can be seen from the ICS graphs (figures 4.6 and 4.7) and tables (4.1 and 4.2). The choice of energy points below 20 eV are those presented in the experimental results in figures 4.6 and 4.7. Apart from the RDW calculations of Khakoo *et al.* (2004), other non-relativistic (DWB) and semi-RDW calculations for both excited states give slightly larger cross sections than the experimental measurements. Apart from the effect of the absorption of incident electrons to other open scattering channels, which leads to lower DCSs, relativistic effects may also be attributed to better cross sections unlike non-relativistic calculations. Furthermore, the absorption potential becomes dominant at higher impact energies, say for

example above 50 eV, since there are more available open scattering channels apart from the inelastic channel under consideration.

4.2.3 Lambda parameter for argon

For an electron that transits from a ‘p’ to an ‘s’ orbital, the lambda parameter is useful in predicting the population of the three magnetic sub-states $M_b = 0, \mp 1$ during the excitation process. As λ approaches zero, it shows that more electrons get excited from the magnetic sublevel $M_b = 1$ and vice versa. This can be explained from the formula (equation (43)) as stated in chapter 3.

There being no other data available for this specific excitation problem, present data is compared within the framework of results obtained using the four choices of distortion potential, that is ; S-RDWBA, SE-RDWBA, SEP-RDWBA and SEPA-RDWBA. Results presented here are useful to other theoretical and experimental researchers aiming to study this similar excitation problem for making reference with their findings. In figures 4.8 and 4.9, present results for lambda parameter are shown for electron impact excitation energies of 20, 30, 50 and 100 eV. At low impact energy of 20 eV, peaks are seen at scattering angles of near 40^o, 80^o and 140^o, but as energy increases, the highest peak is seen at around 80^o and 140^o, and then for energies above 30 eV the peak is mainly around 80^o. From the explanation of the lambda parameter, the peaks predict that most electrons get excited from the magnetic sub level $M_b = 0$.

From the findings shown in figures 4.8 and 4.9, it is also evident that the electron impact energy and hence the effect of the distortion potential affects the relative number of excitations from different magnetic sub-states because for energies above 30 eV, all the present results give results almost similar in shapes and magnitude whereas at 20 and 30 eV they are much different.

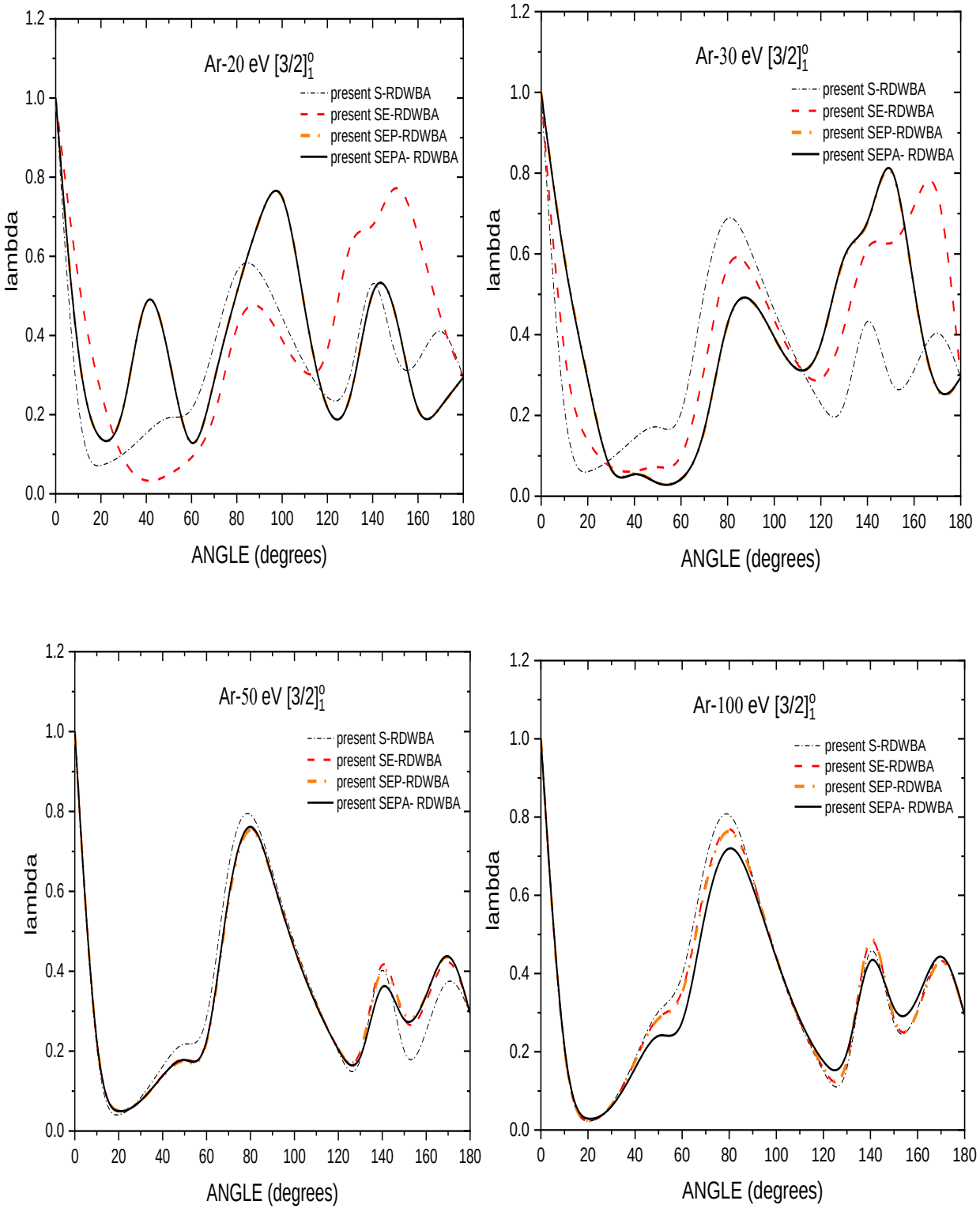

Figure 4.8: Present lambda parameters for excitation of the $4s[3/2]^o_1$ state of argon: S-RDWBA, SE-RDWBA, SEP-RDWBA and SEPA-RDWBA.

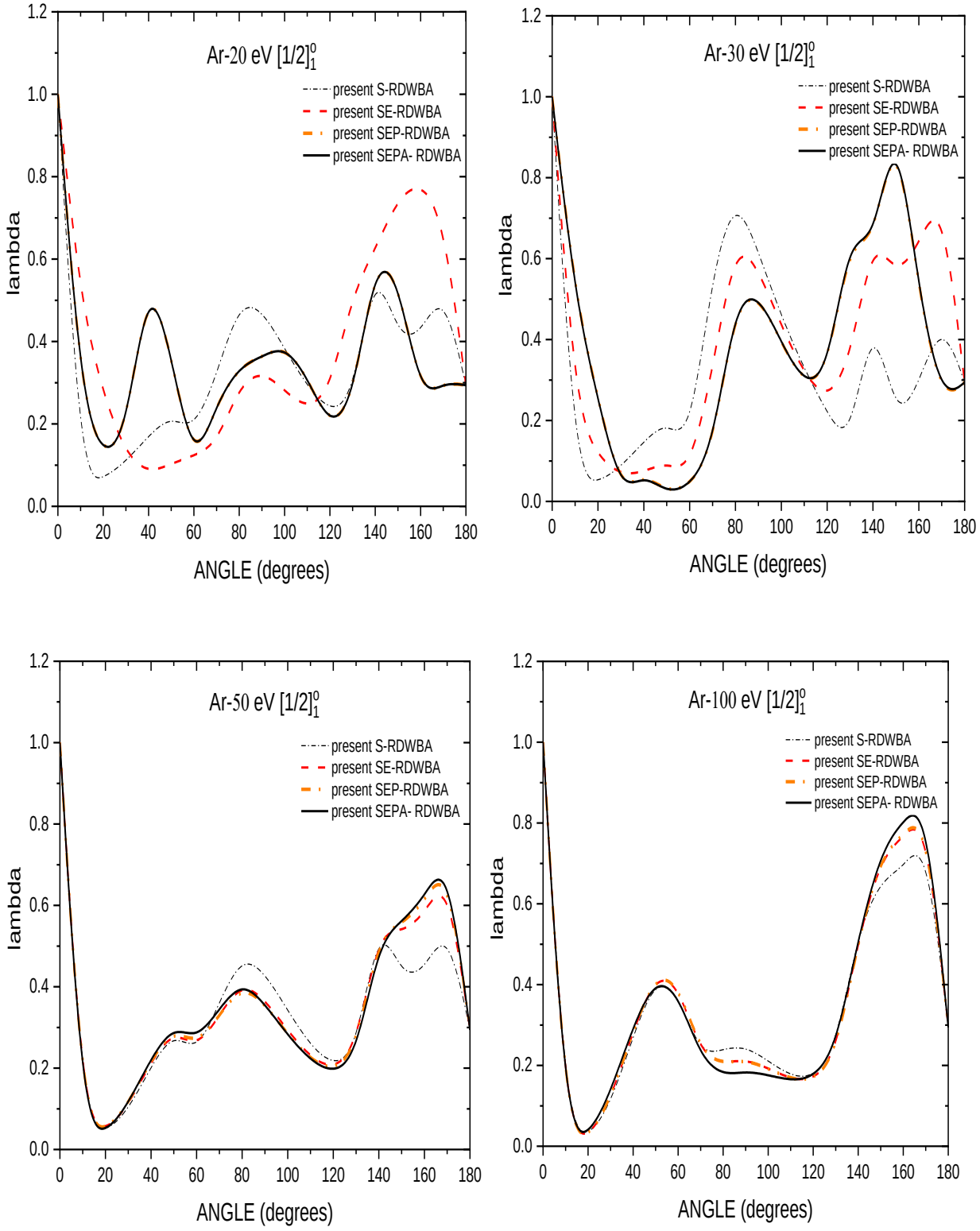

Figure 4.9: Present lambda parameters for excitation of the $4s[1/2]^o_1$ state of argon: S-RDWBA, SE-RDWBA, SEP-RDWBA and SEPA-RDWBA.

4.2.4 Stokes parameters for argon

Because of the limited or lack of other results for Stokes parameters for excitation of argon, we only compare present linear polarization Stokes parameter results P_1 at 20 and 30 eV impact energy with the available experimental results of Corr *et al.* (1992) and calculations of Zuo *et al.* (1992) done using RDW. At 20 eV present result compares well in shape (but not in magnitude) with the experimental results of Corr *et al*. (1992), though with a shift horizontally between 40^o and 70^o scattering angle. For circular polarization, Bartschat and Madison (1987) presented only the P_3 parameter for 20 eV. Comparing this with our present SEPA-RDWBA result at scattering angles less than 50º, their result differ significantly in shape with ours probably due to the choice of distortion potential and relativistic effects in the calculation scattering electron wavefunctions.

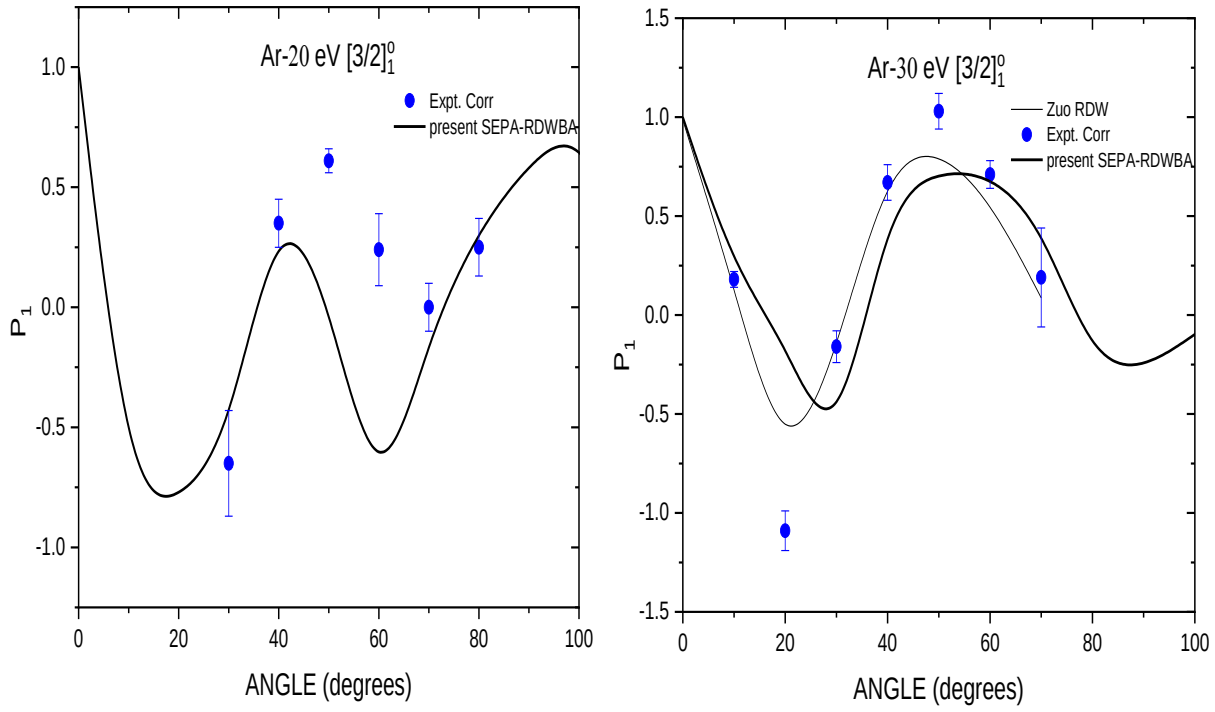

Figure 4.10: P_1 parameter for electron impact excitation of the $[3/2]^o_1$ state of argon at 20 eV and 30 eV. Experimental results: Expt. Corr, Corr *et al.* (1992). Calculations: Zuo RDW, Zuo *et al.* (1992); Present SEPA-RDWBA.

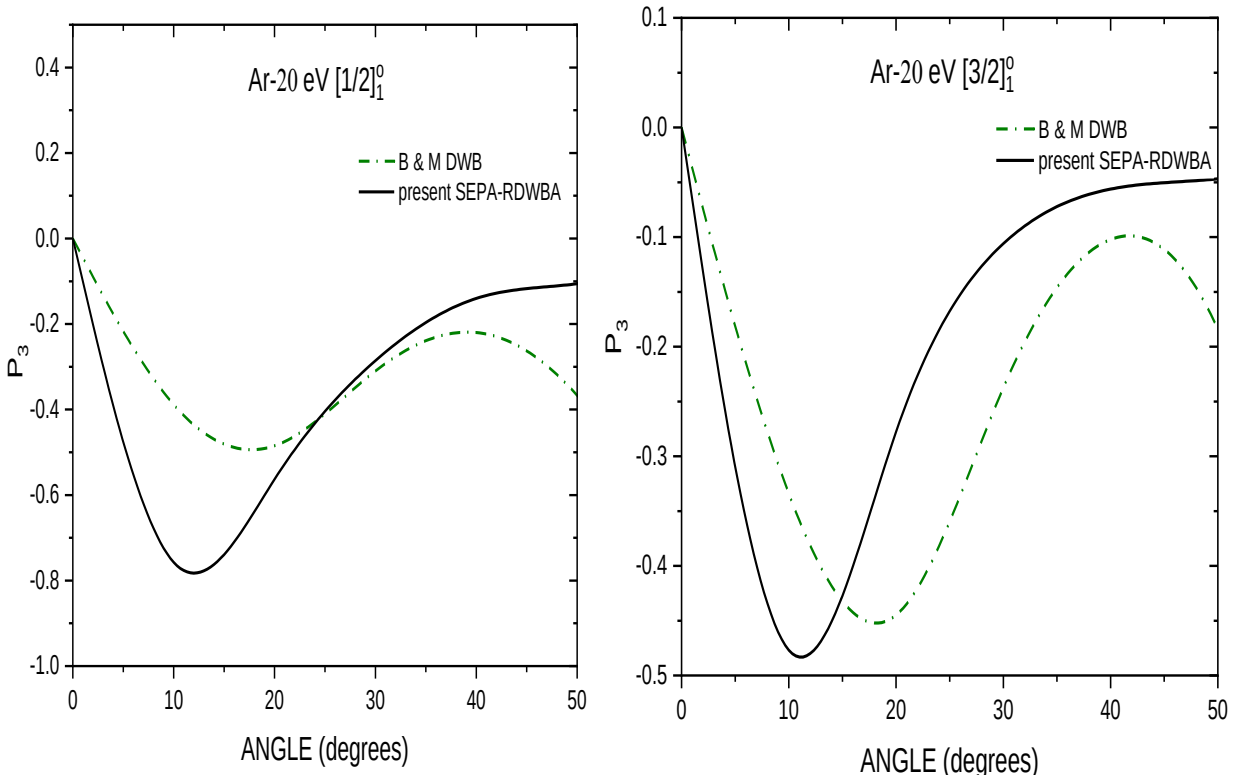

Figure 4.11: P_3 parameter for electron impact excitation of argon at 20 eV. Calculations: B & M DWB, Bartschat and Madison (1987); Present SEPA-RDWBA.

At 30 eV (figure 4.10), the present results of the P_1 parameter predict shape which matches with the experiments (Corr *et al*., 1992) and theoretical (Zuo *et al*., 1992) results, though there is horizontal shift of about10^o of the scattering angle of present results from the experimental results of Corr *et al.* (1992) between 20^o and 40^o. In table 4.3, present Stokes parameters at low energy of 17.5 eV are given, since our interest is mainly on results for scattering at low impact energies. Although there is no other result to compare with, this result is still useful in future as reference for other researchers investigating a similar excitation both experimentally and theoretically.

Table 4.3: Stokes parameters for argon at 17.5 eV

	$4s[3/2]_1^o$ state			$4s[1/2]_1^o$ state		
ANGLE (degrees)	P_1	P_2	P_3	P_1	P_2	P_3
0	1.00000	0.00000	0.00000	1.00000	0.00000	0.00000
10	-0.75728	-5.79E-02	0.11612	-0.77034	-4.31E-02	4.89E-02
20	-0.75605	0.10894	1.80E-02	-0.77103	6.77E-02	6.59E-02
30	-0.56868	-0.20486	-1.76E-02	-0.59287	-0.30337	6.39E-02
40	7.80E-02	-9.65E-02	-4.35E-03	2.77E-02	-0.31976	-1.12E-02
60	-0.67667	-9.51E-03	5.06E-03	-0.55633	-0.19678	-1.40E-02
80	0.44389	-5.14E-03	-3.32E-03	-5.25E-02	-6.54E-02	1.78E-02
100	0.42208	1.55E-02	-3.43E-03	-8.85E-02	9.21E-02	1.41E-02
120	-0.30937	2.94E-02	-4.61E-04	-0.36348	0.202182	-6.68E-04
140	0.35364	9.24E-03	6.18E-03	0.20911	0.20648	-2.84E-02
160	-0.54643	2.27E-03	-6.40E-03	-0.23675	5.90E-02	3.85E-02
180	-7.27E-02	0.00000	0.00000	-7.27E-02	0.00000	0.00000

4.3 Electron- Krypton Inelastic Scattering

4.3.1 Differential cross sections for krypton

Present DCS results for electron impact excitation of the lowest resonance states of krypton are compared with the experimental results of Trajmar *et al.* (1981), Allan *et al.* (2011) and Guo *et al.* (2000), and with calculations of Guo *et al.* (2000) using UFOMBT method, Bartschat and Madison (1987) using semi-relativistic distorted-wave method and Zuo *et al.* (1992) using fully-RDW methods for impact energies of 15 eV, 20 eV, 30 eV and 50 eV.

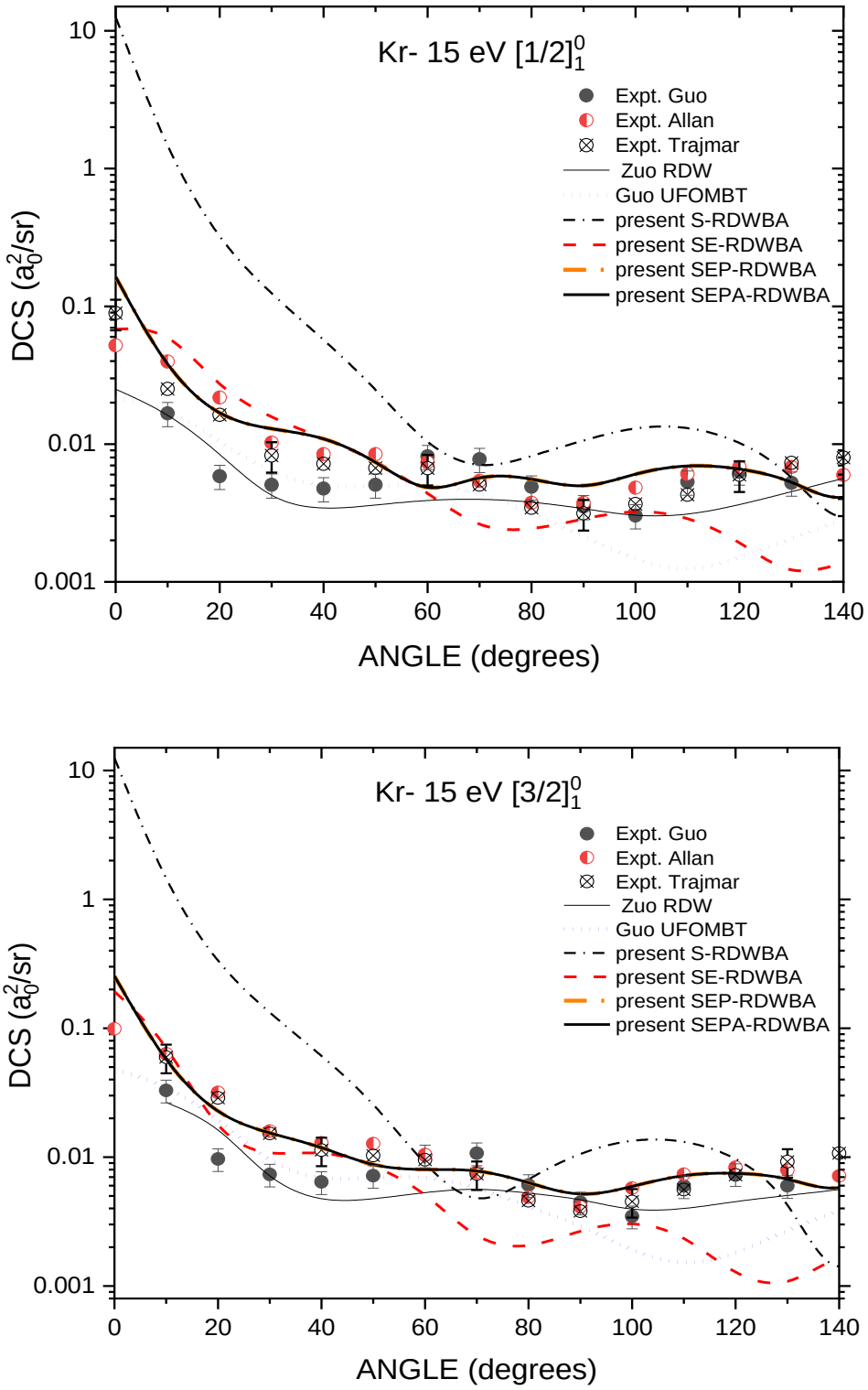

Figure 4.12: DCS results for electron impact excitation of the lowest resonance states ($[1/2]^o_1$ and $[3/2]^o_1$) of krypton at 15 eV. Experimental results: Expt. Trajmar, Trajmar *et al.* (1981); Expt. Allan , Allan *et al.* (2011); Expt. Guo, Guo et al. (2000). Calculations: Guo UFOMBT, Guo et al. (2000); Zuo RDW, Zuo et al. (1992); Present S-RDWBA, SE-RDWBA, SEP-RDWBA and SEPA-RDWBA.

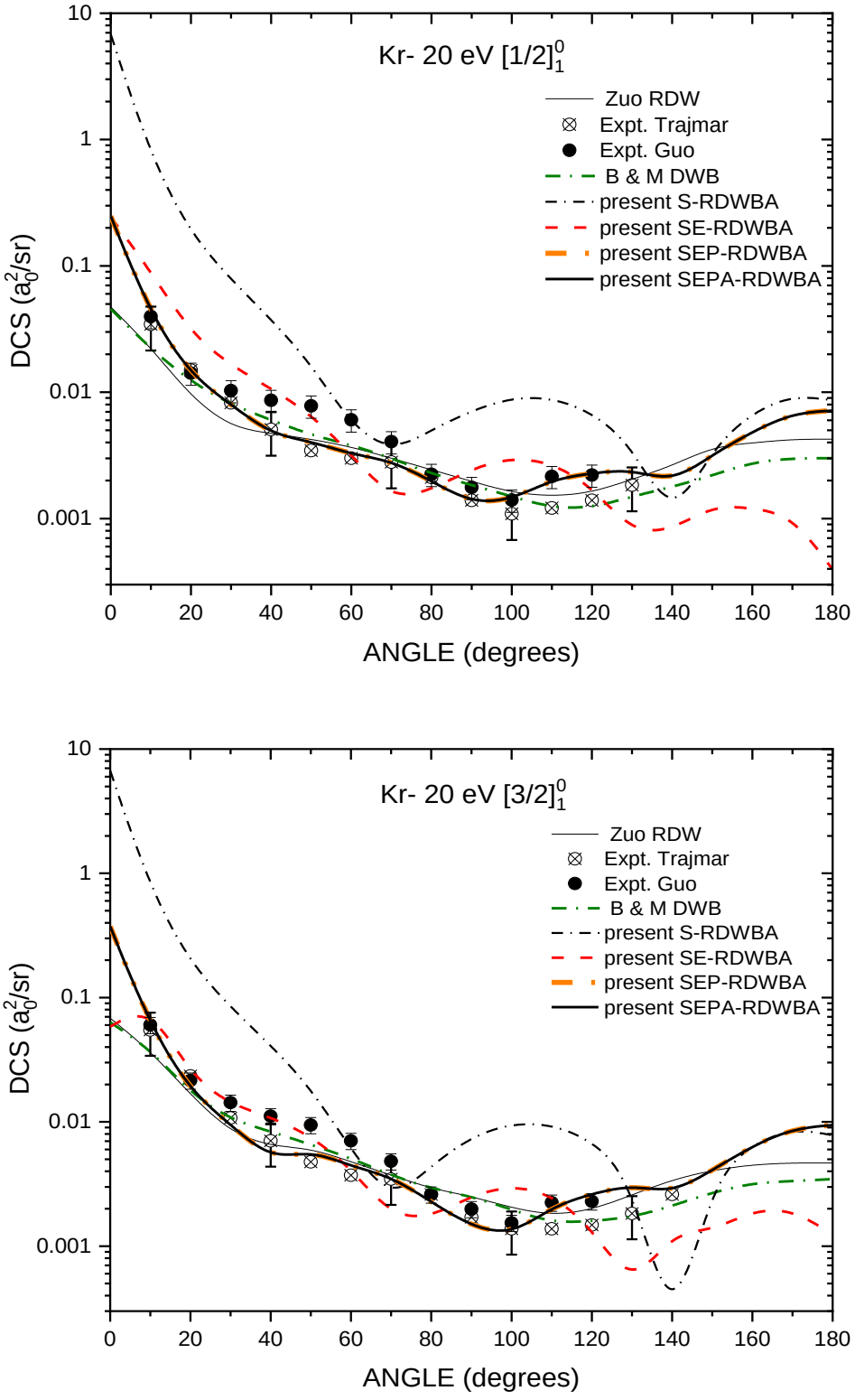

Figure 4.13: DCS results for electron impact excitation of the lowest resonance states ($[1/2]^o_1$ and $[3/2]^o_1$) of krypton at 20 eV. Experimental results: Expt. Trajmar, Trajmar et al. (1981); Expt. Guo, Guo et al. (2000). Calculations: B & M DWB, Bartschat and Madison (1987); Zuo RDW, Zuo et al. (1992); Present S-RDWBA, SE-RDWBA, SEP-RDWBA and SEPA-RDWBA.

DCS results at 15 eV (figure 4.12), show that both the present SEPA-RDWBA and SEP-RDWBA results are in good agreement with experimental results of both Trajmar *et al.* (1981) and Allan *et al.* (2011) at all scattering angles in shape and magnitude, unlike the RDW results of Zuo *et al.* (1992) which is not in good agreement with the above experimental results. This may be because the type of polarization potential they adopted in their calculations is not energy dependent and their distortion potential lacks the complex part. The measurements of Guo *et al.* (2000) also have similar trend in shape of DCS with our present SEPA-RDWBA and SEP-RDWBA results though slightly lower at scattering angles below 50^{o}. Present S-RDWBA results disagree with the experimental results throughout while the present SE-RDWBA results disagree for a wide range of scattering angles.

Present DCS results at 20 eV (figure 4.13), that is SEPA-RDWBA and SEP-RDWBA are in good agreement with experimental results of Guo *et al.* (2000) and Trajmar *et al.* (1981) for all the scattering angles. This is also the case for the fully relativistic results of Zuo *et al.* (1992) and the semi relativistic results of Bartschat and Madison (1987). Present SE-RDWBA and S-RDWBA results fail to give satisfactory results at this impact energy, with the latter giving very large DCS results at low scattering angles. This is an indication that the polarization potential plays a crucial role in improving cross sections at low electron impact energies.

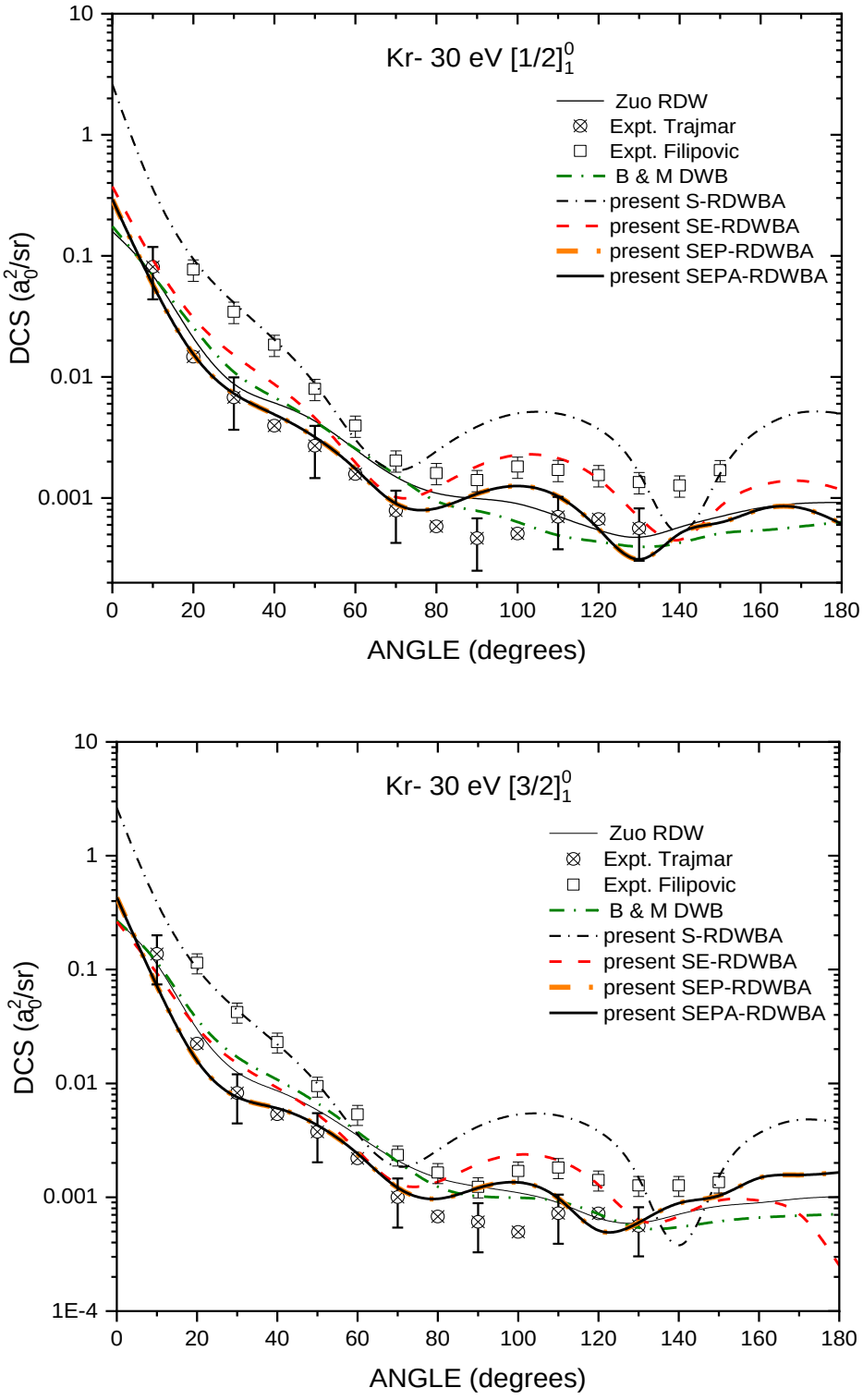

Figure 4.14: DCS results for electron impact excitation of the lowest resonance states ($[1/2]^o_1$ and $[3/2]^o_1$) of krypton at 30 eV. Experimental results: Expt. Trajmar, Trajmar *et al.* (1981); Expt. Filipovic, Filipovic (1988). Calculations: B & M DWB, Bartschat and Madison (1987); Zuo RDW, Zuo *et al.* (1992); Present S-RDWBA, SE-RDWBA, SEP-RDWBA and SEPA-RDWBA.

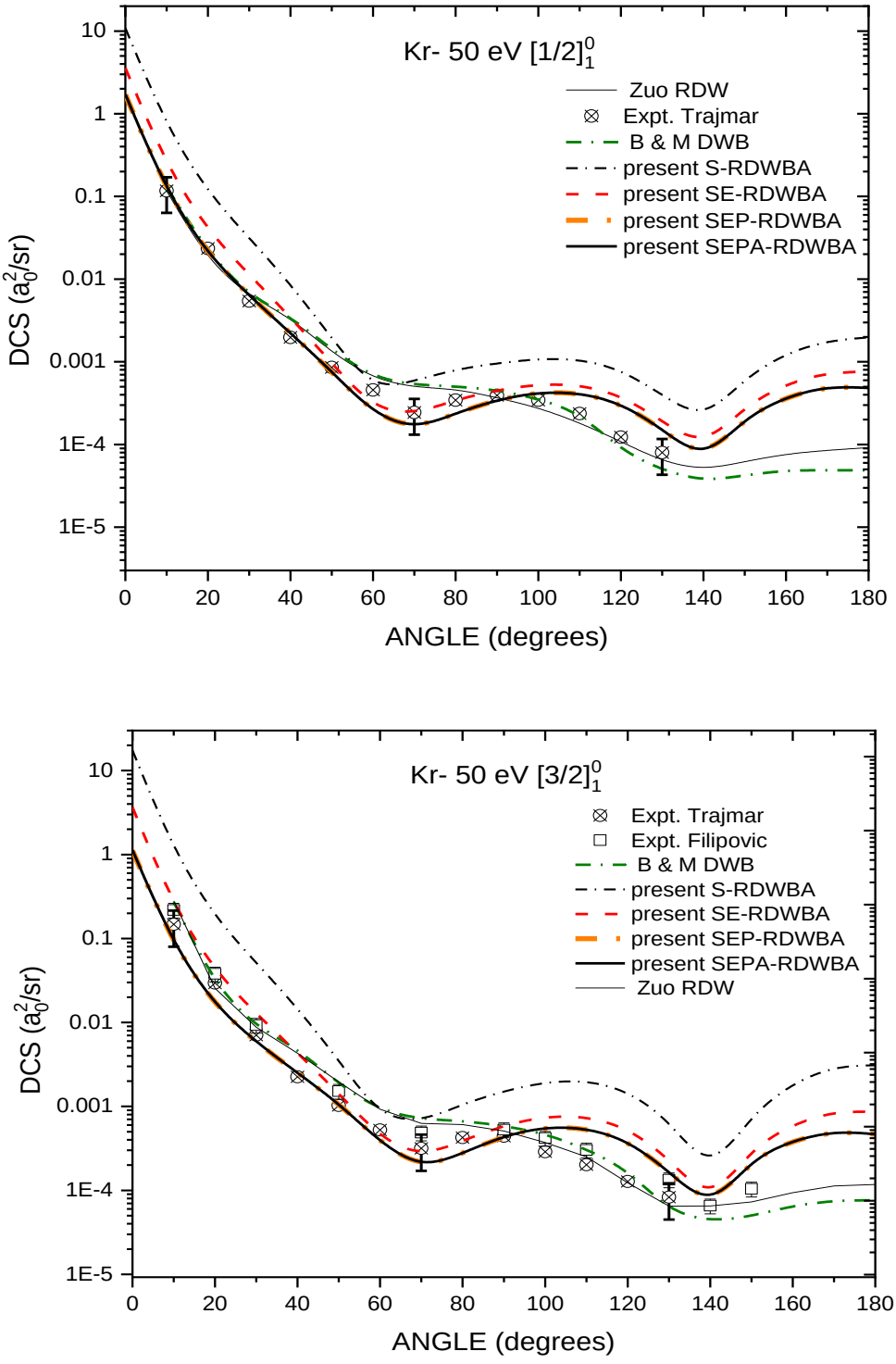

Figure 4.15: DCS results for electron impact excitation of the lowest resonance states ($[1/2]^o_1$ and $[3/2]^o_1$) of krypton at 50 eV. Experimental results: Expt. Trajmar, Trajmar *et al.* (1981); Expt. Filipovic, Filipovic (1988). Calculations: B & M DWB, Bartschat and Madison (1987); Zuo RDW, Zuo *et al.* (1992); Present S-RDWBA, SE-RDWBA, SEP-RDWBA and SEPA-RDWBA.

At 50 eV (figure 4.15), all DCS results begin taking similar shapes and magnitude. The reason behind this is that the interaction between the incident electron and the target atom electrons becomes lesser due to increase in projectile energy so that the effect of the active polarization, exchange and static potentials begin having less effect on the fast moving incident electron.

4.3.2 Integral cross sections for krypton

In figures 4.16 and 4.17, present integral cross sections results (ICS) for electron impact excitation of the lowest resonance states (those with J=1) of krypton are compared with calculations of Dasgupta *et al.* (2001) using DWB, semi-RDW and R-matrix (RM) methods, and with the experimental results of Trajmar *et al.* (1981) and Guo *et al.* (2000) for electron impact energies up to 200 eV.

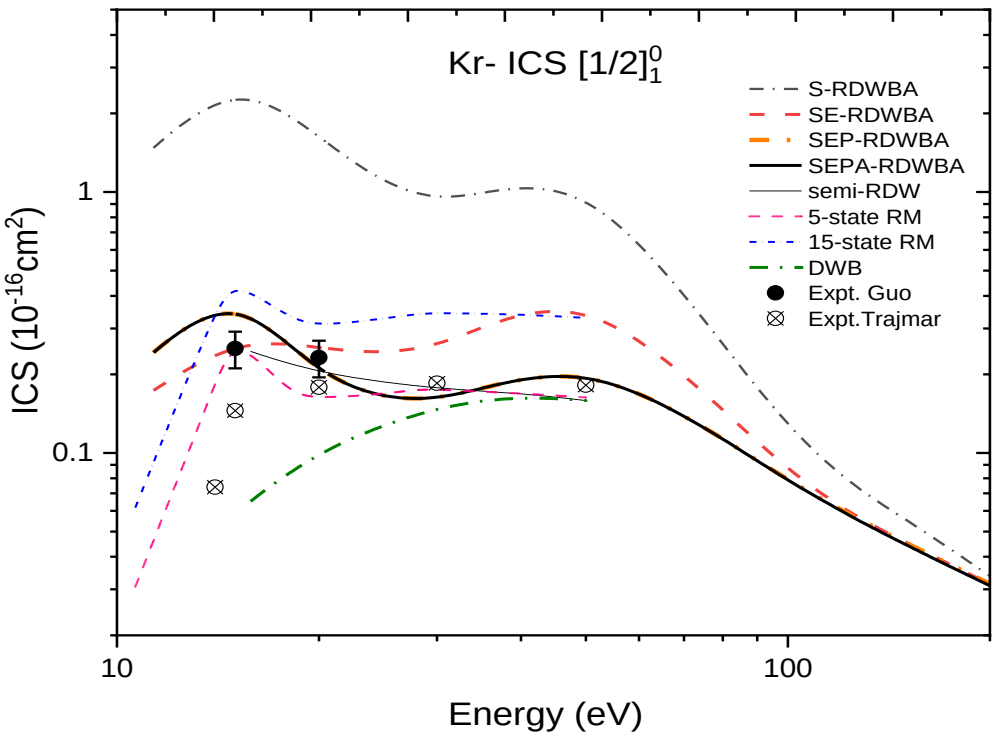

Figure 4.16: ICS results for electron impact excitation of the lowest singlet resonance state ($[1/2]^o_1$) of krypton. Experimental results: Expt. Trajmar, Trajmar *et al.* (1981); Expt. Guo, Guo *et al.* (2000). Dasgupta *et al.* (2001) calculations: DWB, semi RDW, 15-state RM and 5-state RM. Present calculations: S-RDWBA, SE-RDWBA, SEP-RDWBA and SEPA-RDWBA.

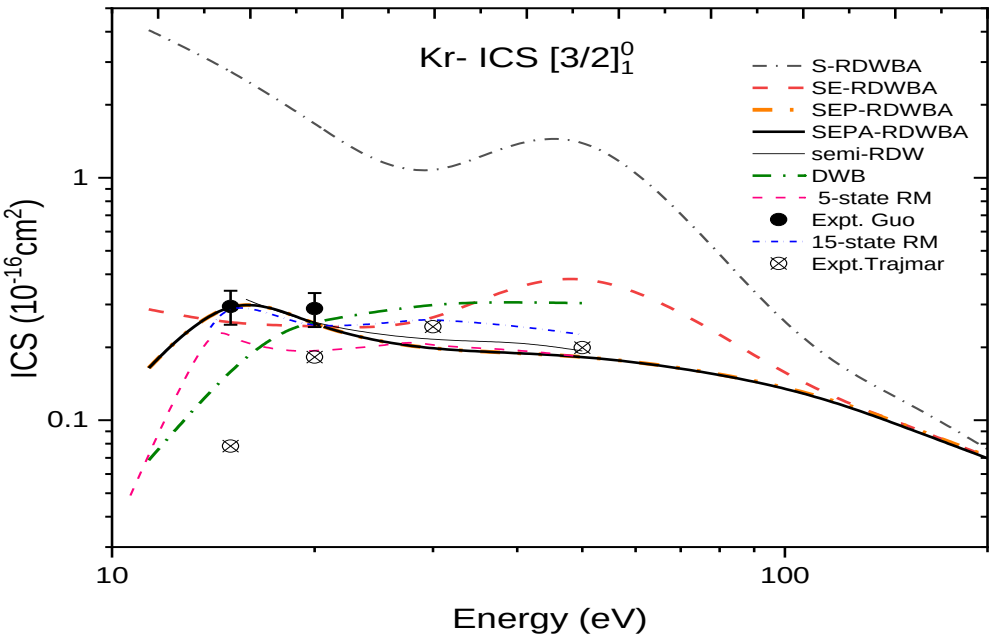

Figure 4.17: ICS results for electron impact excitation of the lowest triplet resonance state ($[3/2]_1^o$) of krypton. Experimental results: Expt. Trajmar, Trajmar *et al.* (1981); Expt. Guo, Guo *et al.* (2000). Dasgupta *et al.* (2001) calculations: DWB, semi RDW, 15-state RM and 5-state RM. Present calculations: S-RDWBA, SE-RDWBA, SEP-RDWBA and SEPA-RDWBA.

For both $5s[1/2]_1^o$ and $5s[3/2]_1^o$ excitations present SEPA-RDWBA and SE-RDWBA results show good agreement with the experimental measurements of Guo *et al.* (2000) at energies near excitation threshold. Unlike the previous measurements of Trajmar *et al.* (1981), present SEPA-RDWBA and SE-RDWBA results suggest presence of a peak close to excitation threshold and these values are close to the experimental results of Guo *et al.* (2000). The 5-state RM (in case of $5s[3/2]_1^o$ excitation 15 state RM) and semi-RDW results of Dasgupta *et al.* (2001) are also close to the measurements of Guo *et al.* (2000). Static potential alone cannot be used to accurately describe the scattering process as shown with the present S-RDWBA ICS results which give very large values throughout the low and intermediate energy region where distortion potential is usually deemed significant. It is seen from tables 4.8 and 4.9 that as impact energy increases beyond 100 eV, ICS results obtained using the complex potential (SEPA-RDWBA) are generally lower than the rest of the present results. Despite this, the absorption potential generally has very

minimal effect on the cross sections of krypton at all energies as can be seen from the graphs (figure 4.16 and 4.17) and tables 4.4 and 4.5 of ICS. The quick rise in cross sections near the excitation threshold suggests large scattering of electrons due to maximum interaction between incident and target atom electrons due to attraction by the positive nucleus, exchange effects and polarization of the target atom electrons by the incident electron. This trend near excitation threshold is same for all the gases discussed in this study. As the kinetic energy of the incident electron increases, the interaction time with the target atom electrons becomes less and less and so the distortion potential has lesser effect on the free electron. This usually leads to convergence of all results at high electron energies.

Table 4.4: Present integral cross section results for relativistic electron impact excitation of $5s\left[1/2\right]_1^o$ state of krypton.

ENERGY (eV)	RDWBA-S ($10^{-16}cm^2$)	RDWBA-SE ($10^{-16}cm^2$)	RDWBA-SEP ($10^{-16}cm^2$)	RDWBA-SEPA ($10^{-16}cm^2$)
11	1.27800	0.15590	0.21130	0.21100
15	2.80433	0.27981	0.44947	0.44947
20	1.63360	0.25159	0.18404	0.18404
50	1.53008	0.51583	0.25772	0.25775
100	0.10640	0.07745	0.07601	0.07600
150	0.05592	0.04527	0.04510	0.04422
200	0.03374	0.03142	0.03150	0.03097

Table 4.5: Present integral cross section results for relativistic electron impact excitation of $5s\left[3/2\right]_1^o$ state of krypton.

ENERGY(eV)	RDWBA-S ($10^{-16}cm^2$)	RDWBA-SE ($10^{-16}cm^2$)	RDWBA-SEP ($10^{-16}cm^2$)	RDWBA-SEPA ($10^{-16}cm^2$)
11	4.41300	0.29611	0.13684	0.13680
15	2.80512	0.24690	0.36830	0.3683
20	1.67582	0.24592	0.23717	0.23717
50	2.45139	0.53998	0.18980	0.18982
100	0.21092	0.14602	0.14313	0.14200
150	0.12178	0.09664	0.09622	0.09417
200	0.07596	0.07071	0.07090	0.06962

4.3.3 Lambda parameter for krypton

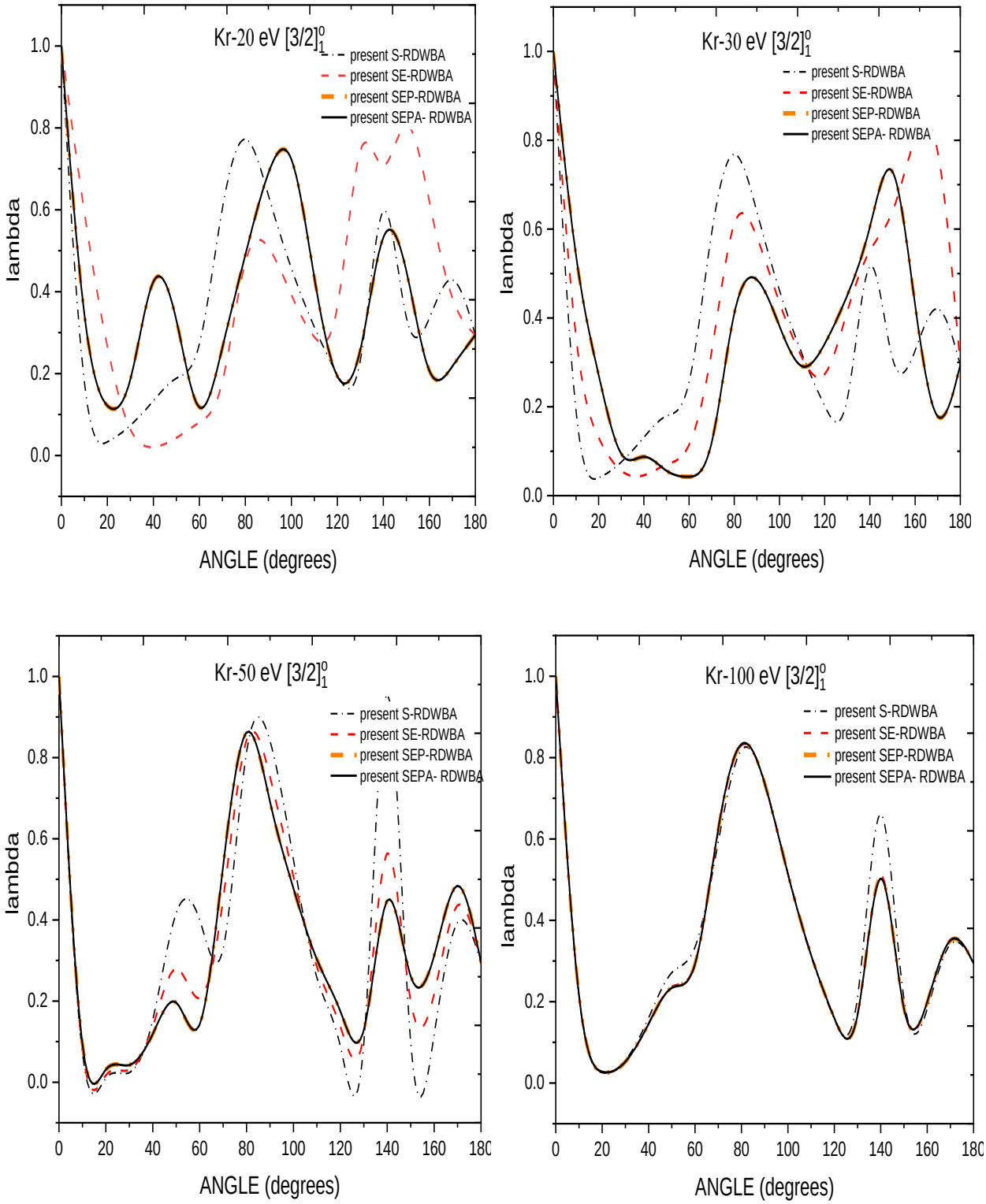

Figure 4.18: Present lambda parameters for excitation of the $5s[3/2]^o_1$ state of krypton: S-RDWBA, SE-RDWBA, SEP-RDWBA and SEPA-RDWBA.

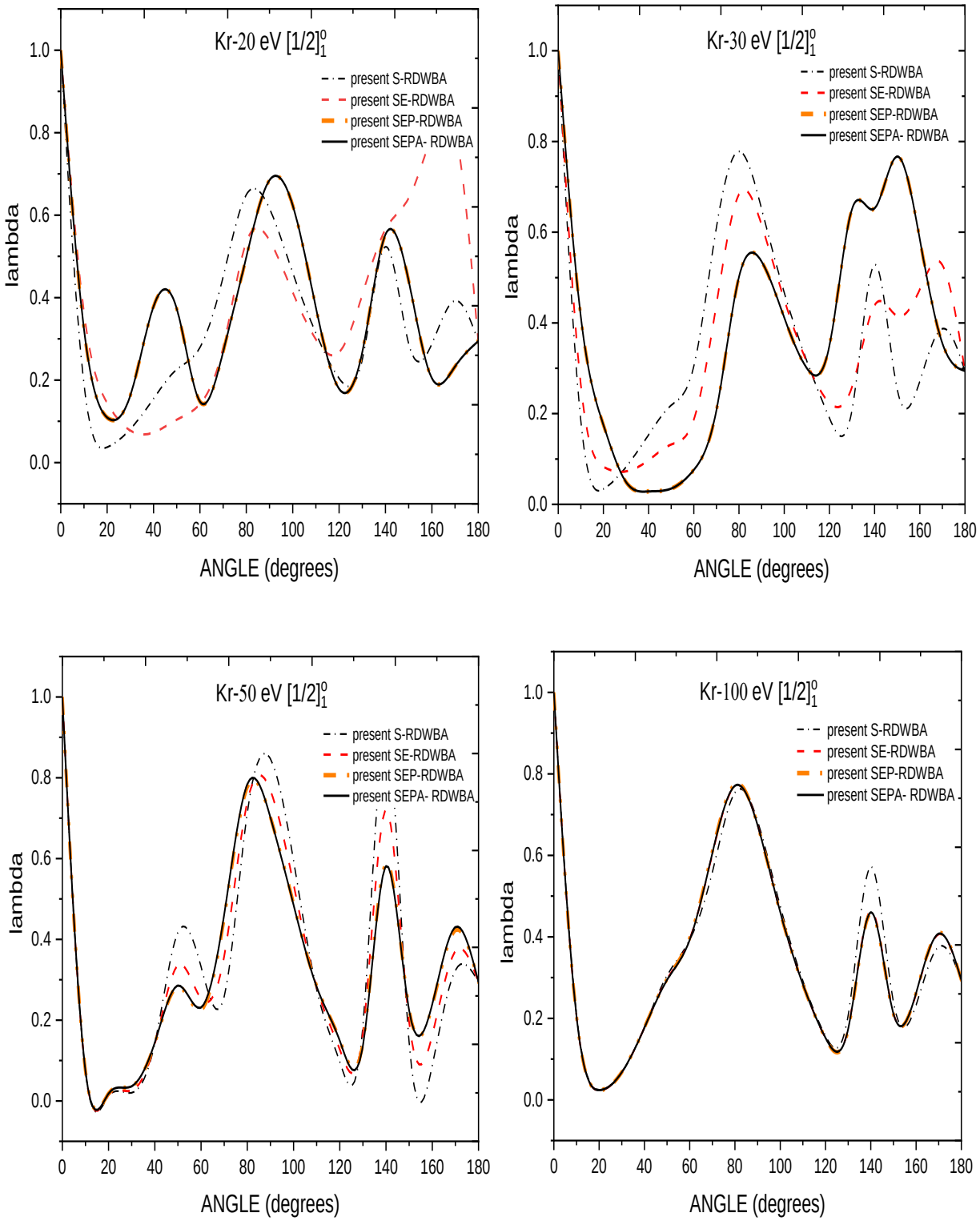

Figure 4.19: Present lambda parameters for excitation of the $5s[1/2]^{o}_{1}$ state of krypton: S-RDWBA, SE-RDWBA, SEP-RDWBA and SEPA-RDWBA.

Usually, for the excited state total angular momentum $J_b = 1$ of the atom, incident electrons occupy the three magnetic sublevels $M_b = 0, \mp 1$before excitation an electron from a 'p' to an 's' orbital. From figures 4.18 and 4.19, it is seen that the forward scattering (around 0^o), after the excitation of the atom, is mostly taking place from the magnetic sublevel $M_b = 0$ for all impact energies, since λ =1 there. Excitation from the magnetic sublevel $M_b = 0$ is also high near 40^o, 80^o and 140^o scattering angles, and mostly around 80^o for energies above 30 eV. As λ approaches zero, this implies that the excitation is mostly taking place from $M_b = 1$ magnetic sub-state. Despite there being no other data available for comparison with respect to this specific excitation of krypton, data presented here will still be useful for other researchers to use in making predictions and comparing with their findings.

4.3.4 Stokes parameters for krypton

Due to the limited or lack of other results for coherence parameters for excitation of krypton, we only compare present linear polarization Stokes (coherence) parameter results P_1 and P_2 at 50 eV impact energy with the available experimental results of Danjo *et al.* (1985) Born approximation results of Martus *et al.* (1991), DWB results of Bartschat and Madison (1987) and RDW results of Zuo *et al.* (1992). The parameters on the positive vertical axis indicate polarization of the photon in the forward direction while the negative axis indicates a backward polarization.

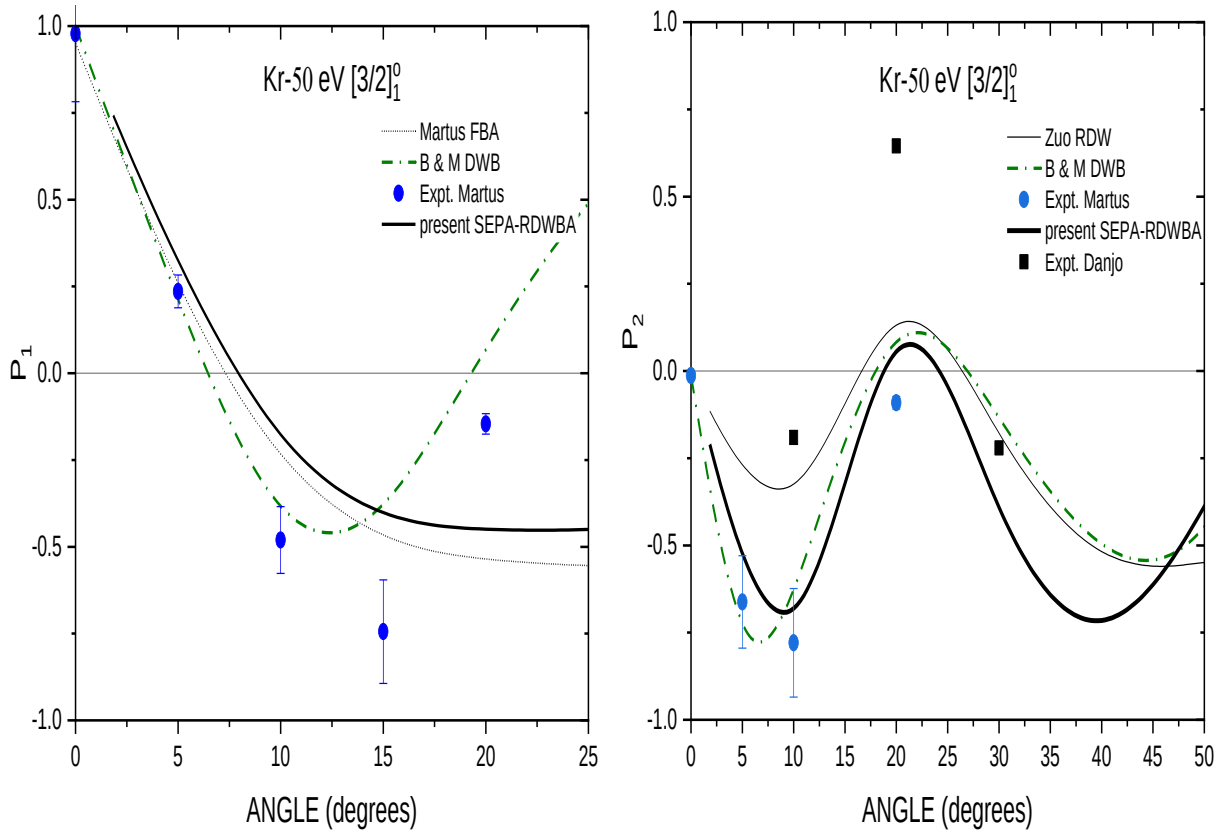

Figure 4.20: P_1 and P_2 parameters for electron impact excitation of the $[3/2]^o_1$ state of krypton at 50 eV. Experimental results: Expt. Martus, Martus *et al.* (1991); Expt. Danjo, Danjo *et al.* (1985). Calculations: B & M DWB, Bartschat and Madison (1987); Martus FBA, Martus *et al.* (1991); Zuo RDW, Zuo *et al.* (1992); Present SEPA-RDWBA.

At 50 eV for P_1 parameter, present SEPA-RDWBA results are similar in shape with first Born approximation (FBA) calculations of Martus *et al.* (1991) but deviates from DWB results of Bartschat and Madison (1987) and experimental result of Martus *et al.* (1991) at scattering angles beyond 15°. For the parameter P_2, present results are in good agreement with the experimental results of Martus *et al.* (1991) and DWB results of Bartschat and Madison (1987). Because this study has more emphasis in comparing scattering data at low impact energy, we have also presented results for Stokes parameters at of 15 eV in table 4.6 to act as reference for other researchers investigating a similar excitation either experimentally or theoretically.

Table 4.6: Stokes parameters for krypton at 15 eV

	$5s[3/2]_1^o$ state			$5s[1/2]_1^o$ state		
ANGLE (degrees)	P_1	P_2	P_3	P_1	P_2	P_3
0	1.00000	0.00000	0.00000	1.00000	0.00000	0.00000
10	-0.49067	-0.56235	0.74232	-0.49297	-0.49434	0.39360
20	-0.49147	0.156085	0.307139	-0.49393	0.113727	0.11448
30	-0.44167	-0.27997	-1.72E-03	-0.44472	-0.24324	-3.86E-02
40	-8.24E-02	-0.24586	-0.12728	-0.16086	-0.22286	-7.48E-02
60	-0.22612	-5.67E-03	3.99E-02	-0.25804	-5.67E-03	-3.04E-03
80	0.249391	-2.13E-02	3.32E-02	0.253586	-2.55E-02	1.09E-02
100	0.249769	2.94E-02	5.06E-03	0.212018	2.86E-02	6.54E-04
120	-0.23744	2.38E-02	-2.00E-02	-0.24058	4.06E-02	-1.50E-02
140	0.302062	-1.84E-02	3.45E-03	0.314305	2.32E-02	1.08E-02
160	-0.38007	2.68E-02	1.43E-02	-0.43875	6.84E-03	5.87E-04
180	-4.55E-02	0.00000	0.00000	-4.55E-02	0.00000	0.00000

4.4 Electron-Xenon Inelastic Scattering

4.4.1 Differential cross sections for xenon

Present DCS results for electron impact excitation of the lowest resonance states of xenon are compared with experimental results of, Filipovic *et al.* (1987) and Khakoo *et al.* (1996) and with theoretical results of Bartschat and Madison (1987) using DWBA, the *R*-matrix of Nakazaki *et al.* (1997), RDW results of Zuo *et al.* (1991) and, FOMBT and UDWA results of Khakoo *et al.* (1996) for impact energies at 15 eV, 30 eV, 50 eV, 80 eV and 100 eV.

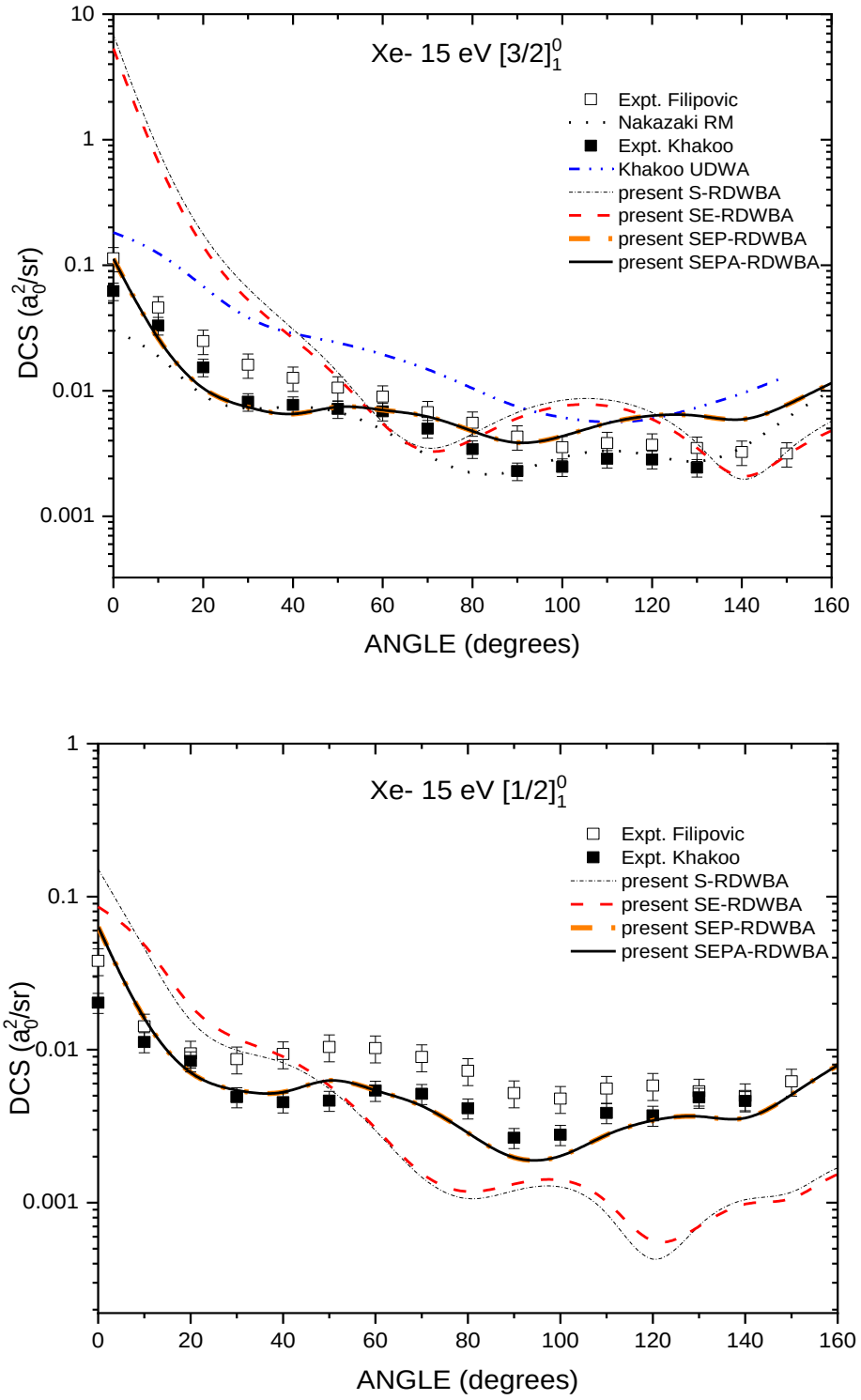

Figure 4.21: DCS results for electron impact excitation of the lowest resonance states $6s[3/2]^o_1$ and $6s[1/2]^o_1$ of xenon at 15 eV. Experimental results: Expt. Khakoo, Khakoo *et al.* (1996); Expt. Filipovic, Filipovic *et al.* (1988). Calculations: Khakoo UDWA, Khakoo *et al.* (1996); Nakazaki *et al.* (1997). Present calculations: S-RDWBA, SE-RDWBA, SEP-RDWBA and SEPA-RDWBA.

At 15 eV (figure 4.21), present SEPA-RDWBA and SEP-RDWBA results overlap, indicating that the absorption potential has negligible effect on cross section results. Furthermore, our results for triplet state $6s[3/2]_1^o$ are in good agreement in shape (but not in magnitude) with the experimental results of Khakoo *et al.* (1996) and the RM results of Nakazaki *et al.* (1997), while the present SE-RDWBA and S- RDWBA results disagree with experimental results at all angles. For $6s[1/2]_1^o$ excitation, present SEPA-RDWBA results are in good agreement with experimental results both in shape and magnitude.

At 30 eV (figure 4.22), experimental results of Filipovic *et al.* (1987) are generally higher in absolute value at all angles as noted by Khakoo *et al.* (1996), though the cross section shapes of both experiments are in agreement with the present SEPA-RDWBA and SEP-RDWBA results. RDW results of Zuo *et al*. (1991) are also close to the experimental results of Khakoo *et al*. (1996). DWB results of Bartschat and Madison (1987) differ in shape for the $6s[3/2]_1^o$ (triplet) state.

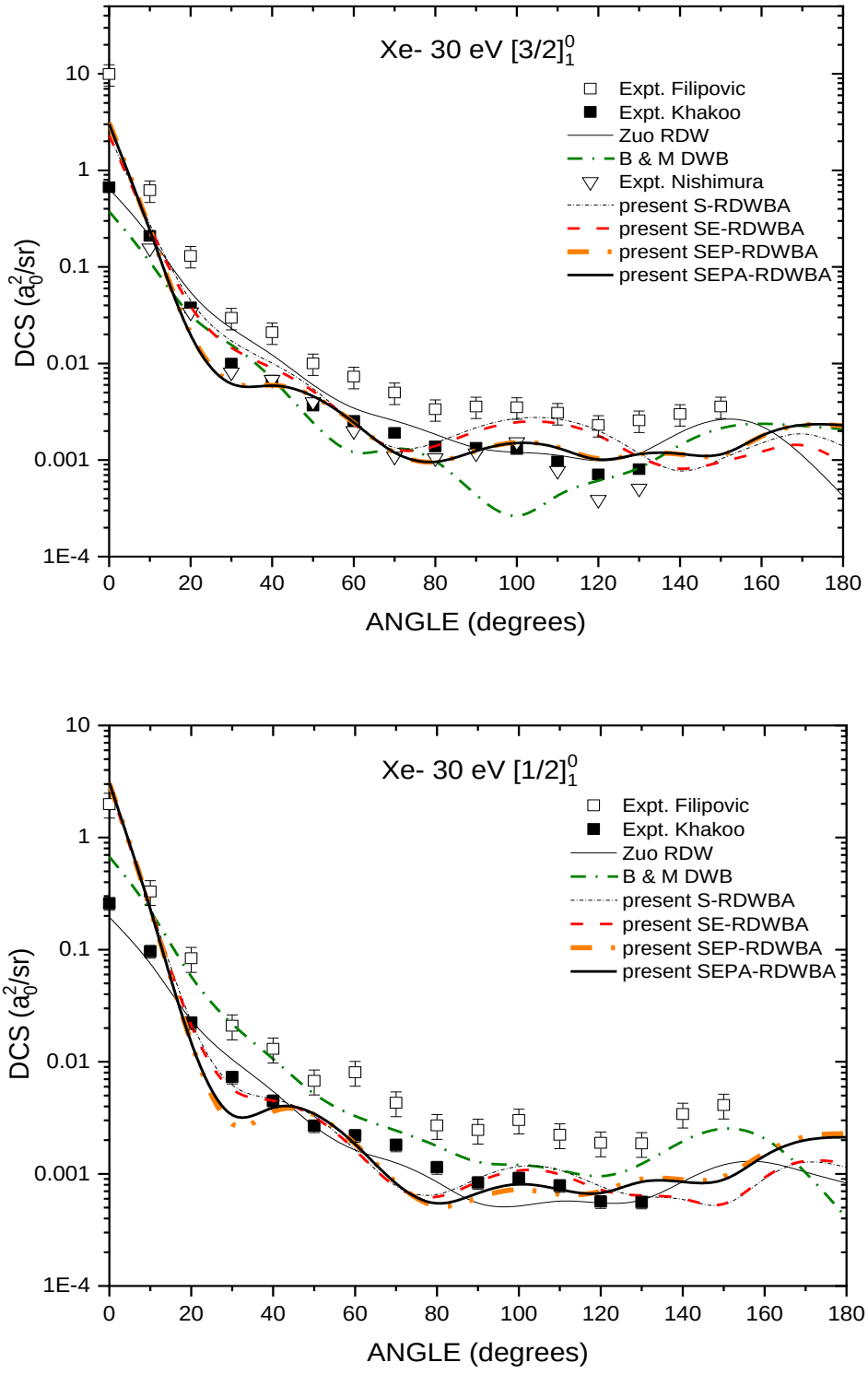

Figure 4.22: DCS results for electron impact excitation of the lowest resonance states $6s[3/2]^o_1$ and $6s[1/2]^o_1$ of xenon at 30 eV. Experimental results: Expt. Khakoo, Khakoo *et al.* (1996); Expt. Filipovic, Filipovic *et al.* (1988); Expt. Nishimura, Nishimura *et al.* (1985). Calculations: B & M DWB, Bartschat and Madison (1987); Zuo RDW, Zuo *et al.* (1991). Present calculations: S-RDWBA, SE-RDWBA, SEP-RDWBA and SEPA-RDWBA.

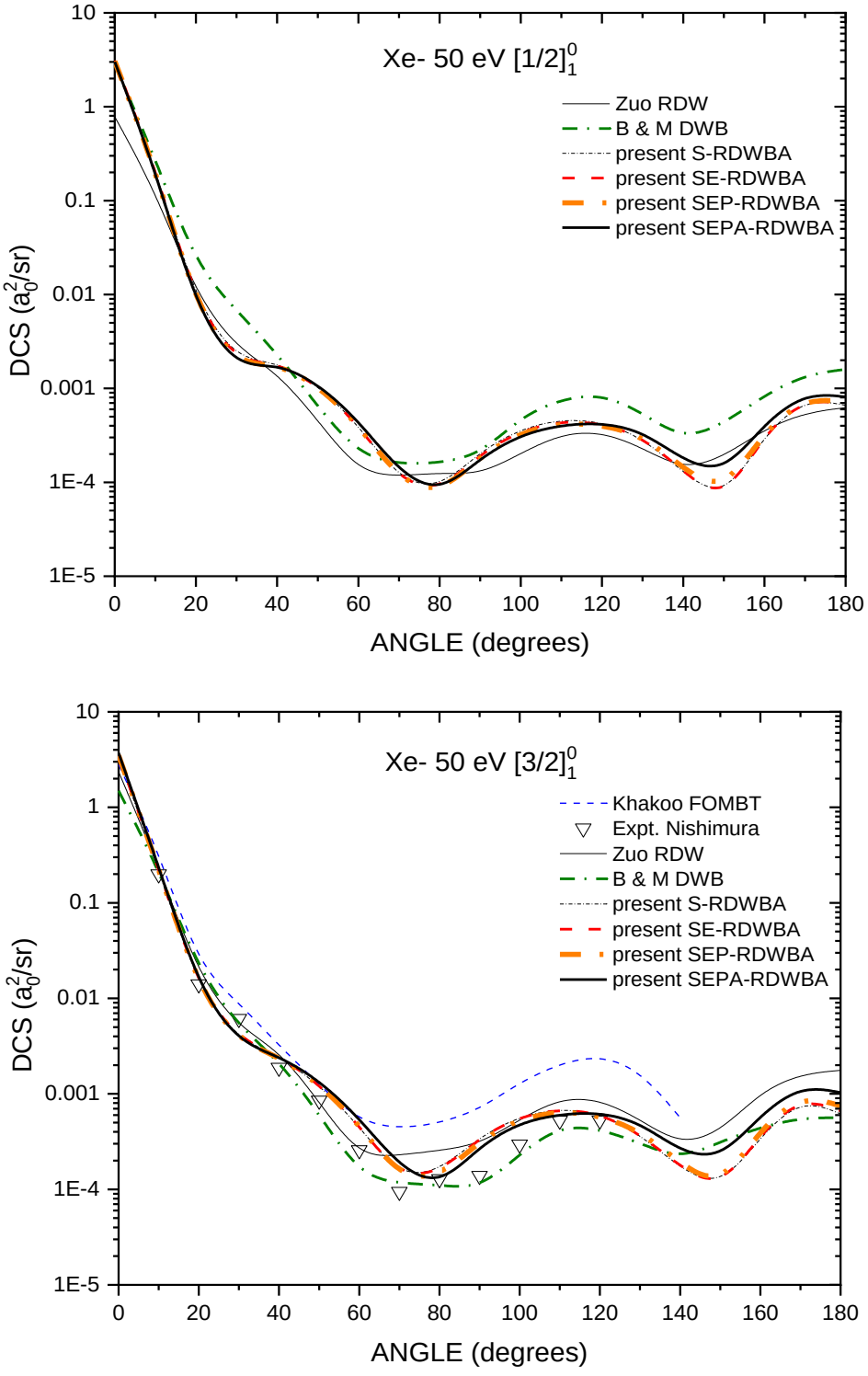

Figure 4.23: DCS results for electron impact excitation of the lowest resonance states $6s[3/2]^o_1$ and $6s[1/2]^o_1$ of xenon at 50 eV. Experimental results: Expt. Nishimura, Nishimura *et al.* (1985). Calculations: B & M DWB, Bartschat and Madison (1987); Zuo RDW, Zuo *et al.* (1991); Khakoo FOMBT, Khakoo *et al.* (1996). Present calculations: S-RDWBA, SE-RDWBA, SEP-RDWBA and SEPA-RDWBA.

At 50 eV (figure 4.23) and 80 eV (figure 4.24) present SEPA RDWBA model again predict DCS results of about the same shape and magnitude as the experimental results of Nishimura *et al.* (1985) and Filipovic *et al.* (1987), and FOMBT and UDWA calculations of Khakoo *et al.* (1996), DWBA calculations of Bartschat and Madison (1987) and RDWA calculations of Zuo *et al.* (1991). Khakoo *et al.* (1996) attributes the satisfactory agreement of calculated values of Zuo *et al.* (1991) and Bartschat and Madison (1987) with experimental results to the type of exchange distortion potential adopted and relativistic effects. Present calculations with complex potential (SEPA-RDWBA) and RDW results of Zuo *et al.* (1991) give very good cross sections shapes (almost matching with experimental results) at 80 eV compared to the non-relativistic (Bartschat and Madison, 1987) and semi-relativistic (Khakoo *et al.*, 1996).results.

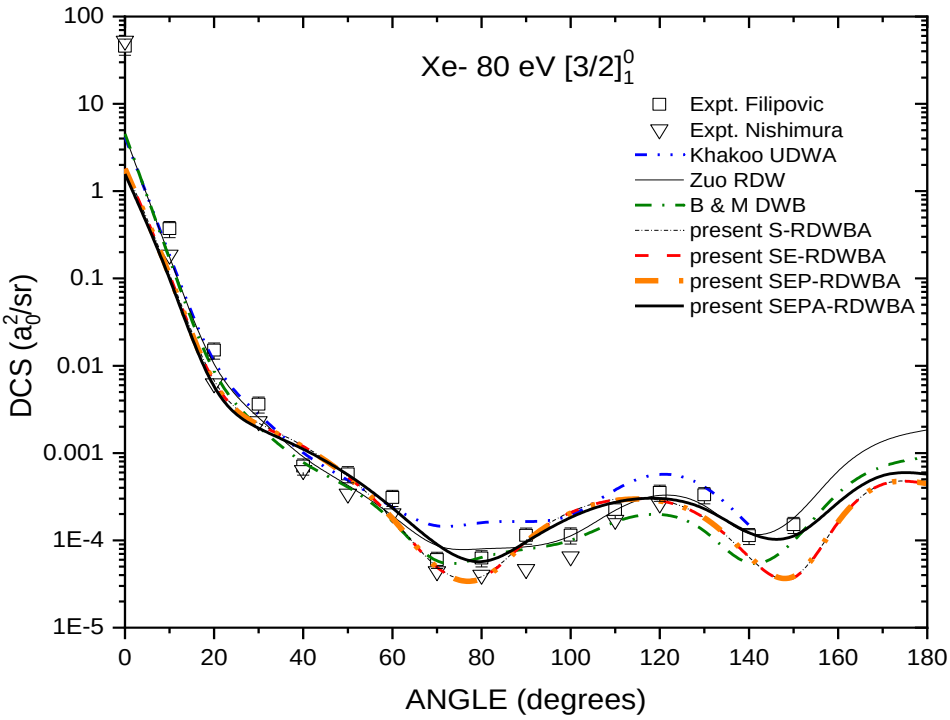

Figure 4.24: DCS results for electron impact excitation of the $6s[3/2]^o_1$ state of xenon at 80 eV. Experimental results: Expt. Nishimura, Nishimura *et al.* (1985); Expt. Filipovic, Filipovic *et al.* (1988). Calculations: B & M DWB, Bartschat and Madison (1987); Zuo RDW, Zuo *et al.* (1991); Khakoo UDWA, Khakoo *et al.* (1996). Present calculations: S-RDWBA, SE-RDWBA, SEP-RDWBA and SEPA-RDWBA.

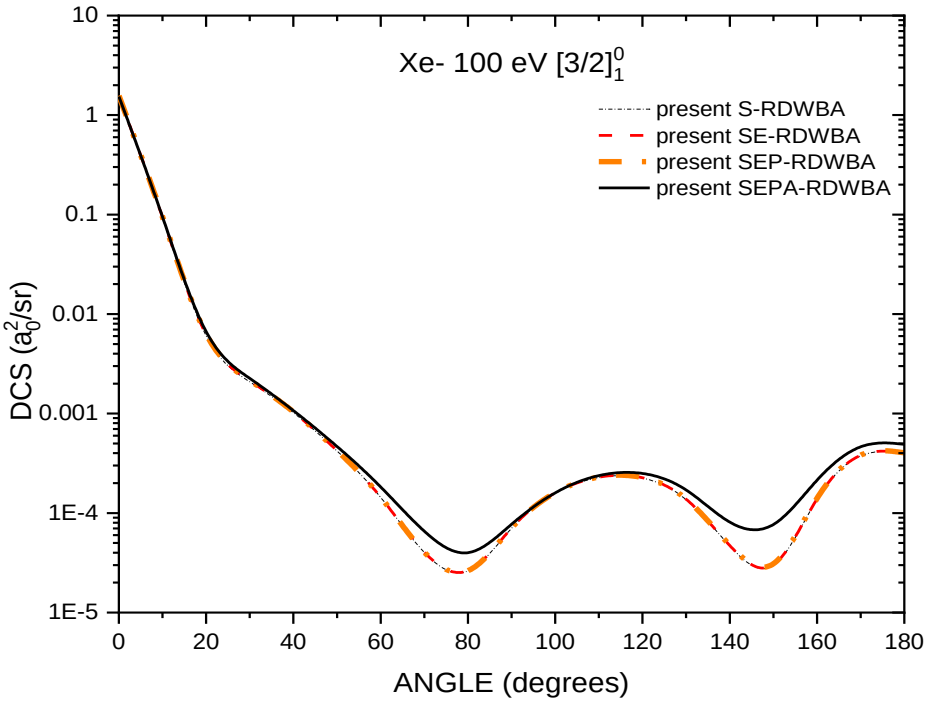

Figure 4.25: DCS results for electron impact excitation of the $6s[3/2]_1^o$ state of xenon at 100 eV. Present calculations: S-RDWBA, SE-RDWBA, SEP-RDWBA and SEPA-RDWBA.

For the same reason as argon and krypton, the similarity in shapes of cross sections as impact energy increases especially above 30 eV is due to the fact that; at impact energies near excitation threshold, there is more interaction between the projectile electron and the target electrons causing electrons to scatter evenly in different directions. At high impact energies, the projectile electron tends to move in a near straight line inside the target atom electron cloud, and encounter less with the target atom electrons resulting in scattering that is at small angles. At energies above 50 eV, the absorption potential plays the most critical role in improvement of cross section results unlike the polarization potential which is more active and critical in giving good DCS shapes at energies close to excitation threshold. For xenon, unlike argon and krypton, absorption potential, which accounts for loss of flux to other open scattering channels, dominates at higher impact energies. This should also be the case for relativistic effects being more dominant as the atomic charge increases, hence giving improved cross sections for predicting experiments as

seen at 80 eV. At 100 eV, as seen in figure 4.25, results generated using with SEPA potentials have a clear distinction from those without (SEP) this complex part of the distortion potential.

4.4.2 Integral cross sections for xenon

In figures 4.26 and 4.27 present integral cross sections results for electron impact excitation of the lowest resonance states of xenon are compared with the experimental results of Filipovic *et al.* (1987), theoretical RM results of Nakazaki *et al.* (1997) and RDW results of Zuo *et al.* (1991).

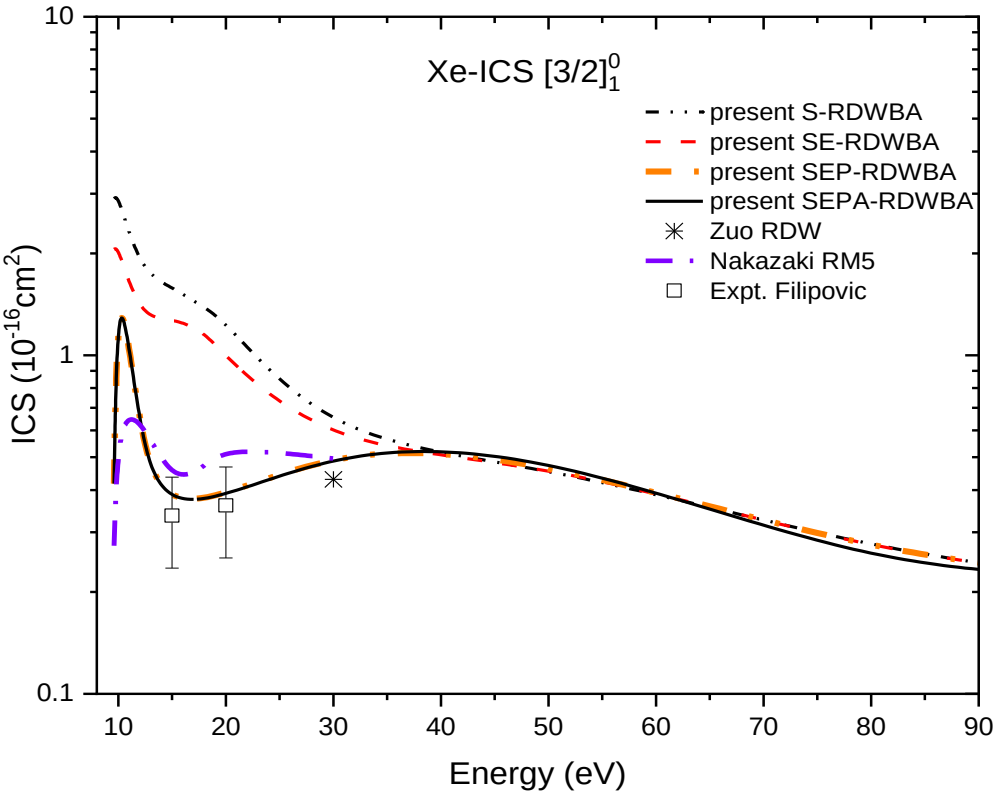

Figure 4.26: ICS results for electron impact excitation of the lowest $6s[3/2]_1^\circ$ resonance state of xenon. Experimental results: Expt. Filipovic, Filipovic *et al.* (1988). Calculations: Zuo RDW, Zuo *et al.* (1991); Nakazaki RM5, Nakazaki *et al.* (1997). Present calculations: S-RDWBA, SE-RDWBA, SEP-RDWBA and SEPA-RDWBA.

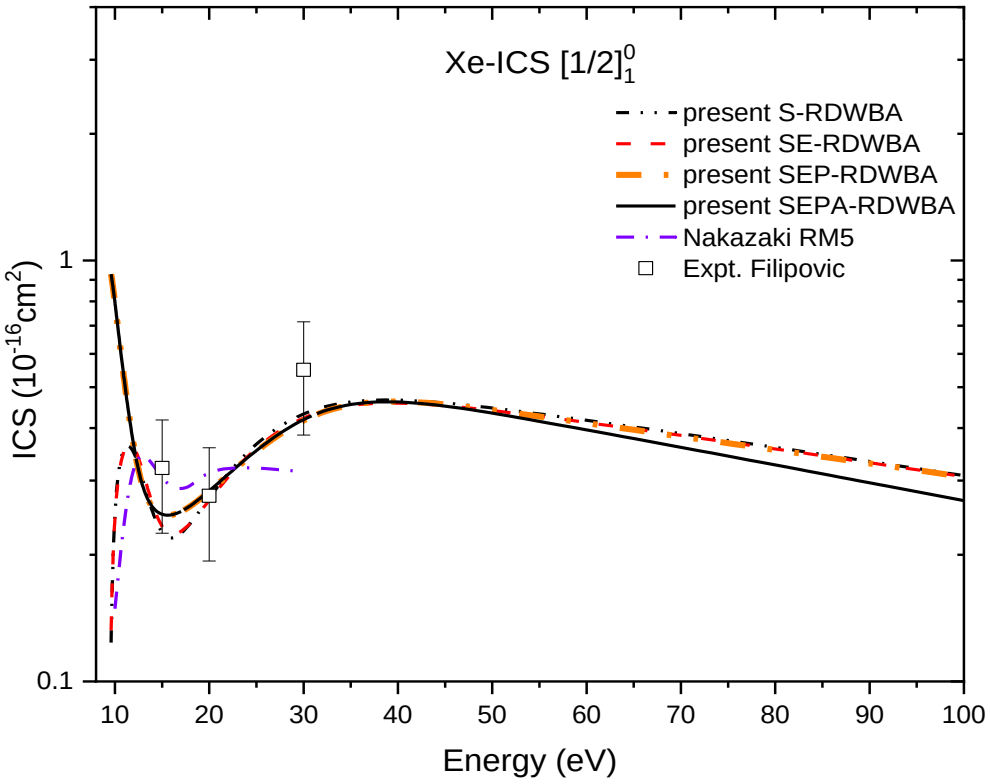

Figure 4.27: ICS results for electron impact excitation of the lowest $6s[1/2]_1^o$ resonance state of xenon. Experimental results: Expt. Filipovic, Filipovic *et al.* (1988). Calculations: Nakazaki RM5, Nakazaki *et al.* (1997). Present calculations: S-RDWBA, SE-RDWBA, SEP-RDWBA and SEPA-RDWBA.

For both $6s[3/2]_1^o$ and $6s[1/2]_1^o$ levels excitation, present SEPA-RDWBA and SEP-RDWBA results predict similar cross sections as the experimental results of Filipovic *et al.* (1987) (though the experimental results are given only for energies below 30 eV). At impact energy above 50 eV, the complex potential (due to absorption) has lower cross sections and further plays the most critical role in improving the cross sections results, as seen from the ICS graphs for both singlet and triplet excitations.

Table 4.7: Present integral cross section results for relativistic electron impact excitation of $6s[1/2]_1^o$ state of xenon.

ENERGY (eV)	RDWBA-S ($10^{-16}cm^2$)	RDWBA-SE ($10^{-16}cm^2$)	RDWBA-SEP ($10^{-16}cm^2$)	RDWBA-SEPA ($10^{-16}cm^2$)
9.6	0.12365	0.13226	0.92880	0.92800
10	0.34500	0.32010	0.80660	0.80670
12	0.40140	0.42660	0.32152	0.32150
15	0.17975	0.18641	0.20022	0.20024
20	0.28410	0.27641	030211	0.30091
30	0.49637	0.48579	0.50883	0.51352
50	0.45386	0.44845	0.44272	0.43830
100	0.30841	0.30665	0.30614	0.26905

Table 4.8: Present integral cross section results for relativistic electron impact excitation of $6s[3/2]_1^o$ state of xenon

ENERGY(eV)	RDWBA-S ($10^{-16}cm^2$)	RDWBA-SE ($10^{-16}cm^2$)	RDWBA-SEP ($10^{-16}cm^2$)	RDWBA-SEPA ($10^{-16}cm^2$)
9.6	2.89970	2.05580	0.41770	0.41780
10	2.98000	2.08900	2.12600	2.12600
12	1.77280	1.28200	0.52990	0.53000
15	1.58629	1.28696	0.31374	0.31362
20	1.25400	0.97860	0.39102	0.39030
30	0.55193	0.52635	0.55643	0.54482
50	0.47570	0.48575	0.49170	0.50576
100	0.22073	0.22386	0.22550	0.22417

4.4.3 Lambda parameter for xenon

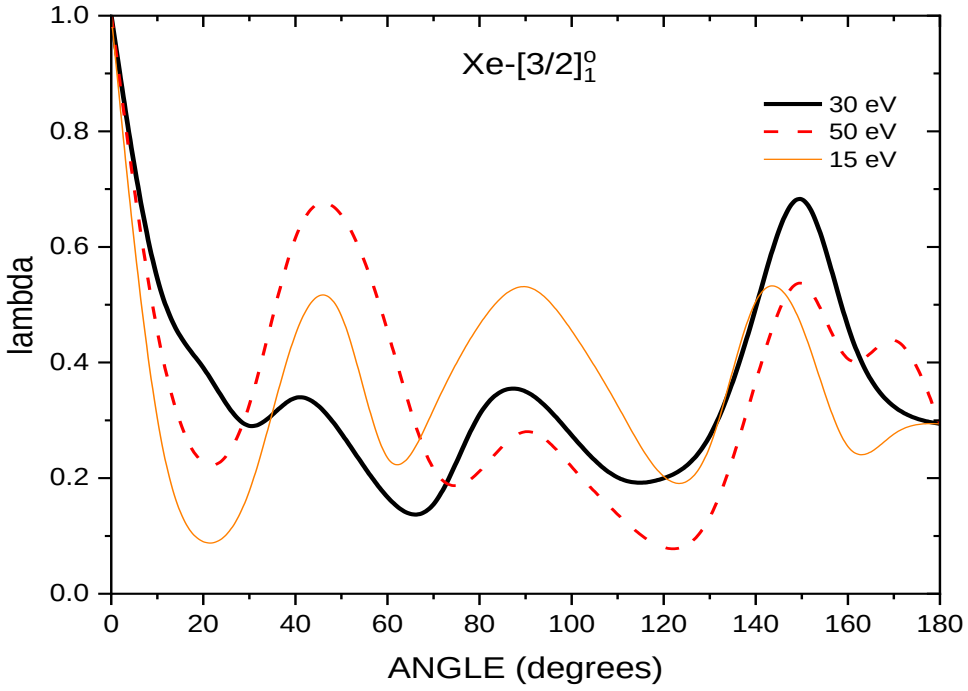

Figure 4.28: Present SEPA-RDWBA lambda parameter results for excitation of the $6s[3/2]^{\circ}_{1}$ state of xenon at 15 eV, 30 eV and 50 eV

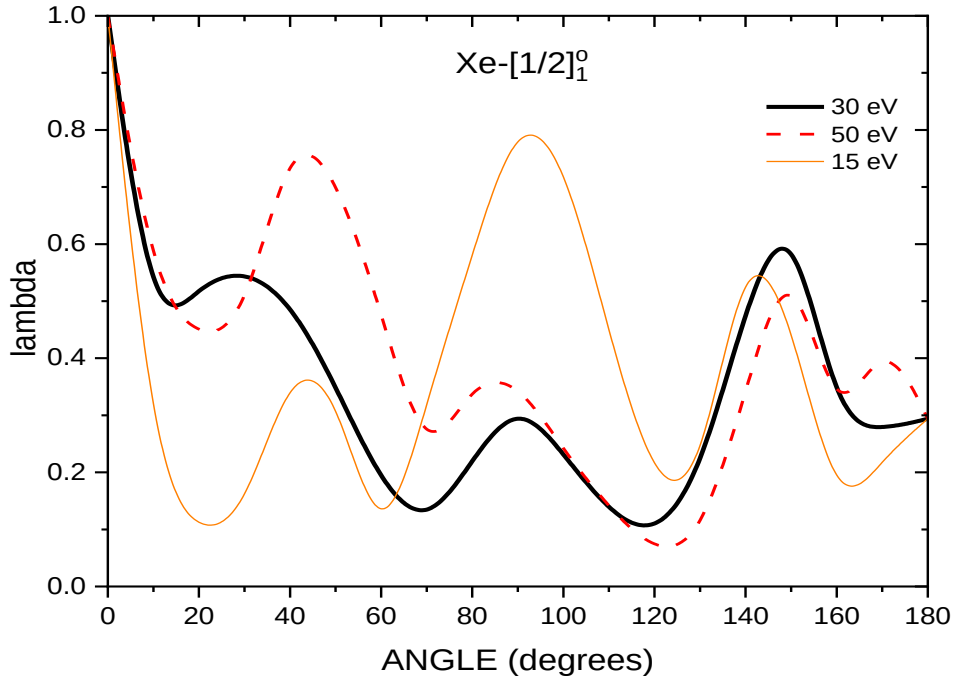

Figure 4.29: Present SEPA RDWBA lambda parameter results for excitation of the $6s[1/2]^{\circ}_{1}$ state of xenon at 15 eV, 30 eV and 50 eV.

From figure 4.28 and 4.29, it is seen that most of the excitations are taking place from the magnetic sublevel $M_b = 0$ when the electron is scattered around 0^o for all energy, since λ =1 there. When the electron is scattered at angles near 40^o, 80^o and 140^o, then also more electrons are excited from the magnetic sublevel $M_b = 0$. On the contrary, if λ approaches zero, then it implies that more electrons get scattered from $M_b = 1$. As stated for argon and krypton, there being no other data available for this specific excitation problem, data presented here can still be useful to other theoretical and experimental researchers for making reference to their findings in future.

4.4.4 Stokes parameters for xenon

Due to limited experimental data on angular correlation parameters in literature, of which if available, measurements are at small scattering angles below 50^o, we have only compared present Stokes parameter for the excitation of the $6s[3/2]_1^o$ state of xenon results at 30 eV with the experimental result of Corr *et al.* (1990) and calculations of Zuo *et al.* (1991).

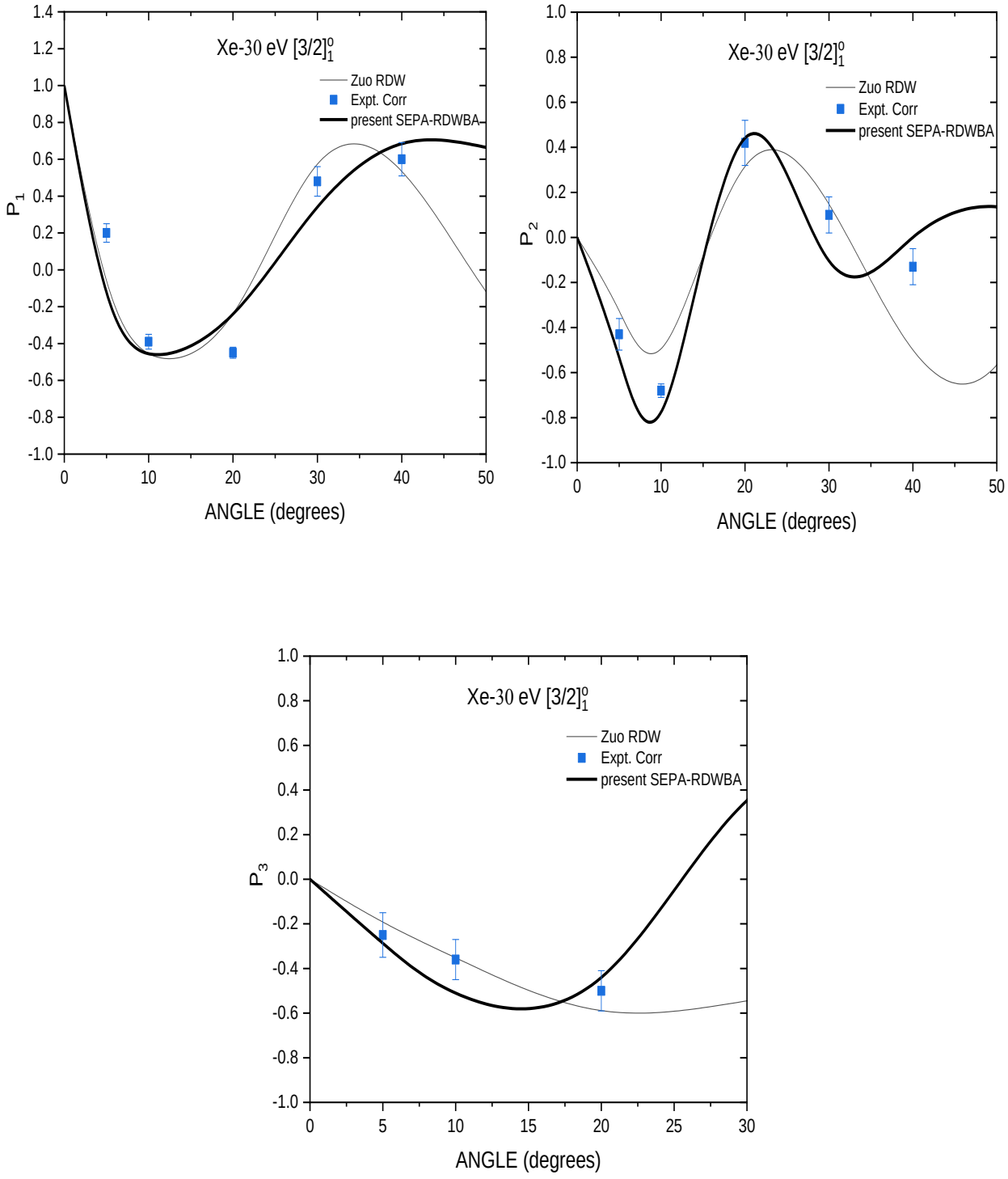

Figure 4.30: Stokes parameters P_1, P_2, and P_3 for excitation of the $6s[3/2]^o_1$ state of xenon at 30 eV. Present SEPA-RDWBA calculations compared with: Expt. Corr, Corr *et al.* (1990) experimental result; Zuo RDW, Zuo *et al.* (1991) calculations.

For the degree of linear polarization parameters P_1 and P_2, present results give satisfactory agreement with the experimental result of Corr *et al.* (1990), while the circular polarizability parameter P_3 predicts a quick rise at 30^o compared to theoretical results of Zuo *et al.* (1991). The difference of results between the present SEPA-RDWBA and RDW result of Zuo *et al.* (1991) is probably due to the difference in the distortion potential applied in calculating the distorted waves as pointed out in literature review (chapter 2). Because of our focus at low energy scattering, we have also presented Stokes parameters at 15 eV in table 4.9, which is still useful as reference for other researchers investigating a similar excitation either experimentally or theoretically.

Table 4.9: Stokes parameters for xenon at 15 eV

	$6s[3/2]_1^o$ state			$6s[1/2]_1^o$ state		
ANGLE (degrees)	P_1	P_2	P_3	P_1	P_2	P_3
0	1.00000	0.00000	0.00000	1.00000	0.00000	0.00000
10	-0.14523	-0.54147	3.71E-01	-0.13778	-1.23371	4.86E-01
20	0.541576	0.902527	3.23E-01	1.00000	0.766072	0.99864
30	0.573036	-0.33589	8.99E-02	0.654933	-0.31626	6.41E-02
40	0.247966	-0.10467	2.81E-02	0.149418	-9.44E-02	-0.11107
60	2.98E-02	-4.00E-02	-3.23E-02	1.64E-03	1.29E-04	7.68E-03
80	1.42E-02	-4.32E-02	3.07E-02	0.101527	1.73E-03	1.20E-02
100	-2.04E-02	2.17E-02	2.75E-02	7.30E-02	1.23E-02	7.59E-03
120	-2.25E-04	6.19E-02	-6.04E-03	5.73E-02	7.17E-03	-2.20E-03
140	6.01E-02	5.54E-02	-4.37E-02	0.110646	-8.13E-03	-5.39E-03
160	3.88E-02	2.63E-02	4.74E-02	3.86E-02	1.34E-02	1.07E-02
180	-5.91E-02	0.00000	0.00000	-5.91E-02	0.00000	0.00000

5 CHAPTER 5

CONCLUSIONS AND RECOMMENDATIONS

5.1 Conclusions

The formulation of the RDW method using a complex potential has resulted in the writing of a new program RDWBA1 for calculation of transition matrix elements, scattering amplitudes, cross sections and angular parameters. Furthermore, the relativistic wavefunctions obtained in a multi-configuration Dirac-Fock approach obtained by modifying the GRASP code, which is an improved version of its predecessor MCDF code, gives improved DCS, ICS and angular correlation parameter results when used as input for our program RDWBA1.

In this study, we were able to compute the scattering amplitudes, differential and integral cross sections for inelastic excitation of argon, krypton and xenon obtained using the RDW approximation with a complex distortion potential at impact energies up to 100 eV from excitation threshold where distorted-wave methods usually fail to agree on results.

Furthermore, angular correlation and Stokes parameters have been obtained but due to lack of available experimental data for a variety of impact energies and large scattering angles, comparison of results is done with present work for the different versions of distortion potentials (S- RDWBA, SE- RDWBA, SEP- RDWBA and SEPA-RDWBA) where no literature reference is found. Nevertheless, present data still serves as a reference for other future works for the problem in context. Results for angular parameters for Ar, Xe and Kr are consistent with most experimental results for all the scattering angle range presented in this study.

Lastly, the present RDW differential cross sections for electron impact excitations and the recent experimental results of Khakoo *et al.* (2004) for argon, Guo *et al.* (2000); Allan *et al.* (2011) for krypton and Khakoo *et al.* (1996) for xenon are in good agreement at all impact energies investigated. This can be attributed mainly to inclusion of relativistic effects and the choice of distortion potential adopted in calculation of wavefunctions. Specifically, calculations with static and exchange potential alone cannot be used to describe an atomic collision process accurately as the DCS obtained are very large especially at low electron impact energies, while the polarization potential lowers cross sections and significantly improves results at the low impact energies. On the other hand, the absorption potential has minimal effect on cross sections results for Ar, Kr and Xe at low energies where the polarization potential dominates, but becomes more significant in improving shapes of cross sections at higher impact energies, more visibly for the heaviest atom (xenon) under this study.

5.2 Recommendations

i From the literature presented in this study, it is evident that there exist limited experimental data for the angular correlation analysis of the emitted photon and the scattered electrons. Therefore, in order to further investigate the RDW method with a complex potential, there is need to extend experimental research for angular correlation and coherence (stokes) parameters to include a wide range of excitation energies and for larger scattering angles, especially above 50 eV. This will provide more data for comparison and further improvement if need arise.

ii This study may also be extended to positron impact excitation of the lowest resonance states of heavy rare gases to see the effect of the complex potential on cross sections.

iii This study is focused on excitation of the lowest resonance states (J=1) of the noble gases. It would also be interesting to carry out the same study for the lowest metastable states (those with total angular momentum of the atom J=0 and J=2).

iv It would also be interesting to do more research that includes higher order terms of the T-matrix with the RDWA approach that has relativistic effects included fully in calculations for the excitation of the lowest resonance and metastable states of the noble gases

REFERENCES

Allan M., Zatsarinny O. and Bartschat K. (2011). Electron impact excitation of the $4p^5$ 5*s* states in krypton. *Journal of Physics B: Atomic and Molecular Physics.* **44,** 065201

Andersen N., Gallagher J.W. and Hertel I. V. (1988). Collisional Alignment and orientation of atomic outer shells. *Physics reports* **165**, 1-188

Andersen N. and Bartschat K. (2017). *Polarization, Alignment, and Orientation in Atomic Collisions*, 2nd Ed. Springer Verlag, Berlin.

Andreas N., Michael D, Hermann S, and Heinzwerner P. (1995). Ab initio energy-adjusted pseudo potentials for the noble gases Ne through Xe: Calculation of atomic dipole and quadrupole polarizabilities. *Chemical Physics* **102**, 8942-8952

Bartschat K. (1996). Computational Atomic Physics. Springer Verlag, Berlin. Pg. 15-27, Pg. 65-86 and Pg. 219-250

Bartschat K. and Madison D. H. (1987).Electron impact excitation of rare gases: differential cross sections and angular correlation parameters for neon, argon, krypton and xenon. *Journal of Physics B: Atomic, Molecular and Optical Physics* **20,** 5839-5863

Bostock C. J., Fontes C. J., Fursa D. V., Zhang H. L. and Bray I. (2013). Calculation of the relativistic rise in electron-impact-excitation cross sections for highly charged ions. *Physical Review* A **88,** 012711

Chen Guo. (1996). Fully-relativistic distorted-wave Born procedure for electron impact excitation. *Physical Review* A **53**, 3227-3237

Chutjian A. and Cartwright D. C. (1981). Electron-impact excitation of electronic states in argon at incident energies between 16 and 100 eV. *Physical Review* A **23,** 2178-2193

Corr J.J., Plessis P. and McConkey J.W. (1990). Coherent excitation of Xe [3/2] 6s by 30eV electrons. *Physical Review* A **42,** 5240-5243

Corr J.J., Wang S. and McConkey J. W. (1992). Coherent excitation of Ar 4*s* [3/2]; by low energy electrons. *Journal of Physics B: Atomic, Molecular and Optical Physics* **25**, 4929-4937

Danjo A., Koike T., Kani K., Sugahara H., Takahashi A. and Nishimura H. **(**1985). Electron-photon angular correlations for the excitation of krypton by electron impact. *Journal of Physics B: Atomic and Molecular Physics.* **18,** 595-600

da Paixao F. J. Padial N. T. Csanak G. (1980). Spin-Orbit Coupling Effects in Parameters that Describe Electron-Photon Coincidence Experiments. *Physical Review Letters* **45,** 1164-1167

da Paixao F. J., Padial N. T. and Csanak G. (1984). Electron-photon coincidence parameters for 4s (1/2) and 4s (3/2) states of argon. *Physical Review* A **30,** 1697-1713

Dasgupta A., Bartschat K., Vaid D., Grum-Grzhimailo A. N., Madison D. H., Blaha M. and Giuliani J. L. (2001). Electron-impact excitation to the $4p5^5s$ and $4p^55p$ levels of KrI using different distorted-wave and close-coupling methods. *Physical Review* A.**64,** 052710

Dyall K.G., Grant I.P., Johnson C.T., Parpia F.A. and Plummer E.P. (1989). A General-purpose Relativistic Atomic Structure Program. *Computer Physics Communications* **55**, 425-456

Filipovic D. (1988). Elastic and inelastic electron scattering by Krypton and Xenon. *PhD Thesis*, University of Belgrade.

Filipovic D. M. (1984). Medium Energy Electron Scattering by Argon. *M.Sc. Thesis* University of Belgrade

Filipovic D. M., Marinkovic B. P., Pejcev V., and Vuskovic L. (2000a). Electron-impact excitation of argon: I. The 4s' [1/2]1, 4p [1/2]1 and 4p' [1/2]0 states. *Journal of Physics B: Atomic, Molecular and Optical Physics* **33**, 677-691

Filipovic D. M., Marinkovic B. P., Pejcev V., and Vuskovic L. (2000b). Electron-impact excitation of argon: II. The lowest resonance 4s [3/2]1 and metastable 4s [3/2]2 and 4s' [1/2]0 states. *Journal of Physics B: Atomic, Molecular and Optical Physics* **33**, 2081-2094

Filipovic D. M., Marinkovic B. P., Pejcev V., and Vuskovic L. (1988). Electron-impact excitation of xenon at incident energies between 15 and 80 eV. Physical Review A **37**, 356-364

Fontes C. J. and Zhang H. L. (2007). Relativistic plane-wave Born theory and its application to electron-impact excitation. *Physical Review* A. **76,** 040703

Furness J.B. and McCarthy I.E. (1973). Semi-phenomenological Optical Model for Electron Scattering on Atoms. *Journal of Physics B: Atomic and Molecular Physics.* **6,** 2280-2291

Grant I. P. (1970). Relativistic calculation of atomic structures. *Advances in Physics* **19**, 747-811

Grant I.P., McKenzie B.J., Norrington P. H. (1980). An Atomic Multi-configurational Dirac-Fock Package. *Computer Physics Communications* **21,** 207-231

Guo X., Mathews D. F., Mikaelian G., Khakoo M. A., Crowe A., Kanik I., Trajmar S., Zeman V., Bartschat K. and Fontes C. J. (2000). Differential cross sections for electron-impact excitation of krypton at low incident energies. *Journal of Physics B: Atomic and Molecular Physics.* **33,** 1895-1919

Hoshino M., Murai H. Kato H., Itikawa Y., Brunger M. J. and Tanaka H. (2013). Resolution of a significant discrepancy in the electron impact excitation of the low lying states of neon. *Chemical Physics Letters*. **585**, 33-36

Itikawa Y. (1986). Distorted-Wave methods in electron-impact excitation of atoms and ions. *Physics Reports* **143**, 69-108

Katiyar K. and Srivastava R. (1988). Distorted-wave calculation of the cross sections and correlation parameters for $e^{\pm}$ collisions. *Physical Review* A **38**, 2767-2781

Kaur S. and Srivastava R. (1999). Excitation of the lowest auto-ionizing np^5 $(n+1)$ s^2, $^2P_{3/2;\ 1/2}$ states of Na (n = 2), K (n = 3), Rb (n = 4) and Cs (n = 5) by electron impact. *Journal of Physics B: Atomic, Molecular and Optical Physics* **32,** 2323-2342

Kaur S., Srivastava R., McEachran R. P. and Stauffer A. D. (1997). Electron impact excitation of magnesium and zinc atoms in the relativistic distorted-wave approximation. *Journal of Physics B: Atomic, Molecular and Optical Physics* **30**, 1027-1042

Kaur S., Srivastava R., McEachran R. P. and Stauffer A. D. (1998). Stokes parameters and differential cross sections for electron impact excitation of the $2p^5 3p$ J =1, 2 and 3states of neon. *Journal of Physics B: Atomic, Molecular and Optical Physics* **31**,157-174

Kessler J. (1985). Polarized electrons (2nd Edition). Springer Verlag, Berlin.

Khakoo M. A., Trajmar S., LeClair L. R., Kanik I., Csanak G. and Fontes C. J. (1996). Differential cross sections for electron impact excitation of Xe. *Journal of Physics B: Atomic, Molecular and Optical Physics* **29**, 3455-3475

Khakoo M, Vandeventer P, Childers J G, Kanik I, Fontes C J, Bartschat K, Zeman V, Madison D H, Saxena S, Srivastava R, and Stauffer A D (2004). Electron impact excitation of the argon $3p^5 4s$ configuration. *Journal of Physics B: Atomic and Molecular Physics* **37,** 247-281

Khare S. P., Ashok K. and Vijayshri (1985). Elastic scattering of electrons and positrons by the Ca atoms. *Journal of Physics B: Atomic and Molecular Physics.* **18,** 1827-1840

Madison D. H., Maloney C. M. and Wang J. B. (1998). Integral and differential cross section for electron-impact excitation of 12 of the lowest states of argon. *Journal of Physics B: Atomic, Molecular and Optical Physics* **31,** 873-893

Martus K. E., Zheng S. H. and Becker K. (1991). Electron-photon coincidence study of heavy-noble-gas excitation at small scattering angles *Physical Review* A **44**, 1682-1693

McEachran R. P. and Stauffer A. D. (1986). Spin polarization of electrons elastically scattered from xenon. *Journal of Physics B: Atomic, Molecular and Optical Physics* **19**, 3523-3538

Mityureva A. A. and Smirnov V. V. (2016) Electron Impact Excitation with the Cascade Population of the $4p^5$ 5*s* Levels of the Krypton Atom. *Optics and Spectroscopy* **121**, 804-809

Nakazaki S., Berrington K. A., Eissner W. B. and Itikawa Y. (1997). Excitation of xenon by electron impact. *Journal of Physics B: Atomic and Molecular Physics* **30**, 5805-5818

Nishimura H., Danjo A. and Matsuda T. (1985). Proceedings of the 14th International Conference on Physics of Electronic and Atomic Collisions (ed Coggiola, M. J. Huestic, D. L. and Saxon, R. P. (Amsterdam: North-Holland) Abstracts Pg. 108

Perger W.F., Halabuka Z. and Trautmann D. (1993). Continuum wave-function solver for GRASP. Computer Physics Communication **76**, 250-262

Sharma K. (2014). Scattering of Spin Polarized Positrons from Heavy Atoms. *Acta Physica Polonica* A **126,** 688-693

Staszewska G., Schwenke W. and Truhlar G. (1984). Investigation of the shape of the imaginary part of the optical-model potential for electron scattering by rare gases. *Physical Review* A **29,** 3078-3091

Trajmar S., Srivastava S. K., Tanaka H. and Nishimura H. (1981). Excitation cross sections for krypton by electrons in the 15-100eV impact-energy range. *Physical Review* A.**23,** 2167-2177

Tsurubuchi S., Miyazaki T. and Motohashi K. (1996). Electron-impact emission cross sections of Ar. *Journal of Physics B: Atomic, Molecular and Optical Physics* **29**, 1785-1801

Zatsarinny O., Yang W. Y. and Bartschat K. (2014). Electron-impact excitation of argon at intermediate energies. *Physical Review* A **89** 022706

Zeman V., McEachran R. and Stauffer A. D. (1994). Relativistic distorted-wave calculation of electron impact excitation of cesium. *Journal of Physics B: Atomic, Molecular and Optical Physics* **27**, 3175-3188

Zuo T., McEachran R. P. and Stauffer A. D. (1991). Relativistic distorted-wave calculation of electron impact excitation of xenon. *Journal of Physics B: Atomic, Molecular and Optical Physics* **24,** 2853-2870

Zuo T., McEachran R. P. and Stauffer A. D. (1992). Relativistic distorted-wave calculation of electron excitation of heavy noble gases. *Journal of Physics B: Atomic, Molecular and Optical Physics* **25,** 3393-3403

APPENDIX A

List of Publications

During the course of this PhD three manuscripts have been published in refereed journals. As a result, matter contained in the thesis has already been reported in the following publications:

i. The role of dynamic absorption and polarization potentials in relativistic excitation of xenon. *European Physical Journal D* **76,** 80 (2022) https://link.springer.com/article/10.1140/epjd/s10053-022-00396-5

ii. Relativistic distorted wave approach to electron impact excitation of argon gas using a complex potential. *Journal of Physics Communication* **5**, 075011 (2021) https://doi.org/10.1088/2399-6528/ac13b6

iii. Relativistic excitation of Krypton gas atoms by electrons moving through a complex distortion potential. *European Physical Journal D* **75,** 225 (2021) https://link.springer.com/article/10.1140/epjd/s10053-021-00221-5

APPENDIX B

B.1 Description of GRASP program

For this study, the only output we required from GRASP program (Dyall *et al.*, 1989) is the atomic wavefunctions; therefore all other output arising from any GRASP program run such as transition oscillator strengths is not used. This program comes with a user manual to enhance its usability. Below is a sample input file to the program GRASP for neutral argon. The same format is used for krypton and xenon, by adjusting the atomic structure parameters accordingly.

```
ARGON                  -Title
5 8 0                  -5 configurations, 8 orbitals, use relativistic formalism
1S
2S
2P-
2P    5 configurations          8 orbitals
3S
3P-   2  2  1  2  1
3P    4  3  4  3  4
4S    0  1  1  1  1
ANG
 2  2
 3  1        Total angular momentum for the excited states (configurations 2, 3, 4 and 5)
 4  1
 5  0
 MCP 7 8       -call subroutine MCP- to calculate coefficients needed by MCDF
 MCDF          -call subroutine MCDF -to initialize calculation of atomic wavefunctions
 8 0 10        -more output options
 18 39.95      -Atomic number, Mass number
OL 2                   -Calculation mode e.g. AL-average level, OL- optimal level
MCT 12 12
-1 1 2
OSCL 7         -call subroutine OSCL-main subroutine for radiative transition data
12 10          -more output options
END              -terminate program once calculations are done.
```

The call of subroutine MCDF will generate the atomic radial wavefunctions $P_{nk}(r)$, $P_{n_s k_s}(r)$, $Q_{nk}(r)$ and $Q_{n_s k_s}(r)$ described in chapter 3 together with their grid *r*.

B.2 Description of RDWBA program

In this section we briefly describe the RDWBA1 program used to determine the transition matrix elements and cross sections for argon as presented in chapter 3 in this thesis. The program RDWBA1 is written in FORTRAN77 language. It is designed to run on windows operating system with minimum of PENTIUM 4 computers in order to produce a runtime of approximately 60 seconds. This time will vary depending on the installed memory (RAM). The entire program contains further supporting subroutines borrowed from the GRASP (Dyall *et al*., 1989) and DWBA1 (Bartschat, 1996) programs. Because of the bulkiness of the RDWBA1 (consist of 175 pages in its current update), we only present the subroutine used for computing transition matrix elements TDIR and TEXC. The whole program (together with its write-up) will be available in open-access as soon as its accuracy is tested with more atoms apart from the rare gases, specifically excitation of group I, II and VII elements. This appendix is meant to encourage readers to develop and avail more programs on excitation of atoms using the RDW method. The input for RDWBA program comprises of the radial bound state wavefunctions $\mathrm{P}_{n_s\kappa_s}(\mathrm{r})$, $Q_{n_s\kappa_s}(\mathrm{r})$, $\mathrm{P}_{n\kappa}(\mathrm{r})$ and $Q_{n\kappa}(\mathrm{r})$ together with their logarithmic grid. Also needed are the atomic number, orbital occupation numbers, quantum numbers for every orbital and the configuration mixing coefficients for the *J*=1 excited states of the target atom. All this information is available from the GRASP program (Dyall *et al*., 1989) once the wavefunctions have been obtained. The subroutine for obtaining the distorted waves $f_{\epsilon_a\kappa_a}(r)$, $f_{\epsilon_b\kappa_b}(r)$, $g_{\epsilon_a\kappa_a}(r)$ and $g_{\epsilon_b\kappa_b}(r)$ follows the same formulation like that of Perger *et al.* (1993) which uses the WKB approximation to solve Dirac equations (equations (16a) and (16b)). The grid points (N) used in calculating the radial (distorted) wavefunctions is set ranging between 2000 and 30000 with the grid changing from

exponential to linear after around 200 grid points. This can still be varied. The wavefunctions are then interpolated to match with the grid with N=400 used for bound state wavefunctions, similar to that of the GRASP program (Dyall *et al*., 1989), in order to calculate the slater integrals $\Gamma_{J_b}(n_s\kappa_s, n\kappa; \in_a \kappa_a, \in_b \kappa_b)$ of subroutine SLATER, $\Gamma_\lambda(n\kappa, \in_a \kappa_a; n_s\kappa_s, \in_b \kappa_b)$ of subroutine SLATER1, and $\Gamma_\lambda(PW)$ for subroutine SLATERT which comprises of plane waves used for the high l partial waves as described in chapter 3. The slater integrals will then be used by subroutines TDIR and TEXC to obtain the direct and exchange T-matrix elements, scattering amplitudes and cross sections. A call to subroutine YYLM of the DWBA1 program of Bartschat, (1996) is made to obtain spherical harmonics to be multiplied with the output from subroutines TDIR and TEXC to obtain transition matrix elements or scattering amplitudes in order to calculate cross sections.

The symbolic names below represent the corresponding quantity (in italic) as used in this thesis followed by a sample of the subroutines TDIR and TEXC used for computing the direct $T^D_{a\to b}$ and exchange $T^E_{a\to b}$ matrix elements respectively;

- PHASKA ,PHASKB, PJAB, PJBB, PJS, PJSS, PJSS1 - $\eta_{\kappa_a}, \eta_{\kappa_b}, J_a, J_b, j, j_s$
  (PJSS for j_s *=1/2* or $\overline{p}$ electron*;* PJSS1 for j_s *=3/2* or p electron)
- LS, LSS, LAS, LBS, MSA, MSB, MBB - $l, l_s, l_a, l_b, \mu_a, \mu_b, M_b$
- KPARTY (M) - $l_a + l_b + J_B$ = even or $l + l_s + J_B$ = even
- ECONT, C,WNA, WNB, PI - impact energy in eV, relativistic speed of light, κ_a, κ_b, π
- PFS (I,IA), QFS (I,IA) , PFS (I,IC), QFS (I,IC) - $\mathrm{P}_{n_s\kappa_s}(\mathrm{r})$, $Q_{n_s\kappa_s}(\mathrm{r})$, $\mathrm{P}_{n\kappa}(\mathrm{r})$, $Q_{n\kappa}(\mathrm{r})$
- PFCA (400,400), QFCA (400,400) - $f_{\in_a\kappa_a}(r)$, $g_{\in_a\kappa_a}(r)$
- PFCB (400,400), QFCB (400,400) - $f_{\in_b\kappa_b}(r)$, $g_{\in_b\kappa_b}(r)$
- YP (400) , CC1, CC2 - $U(r)$, c_1, c_2
- PFB(J,400), QFB(J,400), PFD(J,400), QFD(J,400) - *spherical Bessel functions*
- NW, J -number of orbitals for the ground state atom, λ

```
**********Some declarations before call to TDIR and TEXC**********
ENA=ECONT / 27.211396D0
ENB=ENA-ELOST
IF (ENA.GT. TEN) THEN
CS=C*C
WNA= SQRT (((ENA+CS) **2-CS**2)/CS)
WNB= SQRT (((ENB+CS) **2-CS**2)/CS)
ELSE
CS=1.
WNA= SQRT (2.*ENA)
WNB= SQRT (2.*ENB)
END IF
TDW1=SQRT ((ENA+2.*CS) / (2.*ENA+2.*CS))*SQRT ((ENB+2.*CS) / (2.*ENB+2.*CS))
************************************************************************
IA1 = (NW-2)       ! For P- electron orbital
IA2 = (NW-1)       ! For P electron orbital
IC = NW            ! For S electron orbital
************************************************************************
CALL TEXC (1. /2. , -1. / 2. , MBB, IA1, J, TDW1, EXC1A)
CALL TEXC (1. /2. , 1. / 2. , MBB, IA2, J, TDW1, EXC2B)
CALL TDIR (1. / 2. , 1. / 2. , MBB, IA1, J, TDW1, DIR1A, DIRS1)
CALL TDIR (1. / 2. , 1. / 2. , MBB, IA2, J, TDW1, DIR2B, DIRS2)
************************************************************************
SUBROUTINE TDIR (MSA, MSB, MBB, IA, J, TDW1, DIR, DIRS)
IMPLICIT DOUBLEPRECISION (A-H, O-Z)
COMMON/NUMS/ZERO, HALF, TENTH, ONE, TWO, THREE, TEN, FOUR, SIX, PI
COMMON/GRID/ R (400), N, Z
COMMON /QNUMJ/ PJAB, PJBB, PJS, PJSS, PJSS1, LS, LSS
COMMON /SLAT/ IB, IC, ID, IA1, IA2
COMPLEX*16 DIR (400,-1: 1,-0: 0), SLATER, TDV, TDV3
COMPLEX*16 DIRS (400,-1: 1,-0: 0)
REAL*8 LAS, LBS, MSA, MSB, MBB, SUMM
KPARTY (M) = MOD (M, 2) + 1
DO 533 MLS=-LS, LS
DO 522 MLSS=-LSS, LSS
DO 511 I=1, N
DIR (I, MLSS, MLS) = (0.0D0, 0.0D0)
DIRS (I, MLSS, MLS) = 0.0D0
511 CONTINUE
522 CONTINUE
533 CONTINUE
DO 401 MLSS=-LSS, LSS
LAS=J+MLSS
IF (LAS.  LE.  0.0) GOTO 401
DO 501 MLS=-LS, LS
LBS=J+MLS
IF (LBS. LT. 0) GOTO 501
PJBS=LBS+1. / 2.
IF (IA.EQ.IA1) THEN
PJAS=LAS-1. / 2.
PPJ=PJSS
ENDIF
IF (IA.EQ.IA2) THEN
PJAS=LAS+1. / 2.
PPJ=PJSS1
ENDIF
KPCK= LAS+LBS+PJBB
IF (KPARTY (KPCK). NE. 1) GOTO 501
TDV1=2. / PI*TDW1*SQRT ((2.*PPJ+1.) * (2.*PJS+1)*(2.*PJAS+1)*(2.*PJBS+1))
CALL SYM3 (2.*PJS, 2.*PJBB, 2.*PPJ, 2.*1. /2., 2.*0,-2.*1./2.,0,C1)
IF (C1.EQ.0.0) GOTO 501
CALL SYM3 (2.*PJAS, 2.*PJBB, 2.*PJBS, 2.*1./2.,2.*0,-2.*1./2.,0,C2)
IF (C2.EQ.0.0) GOTO 501
TDV2=C1*C2 / SQRT (3.)
```

```
TDV3=SLATER (J, IC, IA, IB, ID, INT (PJBB))
TDV4=SLATERT (J, IC, IA, IB, ID, INT (PJBB))
TDV = TDV1*TDV2
DO 33 MBB=-PJBB, PJBB
DIR (I, MLSS, MLS) = DIR (I, MLSS, MLS) +
:TDV*TDV3*SUMM(IA,J,LAS,PJAS,LBS,PJBS,MSA,MSB,MBB,2)
DIRS (I, MLSS, MLS) = DIRS (I, MLSS, MLS) +
:TDV*TDV4*SUMM(IA,J,LAS,PJAS,LBS,PJBS,MSA,MSB,MBB,2)
33 CONTINUE
21 CONTINUE
11 CONTINUE
501 CONTINUE
401 CONTINUE
RETURN
END
**************************************************************************
SUBROUTINE TEXC (MSA, MSB, MBB, IA, J, BBS, EDW1, EXC)
IMPLICIT DOUBLEPRECISION (A-H, O-Z)
COMMON/NUMS/ZERO, HALF, TENTH, ONE, TWO, THREE, TEN, FOUR, SIX, PI
COMMON/GRID/R (400), N, Z
COMMON /QNUMJ/ PJAB, PJBB, PJS, PJSS, PJSS1, LS, LSS
COMMON /SLAT/ IB, IC, ID, IA1, IA2
COMMON/TATB/ TA (410), TB (410)
COMPLEX*16 EXC (400,-1: 1,-0: 0), SLATER1, EDV
REAL*8 LAS, LBS, MSA, MSB, MBB, PARS, L, SUMM
KPARTY (M) = MOD (M, 2) +1
DO 533 MLS=-LS, LS
DO 522 MLSS=-LSS, LSS
DO 511 I=1, N
EXC (I, MLSS, MLS) = (0.0D0, 0.0D0)
511 CONTINUE
522 CONTINUE
533 CONTINUE
DO 40 MLSS=-LSS, LSS
LAS=J+MLSS
IF (LAS. LE. 0.0) GOTO 40
DO 50 MLS=-LS, LS
LBS=J+MLS
IF (LBS. LT. 0) GOTO 50
PJBS=LBS+1. / 2.
IF (IA.EQ.IA1) THEN
PJAS=LAS-1. / 2.
PPJ=PJSS
ENDIF
IF (IA.EQ.IA2) THEN
PJAS=LAS+1. / 2.
PPJ=PJSS1
ENDIF
KPCK= LAS+LBS+PJBB
IF (KPARTY (KPCK).NE.1) GOTO 50
EDV1=2. / PI*EDW1*SQRT ((2.*PPJ+1.) *(2.*PJS+1.)*(2*PJAS+1)*(2*PJBS+1))
DO 7 L=ABS (PJS-PJAS), PJS+PJAS, 2
CALL SYM3(2.*PJS,2.*L,2.*PJAS,2.*1./2.,2.*0.,-2.*1./2.,0,C0)
IF (C0.EQ.0.0) GOTO 7
CALL SYM3(2.*PPJ,2.*L,2.*PJBS,2.*1./2.,2.*0.,-2.*1./2.,0,C1)
IF (C1.EQ.0.0) GOTO 7
CALL SYM6 (2.*PJAS, 2.*PJBS, 2.*PJBB, 2.*PPJ, 2.*PJS, 2.*L, 0, C2)
IF (C2.EQ.0.0) GOTO 7
EDV2=C0*C1*C2*SQRT (3.)*(-1) ** (INT(L))
EDV=EDV1*EDV2*SLATER1 (J, IC, IA, IB, ID, INT (L))
DO 33 MBB=-PJBB, PJBB
IF (IA.EQ.IA2) THEN
PARS=BBS
ELSE
```

```
PARS=PJBB
ENDIF
EXC (I, MLSS, MLS) = EXC (I, MLSS, MLS) +
:PARS*EDV*SUMM(IA,J,LAS,PJAS,LBS,PJBS,MSA,MSB,MBB,1)
33 CONTINUE
7 CONTINUE
2 CONTINUE
1 CONTINUE
50 CONTINUE
40 CONTINUE
RETURN
END
**************************************************************************
FUNCTION SLATER (J, IC, IA, IB, ID, K)
IMPLICIT DOUBLEPRECISION (A-H, O-Z)
COMMON/GRID/R (400), N, Z
COMMON/TATB/ TA (410), TB (410)
COMMON /WAVES/ PFS (400, 25), QFS (400, 25)
COMMON/RFC/ PFCA (400,400), QFCA (400,400), PFCB (400,400), QFCB (400,400)
COMPLEX*16 PFCA, PFCB, QFCA, QFCB, SLATER
DO 1 I = 1, N
TA(I) =((PFS(I,IA)*PFS(I,IC)+QFS(I,IA)*QFS(I,IC)))*R(I)
1 CONTINUE
CALL YZK (K)
DO 12 I = 1, N
TA(I)=REAL((PFCA(I,J)*PFCB(I,J)+QFCA(I,J)*QFCB(I,J)))*TB(I)/R(I)
12 CONTINUE
CALL QUAD (DRECTR)
IF (STEP.EQ.2) THEN
DO 122 I = 1, N
TA(I)=AIMAG((PFCA(I,J)*PFCB(I,J)+QFCA(I,J)*QFCB(I,J)))*TB(I)/R(I)
122 CONTINUE
CALL QUAD (DRECTI)   ! Integrate TA (I) from zero to infinity
SLATER =DCMPLX (DRECTR, DRECTI)
RETURN
END
**************************************************************************
FUNCTION SLATER1 (J, IC, IA, IB, ID, K)
IMPLICIT DOUBLEPRECISION (A-H, O-Z)
COMMON /GRID/R (400), N, Z
COMMON /TATB/TA (410), TB (410)
COMMON /WAVES/PFS (400, 25), QFS (400, 25)
COMMON/RFC/PFCA (400,400), QFCA (400,400), PFCB (400,400), QFCB (400,400)
COMPLEX*16 PFCA, PFCB, QFCA, QFCB, SLATER1
DIMENSION TBI (400), TBR (400)
DO 100 STEP=1, 2
IF (STEP.EQ.1) THEN
DO 1 I = 1, N
TA(I)=R(I)*REAL((PFS(I,IC)*PFCA(I,J)+QFS(I,IC)*QFCA(I,J)))
1 CONTINUE
CALL YZK (K)
DO 10 I=1, N
TBR (I) = TB (I)
10 CONTINUE
ENDIF
IF (STEP.EQ.2) THEN
DO 11 I = 1, N
TA(I)=R(I)*AIMAG((PFS(I,IC)*PFCA(I,J)+QFS(I,IC)*QFCA(I,J)))
11 CONTINUE
CALL YZK (K)
DO 101 I=1, N
TBI (I) =TB (I)
101 CONTINUE
ENDIF
```

```
100 CONTINUE
DO 200 STEP=1, 2
IF (STEP.EQ.1) THEN
DO 2 I = 1, N
TA(I)=(PFS(I,IA)*REAL(PFCB(I,J))+QFS(I,IA)*REAL(QFCB(I,J)))*TBR(I)
2 CONTINUE
CALL QUAD (RESULR)
ENDIF
IF (STEP.EQ.2) THEN
DO 22 I = 1, N
TA(I)=(PFS(I,IA)*AIMAG(PFCB(I,J))+QFS(I,IA)*AIMAG(QFCB(I,J)))*TBI(I)
22 CONTINUE
CALL QUAD (RESULI)
ENDIF
200 CONTINUE
SLATER1 = DCMPLX (RESULR, RESULI)
RETURN
END
*************************************************************************
FUNCTION SLATERT (J, IC, IA, IB, ID, K)
IMPLICIT DOUBLEPRECISION (A-H, O-Z)
COMMON /GRID/R (400), N, Z
COMMON /TATB/TA (410), TB (410)
COMMON/WAVES/PFS (400, 25), QFS (400, 25)
COMMON /RWFT/ PFB (400,400), QFB (400,400), PFD (400,400), QFD (400,400)
DO 1 I = 1, N
TA(I) =((PFS(I,IA)*PFS(I,IC)+QFS(I,IA)*QFS(I,IC)))*R(I)
1 CONTINUE
CALL YZK (K)
DO 2 I = 1, N
TA(I)=(PFB(J,I)*PFD(J,I)+QFB(J,I)*QFD(J,I))*TB(I)/R(I)
2 CONTINUE
CALL QUAD (DRECT)
SLATERT =DRECT
RETURN
END
*************************************************************************
FUNCTION SUMM (IA, J, LAS, PJAS, LBS, PJBS, MSA, MSB, MBB, IP)
!  Summation over magnetic sublevels M
IMPLICIT DOUBLEPRECISION (A-H, O-Z)
COMMON/NUMS/ZERO, HALF, TENTH, ONE, TWO, THREE, TEN, FOUR, SIX, PI
COMMON /QNUMJ/ PJAB, PJBB, PJS, PJSS, PJSS1, LS, LSS
REAL*8 LAS, LBS, MSA, MSB, MB, MBB, MLB, SUMM
IF (IA.EQ.IA1) THEN
PPJ=PJSS
ENDIF
IF (IA.EQ.IA2) THEN
PPJ=PJSS1
ENDIF
MB=MSA-MBB
MLB=MB-MSB
CALL SYM3 (2.*LAS, 2.*1. /2.,2.*PJAS,2.*0.,2.*MSA,2.*MSA,1,C6)
IF (C6.EQ.0.0) GOTO 3
CALL SYM3 (2.*LBS,2.*1./2.,2.*PJBS,2.*MLB,2.*MSB,2.*MB,1,C7)
IF (C7.EQ.0.0) GOTO 3
CALL SYM3 (2.*PJAS,2.*PJBB,2.*PJBS,-2.*MSA,2.*MBB,2.*MB,0,C8)
IF (C8.EQ.0.0) GOTO 3
SUMM=C6*C7*C8*(-1.)** (INT (PPJ+ (-1) **IP*MSA))*SQRT ((2*LAS+1)/ (4.*PI))
3 CONTINUE
2 CONTINUE
RETURN
END
*************************************************************************
TDTE=EXP ((0.0D0, 1.0D0)*(PHASKA+PHASKB))*(0.0D0, 1.0D0) ** (INT (LAS-LBS))
```

```
TDTD= (0.0D0, 1.0D0) ** (INT (LAS-LBS))
TDTD2= (-(0.0, 1.0)) **PJBB
*** For excitation to singlet state [1/2] J=1, configuration mixing considered
IF (JLEV.EQ.1./2.) THEN
DIRAMP (J, MLSS, 0) = (CC1*DIR1A-CC2*DIR2B)
DIRAMT (J, MLSS, 0) = (CC1*DIRS1-CC2*DIRS2)
EXCAMP (J, MLSS, 0) = (CC1*EXC1A-CC2*EXC2B)
ENDIF
*** For excitation to a triplet state [3/2] J=1, configuration mixing considered
IF (JLEV.EQ.3./2.) THEN
DIRAMP (J, MLSS, 0) = (CC2*DIR1A+CC1*DIR2B)          ! Direct T-matrix
DIRAMT (J, MLSS, 0) = (CC2*DIRS1+CC1*DIRS2)          ! Top-up
EXCAMP (J, MLSS, 0) = (CC2*EXC1A+CC1*EXC2B)        ! Exchange T-matrix
ENDIF
*************************************************************************
```

Spherical Bessel functions are obtained using subroutine SBESJY (Bartschat, 1996); subroutines QUAD and YZK in the program GRASP (Dyall *et al.*, 1989), while subroutine SYM3 is used in calculation of Clebsch-Gordan coefficients or Wigner-3J symbols while subroutine SYM6 is used to calculate Wigner-6J symbols. These two subroutines can be found in the program DWBA1 (Bartschat, 1996).

APPENDIX C

RDW differential cross section results

In this appendix we list the RDW DCS results for figures given in chapter 4, obtained using the complex distortion potential (present SEPA-RDWBA) for argon, krypton and xenon at different electron impact energies.

Table C-1: DCS results (a_0^2 / sr) for SEPA-RDWA approach to electron impact excitation of the $4s[1/2]_1^o$ state of argon

Scattering angle θ (degrees)	Energy(eV)			
	17.5	20	30	50
0	0.09229	0.08315	0.21668	1.04513
10	0.01855	0.01709	0.03586	0.07859
20	0.00826	0.00634	0.00812	0.01772
30	0.00676	0.00409	0.00405	0.00787
40	0.00564	0.00261	0.00342	0.00406
50	0.00457	0.00420	0.00238	0.00203
60	0.00410	0.00358	0.00139	8.42E-04
70	0.00443	0.00304	6.75E-04	5.25E-04
80	0.00361	0.00209	5.91E-04	6.81E-04
90	0.00300	0.00157	7.98E-04	0.00102
100	0.00360	0.00149	9.24E-04	0.00131
110	0.00445	0.00199	7.59E-04	0.00138
120	0.00495	0.00238	3.94E-04	0.00116
130	0.00476	0.00267	2.32E-04	7.72E-04
140	0.00382	0.00253	4.73E-04	4.11E-04
150	0.00496	0.0034	4.22E-04	6.08E-04
160	0.00724	0.00485	7.42E-04	9.30E-04
170	0.01083	0.00623	7.46E-04	0.00132
180	0.00964	0.0058	6.17E-04	6.69E-04

Table C-2: DCS results (a_0^2 / sr) for SEPA-RDWA approach to electron impact excitation of the $4s[3/2]_1^o$ state of argon

Scattering angle θ (degrees)	Energy (eV)				
	17.5	20	30	50	100
0	0.02825	0.02750	0.06477	0.30231	0.16293
10	0.00709	0.00699	0.01542	0.02728	0.01149

20	0.00349	0.00295	0.00387	0.00671	0.00214
30	0.00297	0.00202	0.00201	0.00299	7.50E-04
40	0.00241	0.00118	0.00184	0.00150	2.94E-04
50	0.00178	0.00185	0.00132	7.00E-04	1.09E-04
60	0.00163	0.00144	7.75E-04	2.25E-04	2.91E-05
70	0.00170	0.00118	3.78E-04	1.16E-04	2.01E-05
80	0.00118	6.87E-04	3.23E-04	1.82E-04	3.03E-05
90	8.16E-04	4.18E-04	4.32E-04	2.97E-04	4.80E-05
100	0.00111	3.51E-04	4.95E-04	3.82E-04	6.34E-05
110	0.00152	6.44E-04	3.99E-04	3.83E-04	6.59E-05
120	0.00175	8.90E-04	1.96E-04	2.91E-04	5.19E-05
130	0.00168	0.00105	1.35E-04	1.45E-04	2.74E-05
140	0.00131	9.37E-04	2.69E-04	1.55E-05	9.82E-06
150	0.00201	0.00134	2.47E-04	1.39E-04	2.54E-05
160	0.00317	0.00212	4.29E-04	2.67E-04	5.02E-05
170	0.00479	0.00292	4.17E-04	3.74E-04	7.59E-05
180	0.00494	0.00308	3.69E-04	3.18E-04	6.23E-05

Table C-3: DCS results (a_0^2 / sr) for SEPA-RDWA approach to electron impact excitation of the $5s[1/2]_1^o$ state of krypton

Scattering angle θ (degrees)	Energy(eV)			
	15	20	30	50
0	0.16326	0.24756	0.29265	1.70712
10	0.03332	0.04059	0.05520	0.11440
20	0.01522	0.01362	0.01374	0.01975
30	0.01279	0.00799	0.00686	0.00631
40	0.01146	0.00463	0.00498	0.00222
50	0.00766	0.00409	0.00328	7.67E-04
60	0.00409	0.00323	0.00181	2.38E-04
70	0.00617	0.00288	7.85E-04	1.51E-04
80	0.00568	0.00199	7.69E-04	2.39E-04
90	0.00458	0.00132	0.00112	3.49E-04
100	0.00620	0.00141	0.00133	4.30E-04
110	0.00719	0.00205	0.00111	4.25E-04
120	0.00672	0.00228	5.83E-04	3.17E-04
130	0.00557	0.00246	2.26E-04	1.55E-04
140	0.00336	0.00193	6.00E-04	6.26E-05
150	0.00690	0.00319	5.86E-04	2.11E-04
160	0.01017	0.00487	8.57E-04	3.76E-04
170	0.01616	0.00683	8.85E-04	5.06E-04
180	0.01654	0.00715	6.11E-04	4.83E-04

Table C-4: DCS results (a_0^2 / sr) for SEPA-RDWA approach to electron impact excitation of the $5s[3/2]_1^o$ state of krypton.

Scattering angle θ (degrees)	Energy (eV)			
	15	20	30	50
0	0.25361	0.37372	0.42888	1.12991
10	0.05125	0.05900	0.06967	0.08266
20	0.02053	0.01762	0.01346	0.01589
30	0.01522	0.00952	0.00686	0.00582
40	0.01214	0.00496	0.00633	0.00251
50	0.00830	0.00592	0.00444	0.00109
60	0.00790	0.00439	0.00253	3.75E-04
70	0.00815	0.00364	0.00109	1.81E-04
80	0.00638	0.00227	8.84E-04	2.77E-04
90	0.00475	0.00144	0.00124	4.48E-04
100	0.00593	0.00122	0.00145	5.72E-04
110	0.00742	0.00208	0.00110	5.56E-04
120	0.00762	0.00265	4.08E-04	3.95E-04
130	0.00705	0.00312	5.83E-04	1.70E-04
140	0.00496	0.00266	9.70E-04	5.95E-05
150	0.00899	0.00408	9.34E-04	2.37E-04
160	0.01399	0.00640	0.00163	3.94E-04
170	0.02113	0.00884	0.00153	5.10E-04
180	0.02212	0.00942	0.00165	4.67E-04

Table C-5: DCS results (a_0^2 / sr) for SEPA-RDWA approach to electron impact excitation of the $6s[1/2]_1^o$ state of xenon

Scattering angle θ (degrees)	Energy(eV)			
	15	30	50	80
0	0.06335	3.06968	3.01518	2.63706
10	0.01433	0.25219	0.21721	0.17935
20	0.00639	0.01168	0.00713	0.00616
30	0.00536	0.00228	0.00163	0.00248
40	0.00491	0.00450	0.00187	0.00140
50	0.00695	0.00370	0.00113	6.24E-04
60	0.00535	0.00192	4.59E-04	2.67E-04
70	0.00449	7.61E-04	1.29E-04	9.56E-05
80	0.00286	4.75E-04	7.50E-05	3.72E-05
90	0.00182	6.90E-04	1.82E-04	7.78E-05
100	0.00190	8.64E-04	3.23E-04	1.70E-04

110	0.00287	7.24E-04	4.09E-04	2.56E-04
120	0.00352	6.13E-04	4.32E-04	2.78E-04
130	0.00382	9.22E-04	3.52E-04	2.02E-04
140	0.00322	8.48E-04	1.71E-04	7.20E-05
150	0.00508	7.83E-04	1.23E-04	7.74E-05
160	0.00805	0.00153	4.27E-04	3.07E-04
170	0.01142	0.00210	8.98E-04	6.69E-04
180	0.01206	0.00213	8.14E-04	6.76E-04

Table C-6: DCS results (a_0^2 / sr) for SEPA-RDWA approach to electron impact excitation of the $6s[3/2]_1^o$ state of xenon.

Scattering angle θ (degrees)	Energy(eV)			
	15	30	50	80
0	0.11259	3.02045	3.71375	1.57357
10	0.02342	0.25543	0.24199	0.11344
20	0.00936	0.01476	0.01276	0.00365
30	0.00733	0.00492	0.00344	0.00187
40	0.00604	0.00648	0.00250	0.00114
50	0.00796	0.00489	0.00139	5.84E-04
60	0.00695	0.00252	5.61E-04	2.42E-04
70	0.00647	0.00108	1.72E-04	8.33E-05
80	0.00474	8.69E-04	1.06E-04	4.54E-05
90	0.00357	0.00128	2.85E-04	9.73E-05
100	0.00427	0.00159	5.02E-04	1.91E-04
110	0.00564	0.00142	6.13E-04	2.87E-04
120	0.00645	8.93E-04	6.42E-04	3.19E-04
130	0.00654	0.00122	5.06E-04	2.54E-04
140	0.00541	0.00120	2.48E-04	1.11E-04
150	0.00760	9.99E-04	2.05E-04	8.90E-05
160	0.01164	0.00191	6.03E-04	2.87E-04
170	0.01680	0.00243	0.00123	6.44E-04
180	0.01628	0.00230	0.00103	5.74E-04